Sodium Chloride and Freezing Temperatures Increasing the Weathering of a Shale Bedrock Channel

by

Logan Ann Koeth

A thesis

presented to the University of Waterloo

in fulfillment of the

thesis requirement for the degree of

Master of Applied Science

in

Civil & Environmental Engineering

Waterloo, Ontario, Canada, 2019

Author's Declaration

I hereby declare that I am the sole author of this thesis. This is a true copy of the thesis, including any required final revisions, as accepted by my examiners.

I understand that my thesis may be electronically available to the public.

Abstract

Studies on erodibility in shale channels attribute slaking as the primary weathering mechanism, and consider chemical weathering mechanisms as a secondary agent (Tinkler and Parish, 1998). This research examines the roles of freeze-thaw, cation exchange, and slaking mechanisms. The objectives of this study were to determine if slaking is the primary mode of weathering in a shale bedrock channel, investigate the cumulative effects of cation exchange, freeze-thaw and slaking upon weathering and ascertain the contribution of chemical weathering due to anthropogenic sources.

The impact of slaking, freeze-thaw and geochemical weathering on Georgian Bay Formation (GBF) shale was assessed in the laboratory using shale samples collected from Humber Creek (Toronto, Ontario). A modified version of the slake durability test (Franklin and Chandra, 1972) and the weatherability test (Unrug, 1997) was employed to investigate the slaking characteristics of the shale. Three-way ANOVA tests revealed that significant effects from air temperature, NaCl concentration and the interaction effect of the two conditions on Weatherability Index and Inverse Slake Durability Index.

The results of this study indicate that slaking is not the primary weathering agent in shale bedrock channels and suggest that changes to water quality from anthropogenic inputs may be increasing the erodibility of these channels. Despite its exploratory nature, this study offers conditional insight into possible revisions required to the conceptual model of erosion and erodibility within a shale bedrock channel environment.

Acknowledgements

I would like to thank my advisor, Dr. William Annable, for always dedicating the time to discuss recent developments in my research, challenge my process, or check in with my mental health.

I would also like to thank those who assisted in the collection and analysis of data; Lucas Mueller, Jeff Hirvonen, Caleb Jefferies, Dr. Lorenzo Brignoli, Terry Ridgeway, Mark Merlau, Mark Sobon, Marco Shun, Dr. Shaun Frape and Dr. Monica Emelko

Finally, I would like to thank all those who helped improve my writing processes. Special thanks go to Mary McPhearson at the Writing Centre, for your perfectly timed words of support and kindness. As well as Amy Green and Nadine Fladd at the Writing Centre, and Stephen B. Heard for writing “The Scientist's Guide to Writing: How to Write More Easily and Effectively Throughout Your Scientific Career”.

Dedication

Serge and Mica for weathering all my up's and down's throughout this journey. Thank you for your endless support and love.

Table of Contents

List of Figures

List of Tables

List of Symbols

Symbol	Description
C_i	concentration of NaCl in dionized water
$ISDI_i$	Inverse Slake Durability Index for cycle *i*
T_i^{air}	air temperature
$T_i^{H_2O}$	water temperature
W'	weight of oven dried sample before cycle 1
W_i	weight of oven dried sample after cycle(s) *i*
$W_i^{largest}$	weigh of largest oven dried element(s) after weathering cycle(s) *i*
WI_i	Weatherability Index for cycle *i*

1 Introduction

A key aspect of erosion, erodibility, is the capacity of a material to resist particle detachment via flowing water or wind on natural landscapes. The primary contributors to erodibility in bedrock channels are lithological characteristics and environmental conditions, both of which change the effectiveness and prevalence of erosion processes (Hancock et al., 2011; Whipple, 2004; Whipple et al., 2000; Wohl, 1993; Wohl and Ikeda, 1998). The erodibility of bedrock channels are inherently dependent on rock properties such as, hardness, structure, intact strength, porosity, permeability and heterogeneity (Hancock et al., 2011; Wohl and Ikeda, 1998). However, these lithological characteristics change over time depending upon the environmental conditions to which the geologic media is exposed. In many circumstances, these conditions reduce the material strength of the geological unit via physical and chemical weathering, and increase its erodibility (Allen et al., 2002; Murphy et al., 2016; Whipple et al., 2000). Of particular interest in this study are the impacts of weathering on the erodibility of a shale bedrock channel, because of the potential to improve environmental channel rehabilitation by maintaining channel structure integrity.

Weathering mechanisms are complex with interdependent processes occurring simultaneously. In general for shale channels, physical weathering often includes wetting and drying (slaking), freeze-thaw (Matsuoka, 1990), heating and cooling and salt bursting (Allen et al., 2002; Gautam and Shakoor, 2013, 2015; Hale and Shakoor, 2003; Kolay, 2016). The limited literature on physical weathering mechanisms in shale bedrock channels highlights that freeze-thaw in combination with slaking effectively increases the degradation rate of clay-bearing rocks (Erguler and Shakoor, 2009), as opposed to slaking alone (Mugridge and Young, 1983). Chemical weathering mechanisms common in shale channels are ionic exchange, expansion via water absorbing clay minerals (Stock et al., 2005), and dissolution of cementing minerals (Allen et al., 2002; Hale and Shakoor, 2003; Hancock et al., 2011; Hirvonen, 2017; Tinkler and Parish, 1998; Whipple, 2004; Whipple et al., 2000; Wohl, 1993).

Bedrock channels in some geological settings are incising at higher than anticipated rates (Allen et al., 2002; Tinkler and Parish, 1998). Studies have primarily focused on enlargement and incision responses exclusively due to erosion. Discrepancies within these studies are often attributed to the variable erodibility of the channel; however, few have investigated the contribution of lithology and environmental conditions on erosion (Allen et al., 2002; Hancock et

al., 2011; Hirvonen, 2017; Murphy et al., 2016; Sklar and Dietrich, 2001; Tinkler and Parish, 1998; Turowski, Hovius, Wilson et al., 2008; Wohl and Ikeda, 1998). Studies on erodibility in shale channels attribute slaking as the primary weathering mechanism, and consider chemical weathering mechanisms as a secondary agent (Mugridge and Young, 1983; Tinkler and Parish, 1998).

This research examines the relative influence of freeze-thaw, cation exchange, and slaking mechanisms on the erodibility of an urbanized shale bedrock channel, with the hope that this information may aid in urban management strategies to revise practices contributing to channel degradation. This study has three primary objectives:

1. measure parameters (air temperature, water temperature, inundation cycles and water chemistry) that contribute to creating a weathering environment,
2. determine if slaking is the primary mode of weathering in a shale bedrock channel, by investigating the cumulative effects of cation exchange, freeze-thaw and slaking to weathering, and
3. ascertain the contribution of chemical weathering due to anthropogenic sources on enhancing the weathering process.

This study indicates that freeze-thaw, sodium cation exchange and slaking have a greater synergistic impact on shale weathering than slaking alone. Therefore, this study contributes to the research concerning shale bedrock channels by demonstrating (1) that slaking may not be the primary weathering mechanism and (2) changes to water quality from road salting, may be increasing the erodibility of these channel environments. It was beyond the scope of this study to quantify the change in erosion rates due to increased erodibility from physical and chemical weathering.

2 Background

In the context of susceptibility of bedrock channels to erosion, channels composed of shale are of primary interest as they are the prone to eroding over a relatively short time span (human and maintenance context). Sedimentary geologic units, such as those which shales are derived from, comprise the most of what we would consider "degradable" rocks in the context of engineering tests such as durability tests (Walkinshaw and Santi, 1996).

Shale is a common weak argillaceous rock that is formed via the consolidation of fine particles in a sedimentary environment (Gurgenli, 2006; Parish, 2001). They comprise 50% of the sedimentary geologic units present on Earth (Parish, 2001; Walkinshaw and Santi, 1996). Typical characteristics of shale include:

1. composed of varying fractions of silt (0.0625 to 0.004 mm) and clay (<0.004 mm) size particles,
2. mineralogically composed of phyllosilicate (e.g. mica), quartz and feldspar minerals (Parish, 2001), and
3. laminations which are prone to, but not defined by, fissility (Parish, 2001; Potter et al., 1980).

Weak rocks, like shale, are characterized as having; "low compressive strength, low durability (resistance to weathering), high clay content, poor induration and a measureable loss of strength in a human time frame" (Gautam, 2012). Research by Matsuoka (1990) has indicated that when comparing geologic media with similar moisture and temperature conditions, those with a higher clay content are more prone to higher rates of degradation. Shale is also considered a weak rock due to its susceptibility to fissility, and the sedimentary formation environment, which typically has weaker bonds between the mineral types.

2.1 Environmental Weathering Conditions

Weathering processes occurring at any given time or location primarily depends upon five conditions:

1. Climate:
   Climate determines which weathering mechanisms predominate in geographic settings. For instance, in dry cold climate regions, physical weathering is the primary mechanism,

whereas in moist climates there is a combination of physical and chemical weathering processes (Carroll, 1970).

2. Parent rock:

   Geologic media vary in their baseline resistance to erosion, however, the degree to which a given geologic unit is susceptible to weathering depends upon the parent rock chemical composition, texture, and previous weathering that the unit has endured in the past (Carroll, 1970).

3. Biological activity:

   The coherency of a geological unit can be acted upon by vegetative root structures desiccating larger rock units as well as through microbial activity.

4. Topography:

   Topography affects drainage and leaching which can play significant roles in the availability and chemical composition of matrix waters. For some physical, but particularly for chemical weathering mechanisms, the moisture content of a given geologic unit can be critical.

5. Time:

   Certain weathering conditions require larger residence times to work effectively at degrading a geologic unit.

The manifestation of these five conditions is typically described as a complex combination of physical, biological and/or chemical weathering processes. Physical weathering is the process whereby a geologic media is broken down into smaller fractions with little or no chemical change (Carroll, 1970). Biological weathering is the process of biological sources, such as roots of vegetation or microbial activity, breaking down rocks into smaller grain size fractions. Chemical weathering is a reaction between water, the atmosphere and a geologic media, which can be described by a constitutive relationship of the form (Carroll, 1970):

$$Rock + Oxygen + Water + p\int_{sea\ level}^{mountains} \rightarrow Saprolite \rightarrow Soil + Soluble\ inorganic\ and\ organic\ ions/compounds \quad (1)$$

The presence or impact of any given chemical weathering mechanism is heavily dependent upon the environmental conditions (which provide the atmospheric and water content conditions) and the minerology of a given geologic unit (Carroll, 1970). Equation (1) represents a relationship between the substrate chemistry and water, thereby emphasizing that the

effectiveness of any given chemical weathering mechanism is dependent upon the presence of water in liquid or gas form (Carroll, 1970; Murphy et al., 2016; Whipple, 2004).

One of the fundamental rate controls of chemical weathering relates to effective reaction surface area. The greater the surface area exposed to a given reaction, the greater the rate of chemical weathering, as an increase in surface area is proportional to an increase in chemical weathering processes, such as ion exchange (Carroll, 1970). This is particularly the case for clay bearing geologic units, where finer grained materials proportionally exhibit an increase in effective grain surface area (Carroll, 1970).

2.2 Weathering Processes Observed in Bedrock Channels

Natural settings are susceptible to a combination of chemical and physical weathering processes occurring simultaneously in most shale bedrock channels, with various mechanisms dominating seasonally (Allen et al., 2002; Hale and Shakoor, 2003; Hancock et al., 2011; Hirvonen, 2017; Tinkler and Parish, 1998; Whipple, 2004; Whipple et al., 2000; Wohl, 1993).

Physical weathering process in shale bedrock channels include:

- freeze-thaw cycles (Gautam and Shakoor, 2013, 2015; Hale and Shakoor, 2003; Hancock et al., 2011; Hirvonen, 2017; Kolay, 2016; Matsuoka, 1990),
- wetting and drying cycles (slaking), (Allen et al., 2002; Gautam and Shakoor, 2013, 2015; Hale and Shakoor, 2003; Hirvonen, 2017; Kolay, 2016; Tinkler and Parish, 1998), and
- heating and cooling cycles, and (Gautam and Shakoor, 2013, 2015; Hale and Shakoor, 2003; Kolay, 2016).

Chemical weathering mechanisms in channels composed of shale bedrock include:

- leaching of ions (e.g. ionic exchange) (Carroll, 1970),
- expansion via water adsorbing clay minerals (Allen et al., 2002; Hale and Shakoor, 2003; Massong and Montgomery, 2000; Stock et al., 2005; Tinkler and Parish, 1998; Whipple, 2004; Whipple et al., 2000); and,
- dissolution of cementing minerals causing micro- and macro- joint expansion and lose of mineral grain cohesion (e.g. carbonates)(Allen et al., 2002; Hale and Shakoor, 2003; Hancock et al., 2011; Hirvonen, 2017; Tinkler and Parish, 1998; Whipple, 2004).

Previous studies acknowledge chemical weathering as a process increasing the erodibility of channel boundaries composed of shale bedrock (Mugridge and Young, 1983; Murphy et al., 2016; Tinkler and Parish, 1998). In particular, Tinkler and Parish (1998), focused on slaking, ice structures and geochemistry as weathering mechanisms of interest in a shale bedrock channel, and identified slaking as the dominant weathering process.

2.2.1 Slaking

Slaking is "the crumbling and disintegration of earth materials when exposed to air or moisture. More specifically, the breaking up of dried clay when saturated with water, due to either compression of entrapped air by inwardly migrating capillary water or the progressive swelling and sloughing off of the outer layers" (American Geological Institute, 1976). Slaking is often induced during cyclic wetting and drying, such as changes in stage of a riverine environment.

Five mechanisms combine to induce slaking. Some of the mechanisms are more prevalent than others, and depend upon the characteristics of geologic media and water chemistry.

1. Increase of hydration force: Exertion of pressure forces when water hydrates and expands the mineral structure, which may lead to failure. (Parish, 2001),
2. Double layer repulsion force increase: Occurs when clay platelets within a rock structure repel each other, prompting degradation. This is commonly initiated when the structure of a geologic unit is hydrated and the ions within the aqueous solution substitute within the clay platelets. (Parish, 2001),
3. Negative pore pressure: When pores are subjected to negative pore pressure from internal suction, the tensile stress exerted can cause the microstructure of a geologic media to breakdown (Parish, 2001),
4. Pore air compression (PAC): Absorption of water into the matrix pores via capillary action. This causes the air to compress in the pores exerting tensile stresses on pore cavities, resulting in fracturing of the rock microstructure (Parish, 2001). Studies have suggested that PAC is a primary mechanism of slaking in non-swelling clays, however, illite, a non-swelling clay, is less susceptible to PAC (Moriwaki, 1975),
5. Mineral Alteration: Bonds of a given geologic media break due to the increased forces on the micro-structure of the media from recrystallization and growth of small crystals (Parish, 2001).

Montgomery (2004) observed greater lateral erosion rates in sections of a channel prone to cycles of wetting and drying (typically banks) than areas permanently submerged (typically

beds). In bedrock channels with wetted perimeters composed of material susceptible to slaking, the process can have a profound impact upon the erodibility of the channel. Montgomery (2004) observed that in channels composed of marine sandstone and siltstone, erosion rates in areas where slaking was prevalent were two orders of magnitude greater than the long term erosion rates where slaking was not present.

In shale bedrock channels, slaking is considered the primary method of weathering (Allen et al., 2002; Mugridge and Young, 1983; Tinkler and Parish, 1998). The degree to which the process dominates is dictated by the rock type, degree of pre-existing weathering, grain size and the mineralogical arrangement and composition of the geologic media (Gurgenli, 2006; Kolay and Kayabali, 2006; Parish, 2001). The mechanism is typically observed within compacted rather than cemented shales, and in drier rather than more highly saturated media (Mitchell, 1993). However, slaking does not occur in all shale types, as the process is dependent upon the percentage of clay-sized particles and mineral composition (Parish, 2001).

2.2.2 Freeze-Thaw

Freeze-thaw is a physical weathering mechanism that degrades coherent rock units into fractions via the expansion of moisture in freezing temperatures (Fraser, 1959; Matsuoka, 1990). It is termed as “frost action”, “frost shattering”, “ice wedging”, and “frost splitting” (Lienhart, 1993), however, for the purposes of this research the process is referred to as freeze-thaw. This mechanism is most effective during spring thaw (Hale and Shakoor, 2003), or during frost shattering period from October to May (Matsuoka, 1990).

In the literature there is contention around the principle mechanisms that cause a geologic media to breakdown under the conditions of moisture and freezing temperatures. Nonetheless, there is agreement that temperature, moisture content and the geologic properties (pore size distribution, permeability, location and quantity of clay minerals) are the main factors critical to understanding the degradation of a coherent geologic unit due to freeze-thaw action (Matsuoka, 1990; McGreevy, 1981).

The most cited mechanism of freeze-thaw action is the expansion forces of freezing water and adsorptive suction. Water expands by 9.1 % per unit volume when frozen (Fraser, 1959). In the confined space of a rock pore, when the expansion forces become greater than the tensile strength, the micro-structure of the rock fails (Fraser, 1959; Hale and Shakoor, 2003; Lienhart, 1993). For freezing to be effective at destroying the chemical bonds of a geologic structure, the voids filled with water must be a closed system matrix, where there is no relief of the pressure

for the expanding water (Reiche, 1950). The adsorptive suction gradient propagates water towards the freezing front by: "(1) capillary action and (2) suction due to negative pore pressure development just ahead of the freezing front" (Lienhart, 1993).

Sufficient pressure to generate rock failure is conditional upon sufficient moisture and permeability (Hale and Shakoor, 2003). If the geologic media has low permeability, water does not infiltrate, but remains within the surface pores and causes spalling (Lienhart, 1988, 1993). If there is relatively low moisture content, there is insufficient water to reach the centre of the rock causing an open system that can relieve pressure from expanding water (Hale and Shakoor, 2003).

The duration and frequency that a rock unit remains frozen changes the degree of degradation caused to the unit by freeze-thaw (Hale and Shakoor, 2003). Hydrofracturing is caused when there is a long period of freezing, which pulls unfrozen water into the center of the rock resulting in sufficient stress to induce fracturing (Hale and Shakoor, 2003). Higher frequencies of freeze-thaw cycles result in continuous stress cycles on the matrix which is typically exhibited as fatigue in the unit leading to failure (Lienhart, 1988).

2.2.3 Ionic Exchange

Ion exchange in the context of rock weathering is the result of an ionic gradient between a substance or solution and a mineral via valance. The gradient is based upon the type and abundance of minerals present in fine grained fractions of a given rock type and the ionic exchange capacity of aqueous solution. (Carroll, 1970)

There are four common ion exchange processes in the chemical weathering of a geologic unit (Carroll, 1970):

1. exchange between mineral and solution cations, when mineral grains are surrounded by a solution,
2. exchange of cations between minerals, and
3. mineral ions adsorbed through the exchange sites on the root hairs of plants.

Of these mechanisms, the first two listed are the most prevalent in geochemical weathering.

Illite, a common clay mineral observed in shale, is characteristic of having strong cation exchange capacity relative to other non-swelling clay minerals (Carroll, 1970). The ionic gradients are strongly related to both the chemical composition and structure of illite and the

solute such that monovalent ions (Na^+ and K^+) and divalent ions (Mg^{2+} and Ca^{2+}) can be exchanged according to the ease of replacement order, which is: Li < Na < H < K < Mg < Ca. Mineral surface structure further controls the rate of exchange based upon the distribution of ionic bonds, where H^+ commonly has a higher bond strength to exchange sites in minerals compared to Na^+ or K^+ (Carroll, 1970).

Two mechanisms often counter-act the effectiveness of ion exchange being: fixation and clogging. In the case of fixation, a clay mineral structure can be regenerated by the fixing or re-replacement of metal ions available in the surrounding solution into the degraded rock matrix structure. For clogging, the exchange sites on micaceous minerals (mica and illite) are blocked via iron oxide. This process is most common in clay soils and is not particularly relevant to shale formations.

2.3 Resisting and Driving Forces in Bedrock Channels

Wohl and Ikeda (1998) indicate that resistance of bedrock channel substrate dominates over the driving forces that lead to rates of channel adjustment. Channel resisting forces such as sediment cover (Sklar and Dietrich, 2004; Turowski et al., 2007) and lithological properties of substrate (Montgomery 2004; Wohl and David 2008) determine the capacity of a particle to resist erosion. Channel driving forces such as the magnitude and frequency of large discharge events (Craddock et al., 2007; Hancock et al., 2011; Lague et al., 2005; Snyder et al., 2003a; Stark, 2006; Wohl and Merritt, 2001), tectonic forcing (Amos and Burbank, 2007; Duvall et al., 2004; Harbor, 1998; Humphrey and Konrad, 2000; Lavé and Avouac, 2001; Pearce et al., 2004; Snyder et al., 2003b; Turowski et al., 2006; Whittaker et al., 2007b, 2007a), and abrasion via sediment cover (Finnegan et al., 2007; Johnson and Whipple, 2007; Shepherd, 1972; Sklar and Dietrich, 2004; Turowski, Hovius, Meng-Long et al., 2008; Turowski, Hovius, Wilson et al., 2008) promote the detachment of particles. However, weathering mechanisms alter the lithological properties of substrate to decrease the capacity of a particle to resist erosion.

Extensive research has been conducted on the complex combination of detachment mechanisms enhancing erosion and incision in bedrock channels. Depending on the geographic location of a particular channel, all or most of the detachment mechanisms listed in Table 1 are present in the evolution and metamorphosis of the channel.

Table 1 - Detachment mechanisms pertinent to bedrock channels.

Detachment mechanism	Description	References
Cavitation	Preceded by weathering, the bedrock of channel banks or high overflow areas fail as a result of gravity.	(Hancock et al., 1998; Hirvonen, 2017; Whipple, 2004; Whipple et al., 2000)
Scour	Continuous removal of particles along the wetted perimeter of a bedrock channel.	(Allen et al., 2002; Hirvonen, 2017; Massong and Montgomery, 2000; Sklar and Dietrich, 2001; Whipple et al., 2000)
Quarry, plucking, mining, or hydraulic wedging	Episodic removal of fractured or weathered clasts from the bed via hydraulic forces.	(Allen et al., 2002; Hancock et al., 1998; Hirvonen, 2017; Whipple, 2004; Whipple et al., 2000; Wohl, 1993)
Tools and cover effect	Tools are a catalyst for particle detachment through impact with the bed, whereas cover is a layer of alluvium overlying and protecting the bed from tool impact.	(Hirvonen, 2017; Turowski et al., 2007; Turowski and Rickenmann, 2009)
Abrasion (micro-, localized and wear)	Grain-by-grain detachment of particles via suspended bedload.	(Hancock et al., 1998; Whipple, 2004; Wohl, 1993)

Several researchers studying bedrock channels have frequently noted the influence of lithological properties of substrate and weathering conditions on erosion rates (Allen et al., 2002; Hancock et al., 2011; Murphy et al., 2016; Whipple, 2004; Whipple et al., 2000; Wohl and Ikeda, 1998). The inherent lithological factors contributing to the capacity to resist erosion include; rock type(s), hardness, structure, tensile strength, intact strength, porosity, permeability, heterogeneity (micro and macro), joint spacing, mesoscale fault lines and fissures, microscale crystal formation and fissures, (Jansen, 2006; Montgomery, 2004; Montgomery and Gran, 2001; Stock et al., 2005; Wohl and David, 2008), fractures (Erguler and Ulusay, 2009), and geologic

stratification (Shobe et al. 2017; Tinkler and Wohl 1998; Wohl 1999; Wohl and Ikeda 1998). Weathering through dissolution, freeze-thaw cycles (Robinson et al., 2001) and slaking (Tinkler and Wohl, 1998) reduce the tensile strength, thereby increasing the erodibility of the channel geological units (Murphy et al., 2016; Shobe et al., 2017).

Bedrock channels typically erode at slower rates, relative to their alluvial counterparts, which increases the difficulty of measuring and quantifying changes in channel morphology and rates of change as compared to alluvial channels (Wohl and Ikeda, 1998). Alluvial systems balance deposition and erosion, whereas bedrock systems are dominated by erosion, with little to no deposition (Hancock et al., 1998; Montgomery and Buffington, 1997; Tinkler and Wohl, 1998; Whipple, 2004; Wohl and Ikeda, 1998; Wohl and Merritt, 2001). Erosion is exacerbated in bedrock channels because eroded material cannot be re-constituted as in alluvial channels.

The synergistic interactions between geology, climate and hydrology govern the weathering of bedrock channel systems. Erosion mechanisms leading to the detachment of substrate comprise the majority of the research contribution related to geometric adjustments in these channels. However, a scarcity of knowledge exists regarding resisting factors, specifically the capability of channels with perimeters of bedrock to resist erosion (Turowski et al., 2009; Wohl and Ikeda, 1998).

2.4 Anthropogenic Influences on Weathering Processes

Paved surfaces are degrading the quality of water in urbanized watersheds, particularly the practice of road salting (Perera et al., 2010). Watershed landuse is often defined by the percent area of impervious cover, where < 5% cover indicates a rural watershed and > 30% cover indicates an urban watershed such that the hydrologic responses of the channel network can no longer be buffered by the riparian corridor (Kang and Marston, 2006). Impervious cover can be defined as either the much larger transportation component (e.g. roads, driveways and parking lots) or the much smaller non-transportation component (e.g. rooftops) (Kang and Marston, 2006).

Due to reduced infiltration from impervious cover, larger fractions of water are routed into overland runoff. The runoff dissolves and suspends contaminants, decreasing the quality of the water compared to the pre-urbanized condition. With urbanization there can also be significant changes to water quality present in rivers, creeks and/or channels (Henshaw and Booth, 2000).

Under the influence of land use change, bedrock channels are incising and eroding at historically high rates (Allen et al., 2002; Tinkler and Parish, 1998). Significant research has been conducted on bedrock channel erosion and degradation in response to the increase in frequency and magnitude of flow events as a result of urbanization. To date no known study has documented the influence of changes to water quality from urbanization in combination with freeze-thaw and slaking on increasing the erodibility of shale. This research program focuses on the cumulative effects of weathering mechanisms on the degradation of an urbanized shale bedrock channel environment.

3 Study Site Characteristics

Humber Creek (Figure 1), located in Toronto, Ontario was used as the study site to parameterize the laboratory experiments conducted in this study. A 1,200 m reach was selected that transitions from an upstream 300 m semi-alluvial channel with a well-connected floodplain into a 900 m incised bedrock channel that terminates at the confluence with Humber River. This bedrock channel was specifically chosen as the watershed has undergone dramatic anthropogenic changes over the past 50 years and as a result has experienced significant degradation (Hirvonen, 2017).

The landuse of the effective drainage area is classified entirely as urban (City of Toronto, 1999). There is an absence of contemporary storm water management infrastructure within the watershed leaving the stream corridor prone to frequent high magnitude short duration events (Aquafor Beech Limited, 1999). During a typical seasonal range in flows, the alluvial section is discontinuously connected to the floodplain, whereas the bedrock section is entirely disconnected from its flood plain, by as much as 10 m at the downstream limit (Figure 2) (Hirvonen, 2017).

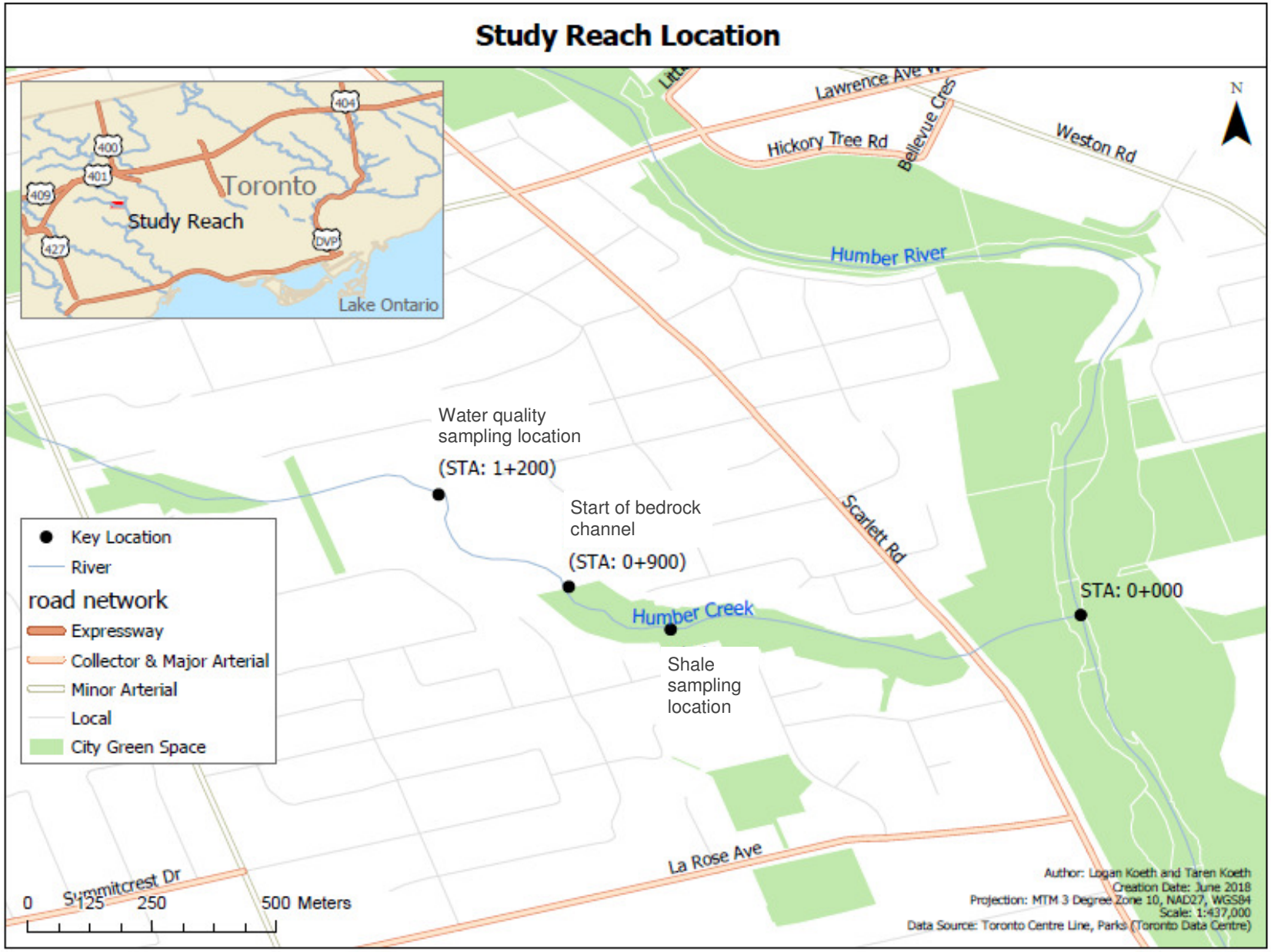

Figure 1 - Study site location and sampling/observation monitoring locations.

Figure 2 - Scale of incision at Humber Creek (Photo date: January 2017).
(Note: people in the photo are approximately 1.7 - 2 m tall)

The bedrock section of the channel has incised within the marine deposited Upper Ordovician Georgian Bay Formation (GBF), which was formed in shallow wave and storm influenced marine environments that deposited a grey-blue shale with interbedded siltstone and limestone (Figure 3) (Ontario Geological Survey, 1991; Rutka and Vos, 1993; Westgate et al., 1999). The Limestone strata are notably more resistant to erosion than the friable shale units resulting in differential weathering rates (Figure 4).

The GBF shale, as with most shale, is primarily comprised of clay minerals. Table 2 lists an estimation of the average composition of shale from around the world as well as the common chemical elements of the GBF from across southern Ontario. The average composition of shale is primarily comprised of clay minerals (~ 60%), followed by lesser quantities of quartz, carbonate and ancillary minerals. A similar compositional ratio was identified for the GBF shale based upon the mineral analysis of shale samples in Toronto, Ontario. These samples were

composed of the clay mineral, illite (35 - 60%), quartz (15 - 30%), carbonate (4 - 30%), and accessory minerals (0 - 11%) (Cao et al., 2014; Russell, 1982; Wilson et al., 2017).

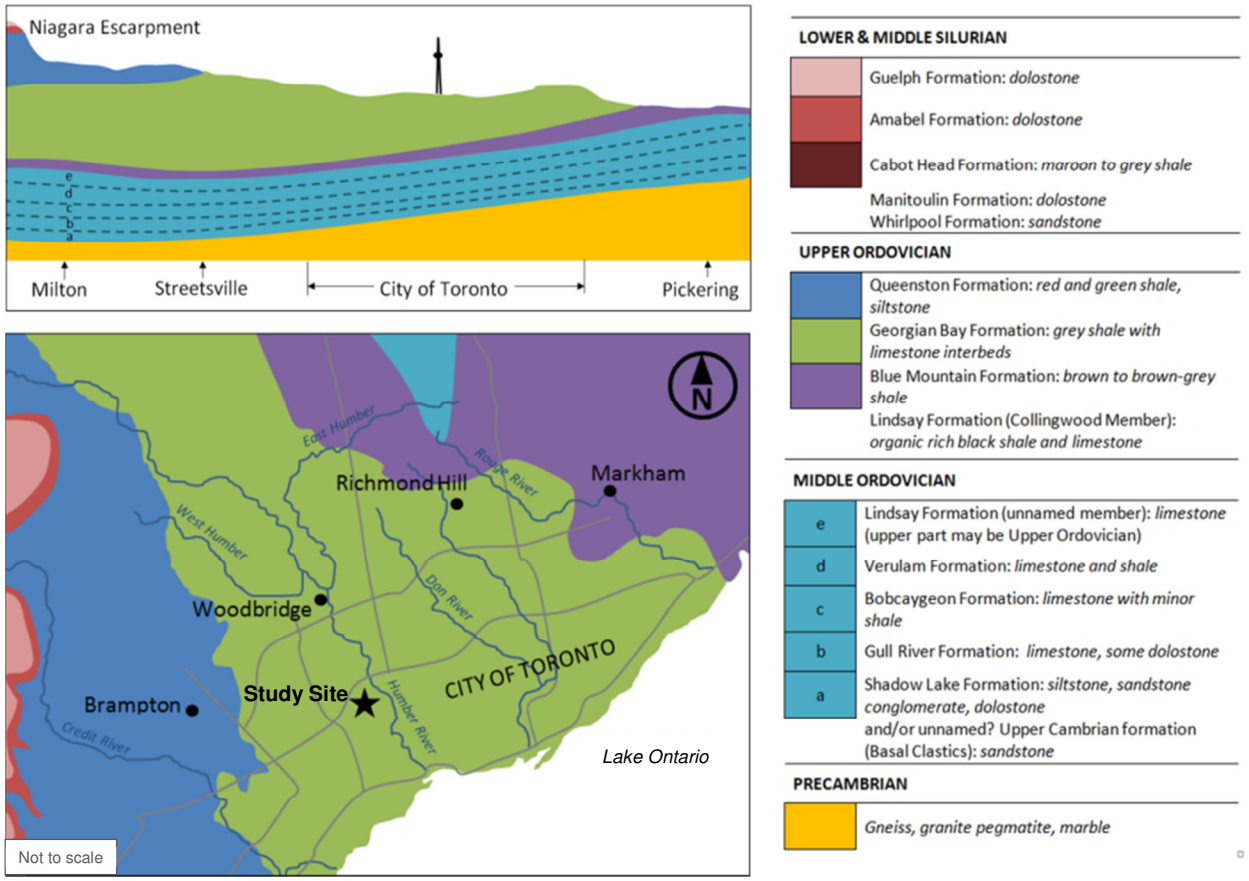

Figure 3 - Bedrock Geology of greater Toronto area and site location (black star). (adopted from (Westgate et al., 1999)**)**

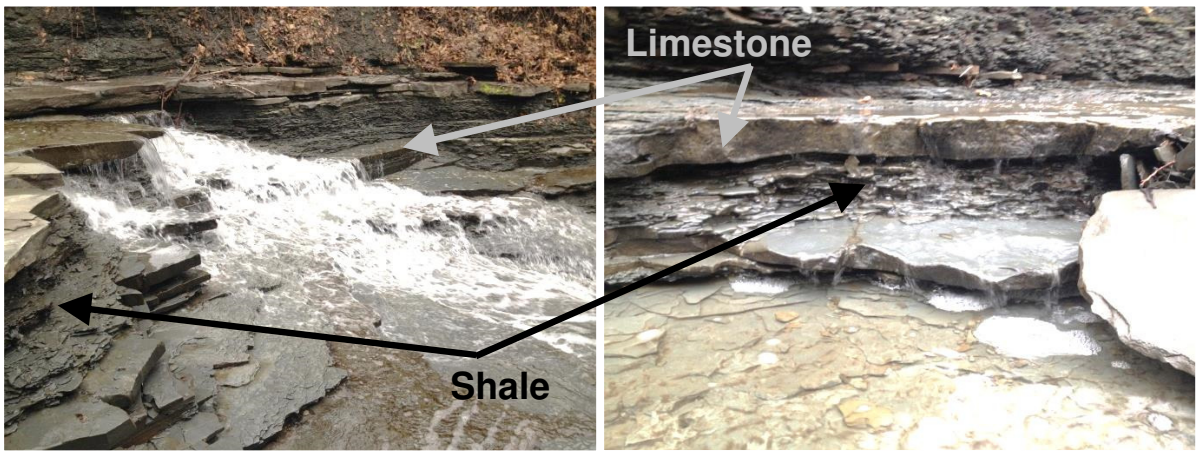

Figure 4 - Differential erosion rates between limestone and shale at Humber Creek. (photo date: January 2017).

Table 2 - GBF and average shale mineral composition from literature.

Geographic Location	Average Shale Composition	Toronto, Ontario	Toronto, Ontario	Toronto, Ontario	Kincardine, Ontario
Formation		GBF	GBF	GBF	GBF
Clay Minerals	59%*	Illite: 55-60 % Vermiculite: 3-5 %	Illite: 35-45 %	60 %*	Illite: 33 %$^{\Psi}$
Quartz [4]	20%	15-18 %	10-30 %	12-34%	26 %
Chlorite		10-15 %	0-15%		15 %$^{\mp}$
Carbonate	7%	4 %[1]	15–30 %	Calcite: 3-17% Dolomite: 0-4%	Calcite: 9 %[2] Dolomite: 10 %[3]
Other Minerals	Feldspar: 8% Iron oxide: 3% Other: 2%	Pyrite: 2-4 %	Feldspar: 0-10%	Feldspar: 0-11%	
Organic Matter	1%				
Shale Classification		Compaction shale			
Reference	(Yaalon, 1962)	(Czurda et al., 1973)	(Cao et al., 2014)	(Guillet, 1967, 1977; Russell, 1982)	(Wilson et al., 2017)

* illite predominates

$^{\Psi}$ illite: $K_{0.6}Mg_{0.25}Al_{1.8}Al_{0.5}Si_{3.5}O_{10}(OH)_2$

$^{\mp}$ Clinochlor magnesium-end member chlorite composition - $Mg_5Al_2Si_3O_{10}(OH)_8$)

[1] equal parts calcite and dolomite

[2] Calcite: $CaCO_3$

[3] Dolomite: $CaMg(CO_3)_2$

[4] Quartz: SiO_2

4 Methods

4.1 Environmental Weathering Conditions

Stage fluctuation, water temperature, surface water chemistry and air temperature of Humber Creek were monitored as potential factors contributing to the weathering of the GBF shale. Stage fluctuation was assessed to estimate the frequency and duration of slaking cycles. Water temperature and air temperature were assessed to evaluate freeze-thaw weathering cycles. Surface water chemistry was assessed to determine foreign ion contributions acting upon the shale units to enhance geochemical weathering.

Fluctuations in creek stage, water temperature, and surface water chemistry were measured at the study reach from January 6, 2017 to April 20, 2017 at monitoring station STA 1+200 previously established upstream of the bedrock section (Figure 1). Stage fluctuations and water temperatures were continuously measured with a HOBO Water Level Logger (± 0.001 mm, ± 0.44℃ from 0° to 50℃; Onset, 2018). Water chemistry samples were collected during precipitation and snow melt events to determine the concentrations of major cations (sodium, magnesium, potassium and calcium) and anions (chloride, nitrate, and sulphate). Samples were analyzed within 48 hours of collection using ion chromatography (DIONEX ICS-1100 with a DIONEX AS-DV). The calibration range for the instrument was 0 - 8 mg/L; samples beyond this range were diluted by a maximum factor of 10 to reduce dilution errors. Temperature, pH, and conductivity were measured in-situ each time water quality samples were collected.

Daily air temperature data was obtained from the Environment Canada weather station at Pearson International Airport (WMO ID: 71624, Climate ID: 6158733 and 6158731) located approximately 8.7 km from the study reach (Environment Canada, 2017b, 2017a).

4.2 Laboratory Experiment

Unweathered shale samples were unearthed from the incised creek bed of Humber Creek with a hammer and crowbar (Figure 1) in the spring and fall of 2017. To maintain saturated conditions, shale samples were sealed in 5-gallon plastic containers filled with creek water and subsequently stored at a temperature of approximately 20 ℃.

A modified version of the slake durability test (SDT) (Franklin and Chandra, 1972; Gamble, 1971; Gautam, 2012; Gurgenli, 2006; International Association for Rock Mechanics, n.d.;

Koncagul, 1998; Oakland and Lovell, 1982) and the weatherability test (WIT) (Gurgenli, 2006; Unrug, 1997; Unrug and Padgett, 2003) were employed to investigate the slaking characteristics of the shale. The slake durability test is the most common method applied to evaluate slaking mechanisms, however, it poorly represents field conditions from the abrasion induced by the method (Czerewko and Cripps, 2001; Franklin and Chandra, 1972). The weatherability test better represents field conditions; however, the method could not be replicated due to the intricate testing mechanism required. The laboratory procedure applied in this study combined features from both the SDT and WIT, and consisted of:

1. Five shale samples ranging in mass between 150 and 250 grams, with a distribution as presented in Table 3, and a combined mass of 990 to 1010 grams were randomly selected. The samples were towel dried, photographed, labelled, weighted and the three major axis (smallest, intermediate and largest) of each individual particle measured,

Table 3 - Sample selection target and tolerance mass.

Sample no.	Target mass (g)	Tolerance (g)
1	150	+ 10
2	175	± 10
3	200	± 10
4	225	± 10
5	250	- 10

2. The five samples were individually wrapped in a 2 mm (No. 10) mesh bag and placed on a tray (Figure 5 (A)). A 2 mm (No. 10) mesh bag was applied to imitate the slake durability test conditions (ASTM, 2016),
3. The tray (Figure 5(A)) was subsequently submerged into a water bath at temperature ($T_i^{H_2O}$) (Figure 5(B)) and concentration (C_i) for duration (D_{wet}) (Figure 5 (C)). Subsequently, the tray was removed from the bath and placed into an environmental chamber at air temperature (T_i^{air}) based upon the factorial design of the field observed environmental factors (Section 5.1) for duration (D_{dry}),
4. Step 3 was repeated for 12 cycles, to ensure measurable difference in mass between the trials,

5. After 12 cycles, samples were air dried for at least 24 hours, and manually sieved in the mesh bag to remove any particles less than 2 mm in size. Samples were then oven dried, weighed and re-photographed.
6. Steps 1 through 5 were repeated for every combination of air temperature, water temperature and ionic concentration, as presented by the nodes of Figure 6.

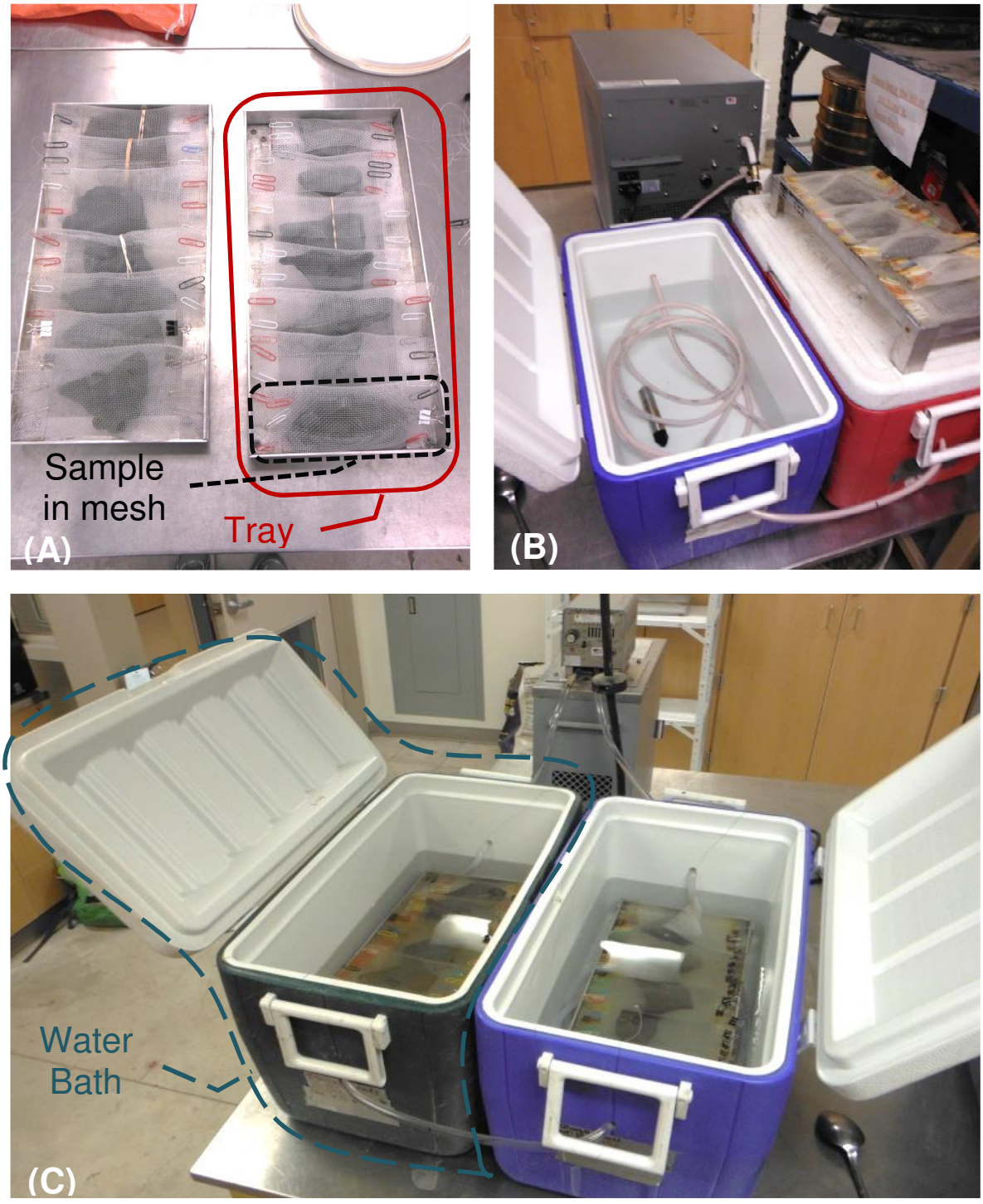

Figure 5 – Laboratory apparatus.
(A) sample tray setup of five samples, (B) water bath temperature control system, and (C) sample trays submerged in water bath.

Experiments were conducted based upon a 2^3 factorial design (Montgomery 2012; van Emden 2008), where 3 factors (i.e. the environmental parameters) were tested at two endpoints (i.e. the high and low values of field measured ranges). A factorial design was applied to optimize the experimental procedures by changing all of the parameters for each of the eight trials; as represented by the nodes of the cube in Figure 6. Water temperatures were controlled via a water bath (+/- 1℃), air temperatures were controlled via an environmental chamber (+/- 2℃), and concentrations were controlled by mixing the appropriate mass of major ions with 20 L of double deionized water.

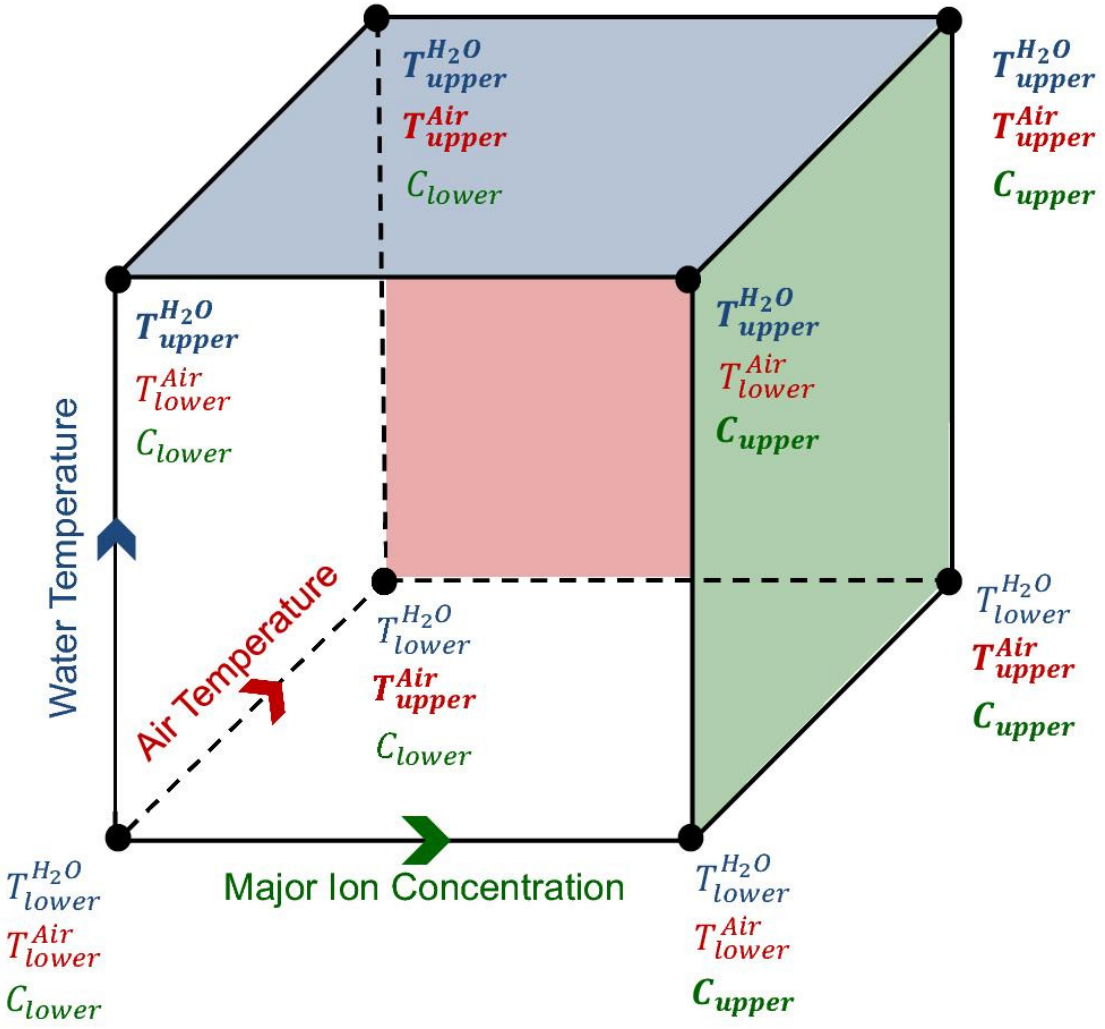

Figure 6 - Laboratory 2^3 factorial design.

The inverse slake durability index (ISDI) and weatherability index (WI) were calculated for each sample, and mean values calculated from the composite samples per trial. Both metrics

produced a value representing the percent of material lost from the original five particles per composite sample. The ISDI yielded the percent weight of dried rock lost after undergoing cycles of SDT. Therefore, the higher the ISDI value, the less durable the geologic media (Franklin and Chandra, 1972; Wood and Deo, 1975). The ISDI was calculated for the i wetting/drying cycle(s) as defined by (Franklin and Chandra, 1972):

$$ISDI_i = \left[\frac{W' - W_i}{W'}\right] \times 100 \qquad (2)$$

where, i is the serial inundation cycle (1 to 12), W' is the oven dried sample weight before cycle 1 and W_i is the oven dried sample weight after cycle(s) *i.* The Weatherability Index (WI) is the percent weight of the largest dried rock element(s) remaining after undergoing the requisite cycles of WIT as defined by (Gurgenli, 2006):

$$WI_i = \left[\frac{W' - W_i^{largest}}{W'}\right] \times 100 \qquad \mathbf{(3)}$$

where, $W_i^{largest}$ is the weight of the largest oven dried element(s) after weathering cycle(s) *i.* A high value of WI corresponds to a particle that is more susceptible to weathering.

A mass calibration curve was developed from a series of shale particles (not used in the ISDI and WI cycling procedure) to define the relationship between the saturated and oven dried mass of GBF shale samples, thereby allowing the unweathered samples to be tested without oven drying. Oven drying is often applied to standardize the before and after weight of samples to determine the change in mass without the influence of moisture. However, as noted by Gamble (1971), oven drying is a severe treatment to the sample, which could change the integrity of the bonds between minerals. Since the current experiments are dependent on maintaining the integrity of the mineral bonds, the samples were not dried prior to the weathering experiment. Therefore, the saturated mass of each sample was measured prior the weathering experiment, and a dried weight was estimated from the saturated mass using the mass calibration curve relationship defined in Figure 7.

Unweathered samples were first weighed for a saturated mass then dried as per the standard test method for laboratory determination of water (moisture) content of soil and rock by mass (ASTMD2216-10) for an oven dried mass. A total of 94 samples with wet masses ranging between 12 to 680 g were tested. A significant linear fit was observed (R^2 = 0.99) between the

oven dried mass and saturated mass of GBF shale samples was obtained (Figure 7). Raw data from the experiment is provided in Appendix A.

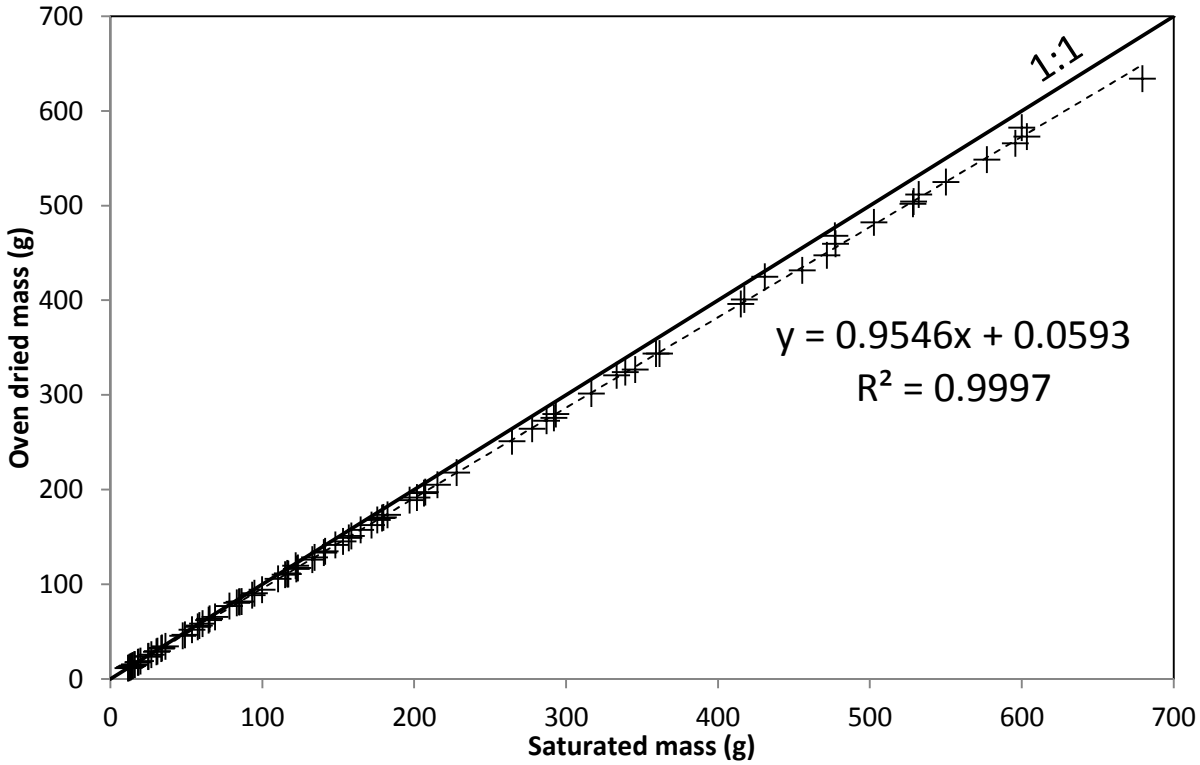

Figure 7 - Model between the saturated and oven dried mass of unweathered GBF shale.

The mean ISDI and WI metric results from each trial were analyzed with a 3-way ANOVA test using the statistical software SAS (SAS Institute Inc., 2017) to determine which parameter(s) or parameter interaction(s) had the greatest impacts upon the shale degradation. A 3-way ANOVA test was applied over a regression analysis since the analysis procedure explored endpoints. At this time, it was not the objective of the study to develop a model.

4.3 Geochemical Model

PHREEQC (Parkhurst and Appelo, 2013) was applied to determine the ionic exchange reactions between the GBF shale and major ions in solution. The simulation was applied using the Debye-Hückel solution as a batch reaction to replicate the laboratory experiment. PHREEQC simulates the ionic exchange reactions based upon a given initial solution and a defined mineral phase. Input values for the solution included pH, temperature and concentration of the initial solution, which were based upon the field measured as well as the

laboratory experiment values. Illite was selected as the mineral phase because it was representative of the units tested from the study site (Table 4). The reaction of 10 moles of illite equilibrated in 1 Kilogram of solution with a fixed pH of 7.

Four water quality solutions were modelled using PHREEQC to evaluate the geochemical conditions, being:

1. LAB: LOWER – representing the low boundary condition of the laboratory experiment with a concentration of C_{lower} (Table 5),
2. LAB: UPPER – representing the high boundary condition of the laboratory experiment with a concentration of C_{upper} (Table 5),
3. FIELD: LOWER – representing the low ionic strength concentration range measured from the water quality results of Humber Creek (Table 5), and
4. FIELD: UPPER – representing the high ionic strength concentration range measured from the water quality results of Humber Creek (Table 5).

Table 4 - Theoretical composition of phases employed in the ionic exchange model.

Phases	Formula
Illite	$K_{0.6}Mg_{0.25}Al_{2.3}Si_{3.5}O_{10}(OH)_2$
Pure Water	H_2O

5 Results & Analysis

5.1 Environmental Weathering Conditions

Field data was analyzed to determine the maximum and minimum values, referred to as the factorial design bounds (FDB), for each of the parameters measured. From discharge stage data, the duration of wetting and drying periods for the slaking cycles were calculated based upon the average time the water levels (solid line, Figure 8) were above (considered wetting) or below (considered drying) the average flow elevation (dotted line, 132.075 masl, Figure 8). An elevation of 132.075 masl was arbitrarily estimated based upon the lowest stage elevation values in the hydrograph as well as the flow ranges provided by Hirvonen (2017). Water temperature values used in the factorial design were based upon the highest and lowest field recorded temperatures over the sampling period. Ten years of air temperature data were analyzed to establish long term average seasonal temperature statistics. The factorial design bounds were adjusted from the values measured in the field to accommodate experimental equipment and study logistics (Table 5).

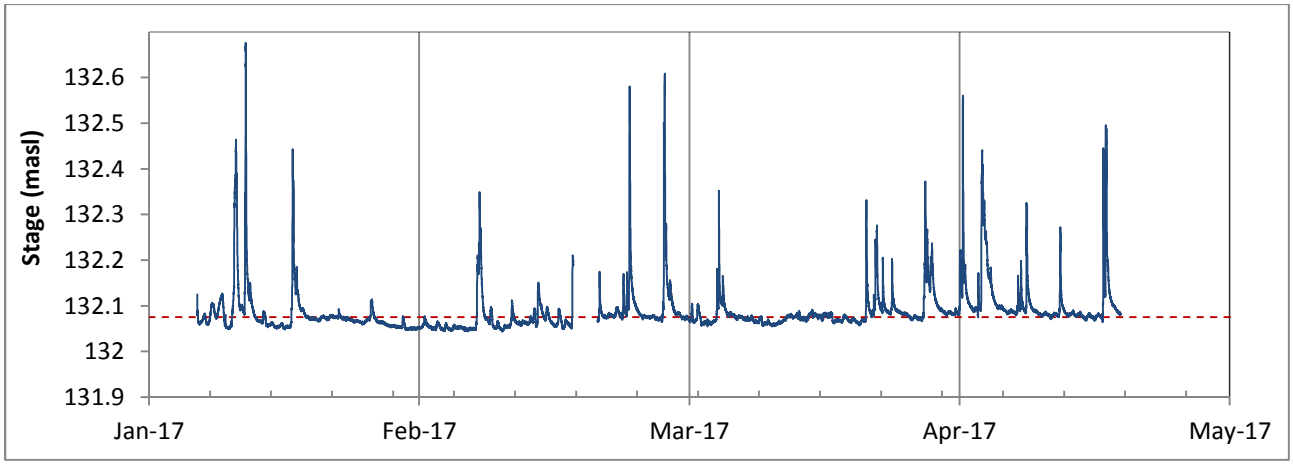

Figure 8 - Stage fluctuations at Humber Creek for the period of record.

Table 5 - Field observed parameter limits on factorial design bounds (FDB).

		Units	Dry	Wet
Slaking Cycle	Calculated	hours	14.0	8.0
	FDB	hours	$D_{dry} = 8.0$[a]	$D_{wet} = 4.0$[a]
		Units	**Upper Bound**	**Lower Bound**
Water Temperature	Measured	℃	17.0	- 0.8
	FDB	℃	$T_{upper}^{H_2O} = 20.0$	$T_{lower}^{H_2O} = 4.0$[b]
Air Temperature	Measured	℃	37.9	- 26.3
	FDB	℃	$T_{upper}^{air} = 20.0$	$T_{lower}^{air} = -20.0$
Ion concentration	Measured	mg/L Na	4,650.3	82.5
	Measured	mg/L Mg	43.2	0.0
	Measured	mg/L K	17.5	4.1
	Measured	mg/L Ca	214.9	11.6
	Measured	mg/L Cl	9,843.4	124.3
	Measured	mg/L Nitrate	8.7	1.4
	Measured	mg/L Sulfate	118.5	15.4
	FDB	mg/L NaCl	$C_{upper} = 5{,}000.0$	$C_{lower} = 0.0$

[a] Applied to duration of wetting and drying periods for slaking cycles (see procedure in section 4.2)
[b] Adjusted to measure impact of water at the densest state on the experiment

From the field sampled water chemistry results it was determined that Na and Cl concentrations were more than 20 times greater than the other ion concentrations present in the surface water samples. Therefore, Na and Cl were deemed to be the ions with the greatest potential impact on the geochemistry weathering processes and were the focus of the experimental design. Since, sodium and chloride dissociate in a 1:1 ratio, the upper water chemistry bound for the factorial design was delineated to 5,000 mg/L NaCl, based upon Na which is the limiting factor for the field observed upper bound (4,650.3 mg/L Na). The lower water chemistry bound, 0 mg/L NaCl, was selected for the factorial design as a control. Analytical results from the field sampling campaign are included in Appendix A.

5.2 Laboratory Experiments

The three-way ANOVA tests revealed that degradation was significantly correlated to air temperature, NaCl concentration and the interaction effects of the two conditions for both WI and ISDI (Table 6). Statistical analyses were conducted to compare the main effects of air temperature, water temperature and NaCl concentrations on the rates of shale degradation and the interaction effect between:

- air temperature and water temperature,
- air temperature and NaCl concentrations,
- water temperature and NaCl concentrations and,
- air temperature, water temperature and NaCl concentrations.

Each factor was investigated for the two bounding limits based upon field observations (Table 5). Experiments were organized according to the nodes of the factorial design cube (Figure 9). Raw data from the weathering experiments can be found in Appendix A, with the statistical analysis outputs from SAS in Appendix B.

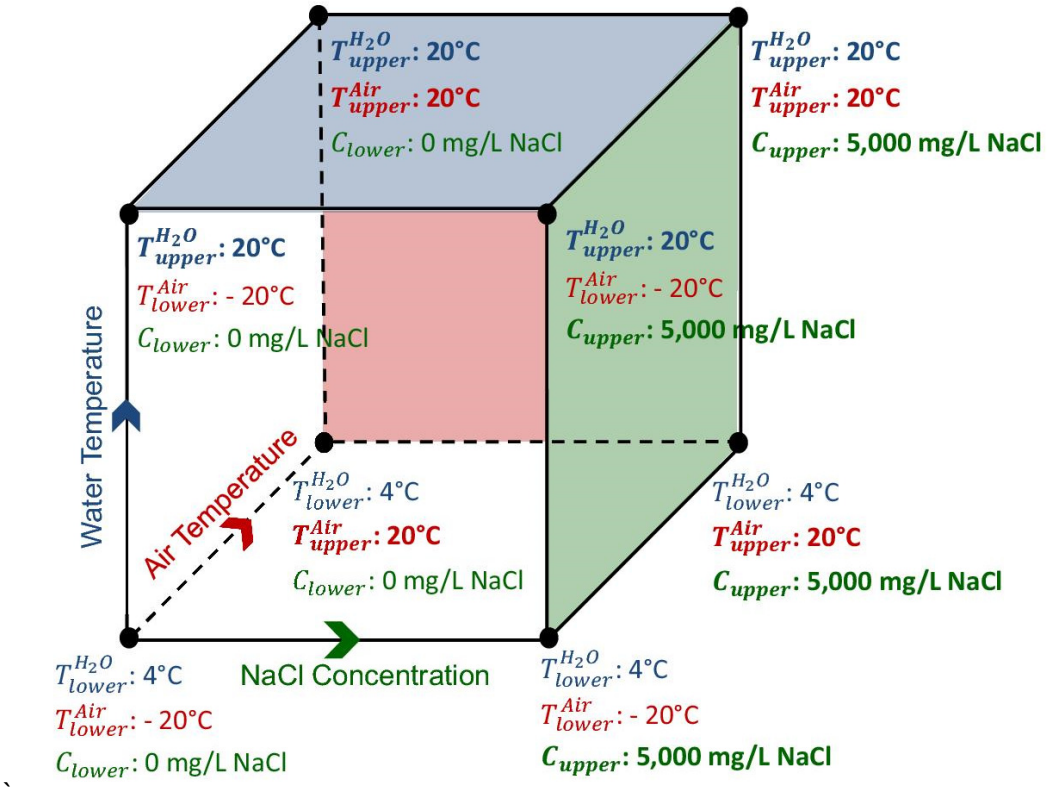

Figure 9 - 2^3 Factorial design plan with values.

Table 6 - ANOVA results for WI and ISDI analysis.

Source	Weatherability Index (WI)				Inverse Slake Durability Index (ISDI)			
	Degrees of Freedom	Mean Square	Variance Ratio (F)	P-value	Degrees of Freedom	Mean Square	Variance Ratio (F)	P-value
T_i^{air}	1	1074.5	42.9	<0.0001	1	115.7	29.2	<0.0001
$T_i^{H_2O}$	1	86.0	3.4	0.0732	1	6.5	1.6	0.2098
C_i	1	284.9	11.4	0.0020	1	59.9	15.1	0.0005
$T_i^{air} * T_i^{H_2O}$	1	58.8	2.3	0.1354	1	5.8	1.5	0.2336
$T_i^{air} * C_i$	1	209.2	8.3	0.0069	1	54.1	13.6	0.0008
$T_i^{H_2O} * C_i$	1	2.0	0.1	0.7783	1	0.2	0.1	0.8271
$T_i^{air} * T_i^{H_2O} * C_i$	1	2.8	0.1	0.7415	1	1.1	0.3	0.5991

T_i^{air} = Air Temperature

$T_i^{H_2O}$ = Water Temperature

C_i = NaCl Concentration

The main effects arising from the experiments identified air temperature and NaCl concentrations, and the interaction effect between the aforementioned factors were statistically of greatest significance ($p \leq 0.01$ for both) for both the WI and ISDI tests (Table 6).

For WI, air temperature yielded a variance ratio (F ratio) of $F(1,32) = 42.9$, $p=<0.0001$, indicating a significant difference in coherent sample mass for trials at 20 ℃ (Mean (*M)* = 0.7, Standard deviation (*SD)* = 1.3) and - 20 ℃ (*M* = 11.1, *SD* = 15.3). NaCl concentrations yielded an F ratio of $F(1,32) = 11.4$, $p=0.0020$, indicating a significant difference for trials at 5,000 mg/L NaCl (*M* = 8.6, *SD* = 17.4) and 0 mg/L NaCl (*M* = 3.2, *SD* = 9.2). The interaction effect was also significant, $F(1,32) = 8.4$, $p = 0.0069$.

The main effects arising from the three-way ANOVA tests for WI, indicated that, in all circumstances, a concentration of 5,000 mg/L NaCl or an air temperature of - 20℃ will result in the greatest percentage loss of a coherent sample mass. A further investigation of the interaction effects revealed enhanced synergistic results (Table 7, Figure 10), which showed that the greatest loss of sample mass (16; bold in Table 7) occurred when the NaCl concentration were the highest and air temperatures the lowest.

Table 7 - WI interaction analysis for air temperature and NaCl concentration. (Note: a higher value indicates a higher reduction in mass from weathering trial).

		NaCl Concentration		
		UPPER (5,000 mg/L NaCl)	LOWER (0 mg/L NaCl)	Temperature Mean
Air Temperature	UPPER (20 °C)	1.1	0.3	0.7
	LOWER (- 20 °C)	**16.0**	6.1	11.1
	Concentration Mean	8.6	3.2	

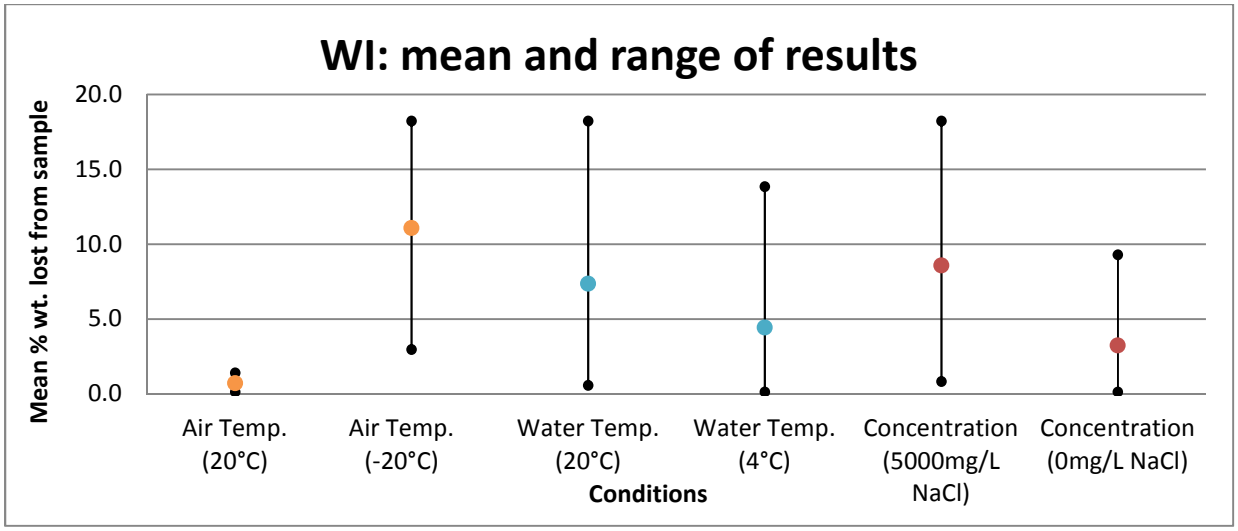

Figure 10 - WI box-and-whisker interaction results.

For the ISDI analysis, air temperature yielded an F ratio of F(1,32) = 29.2, p=<0.0001, indicating a significant difference in sample mass for trials with air temperature of 20 ℃ (*M* = 0.0, *SD* = 0.3) and - 20 ℃ (*M* = 3.4, *SD* = 6.3). NaCl concentration yielded an F ratio of F(1,32) = 15.1, p=0.0005, indicating a significant difference for trials with 5,000 mg/L NaCl (*M* = 3.0, *SD* = 6.8) and 0 mg/L NaCl (*M* = 0.5, *SD* = 1.7). The synergistic interaction effect between air temperature and NaCl concentration was also significant, F(1,32) = 13.6, p = 0.0008.

The principle effects from the three-way ANOVA tests for ISDI, indicated that, in all circumstances, a high concentration of NaCl (5,000 mg/L) or an air temperature of - 20℃ resulted in the greatest percentage loss of coherent sample masses. Similar to the WI analysis the greatest loss of sample mass (5.8 %; bold in Table 8) was measured when the NaCl concentration was high and air temperature was low (Table 8, Figure 11). A binary evaluation in the factorial of the NaCl concentration or a binary reduction in air temperature did not experience an equivalent effect to the combined synergistic interaction.

Table 8 - ISDI interaction analysis for air temperature and NaCl concentration. (Note: a higher value indicates a higher reduction in mass from weathering trails).

		NaCl Concentration		
		UPPER (5,000 mg/L NaCl)	LOWER (0 mg/L NaCl)	Temperature Mean
Air Temperature	UPPER (20 °C)	0.1	0.0	0.0
	LOWER (- 20 °C)	**5.8**	1.0	3.4
	Concentration Mean	3.0	0.5	

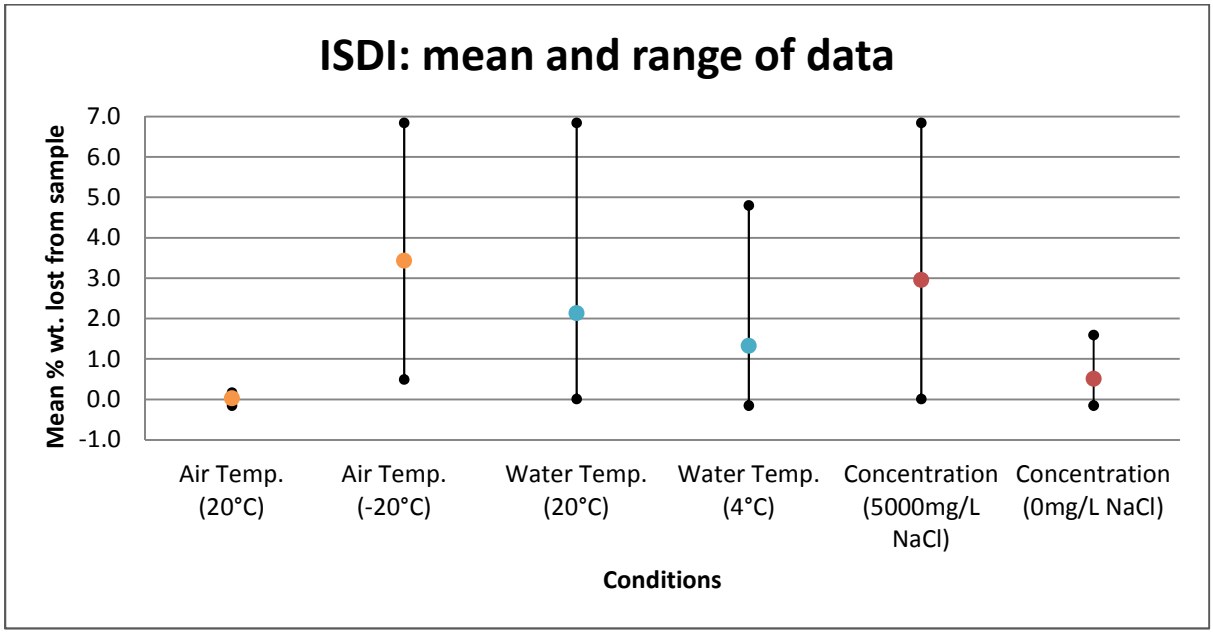

Figure 11 – ISDI box-and-whisker interaction results.

The control condition exclusively representing slaking (i.e. 20 ℃ water temperature, 20 ℃ air temperature and 0 mg/L NaCl) consistently resulted in the lowest mass loss of coherent shale sample. With the exception of the control trial, all other trials exposed the samples to additional weathering mechanisms during slaking cycles. When a negative air temperature (- 20 ℃) was applied, this represented freezing and thawing conditions. When a high NaCl (5,000 mg/L) concentration was applied, this represented the condition when runoff from rain and snowmelt events collected NaCl from winter road salting, which had the potential to encourage chemical weathering such as cation exchange.

5.3 Geochemical Model

The modelling results for all four solutions were inconclusive. The results did not indicate an ionic exchange mechanism between the mineral illite and the input solutions that could be attributed to the shale degradation (Table 9).

An increase in Na, Cl, K, Mg, Al and Si ions in the modelling output solution relative to the input solution were present for both LAB: LOWER and UPPER trials. Increases in concentrations of K, Mg, Al, and Si were expected due to the presence of these elements in the illite mineral structure (Figure 12, Table 4). However, increases in concentrations of Na and Cl were not expected in the output solution, since no source of the ions were present within the batch experiment. As expected, the concentration results of the Ca, Fe and Fe^{+3} remained unchanged from the input solution. The greatest loss of illite mass occurred when the mineral was exposed to the LAB: LOWER numerical experiment.

Solutions for the FIELD: LOWER trial resulted in an increase in Na, Cl, Ca, Fe^{+3}, Mg, Al, Si and Fe ions relative to the input solution, whereas the output solution for the FIELD: UPPER trial resulted in the increase of Fe^{+3}, Al, Si and Fe ions relative to the input solution (Table 9). Similar to the results of the LAB: LOWER and UPPER simulations, increases in ionic concentrations of Mg, Al and Si were expected due to the presence of these elements in the illite mineral structure (Figure 12, Table 4). Increases in the ionic concentration of Na, Cl, Ca, Fe^{+3} and Fe ions were again not expected in the output solution, because no source of the ions were present within the batch experiment. The ionic concentrations for Na, Cl, Ca and Mg in the FIELD: UPPER trial did not increase as in the FIELD: LOWER output, indicating that the FIELD: UPPER trial achieved equilibrium between the mineral and the solution for these ions.

Table 9 - PHREEQC equilibrium solution results.

Solution Type	Solution Stage	Total ions in Solution (moles/kg-water)									Illite Stage	Moles of Illite
		Na	Cl	K	Ca	Fe^{+3}	Mg	Al	Si	Fe		
LAB: LOWER	Input	8.6E-04	8.6E-04	0	0	0	0	0	0	0	Initial	10
	Output	6.2E-03	6.2E-03	4.9E-14	0	0	6.6E-10	3.8E-06	2.9E-03	0	Delta	-8.2E-04
LAB: UPPER	Input	8.6E-02	8.6E-02	0	0	0	0	0	0	0	Initial	10
	Output	8.6E-02	8.6E-02	6.9E-13	0	0	1.4E-08	5.2E-05	3.1E-04	0	Delta	-8.7E-05
FIELD: LOWER	Input	3.6E-03	3.5E-03	1.1E-04	2.9E-04	3.6E-07	0	0	0	3.6E-07	Initial	10
	Output	3.7E-03	3.6E-03	1.1E-04	3.0E-04	7.7E-07	7.2E-10	5.2E-06	5.8E-05	7.7E-07	Delta	-1.7E-05
FIELD: UPPER	Input	2.0E-01	2.8E-01	4.5E-04	5.4E-03	2.1E-05	1.8E-03	0	0	2.1E-05	Initial	10
	Output	2.0E-01	2.8E-01	4.5E-04	5.4E-03	2.2E-05	1.8E-03	7.8E-06	1.5E-05	2.2E-05	Delta	-4.2E-06

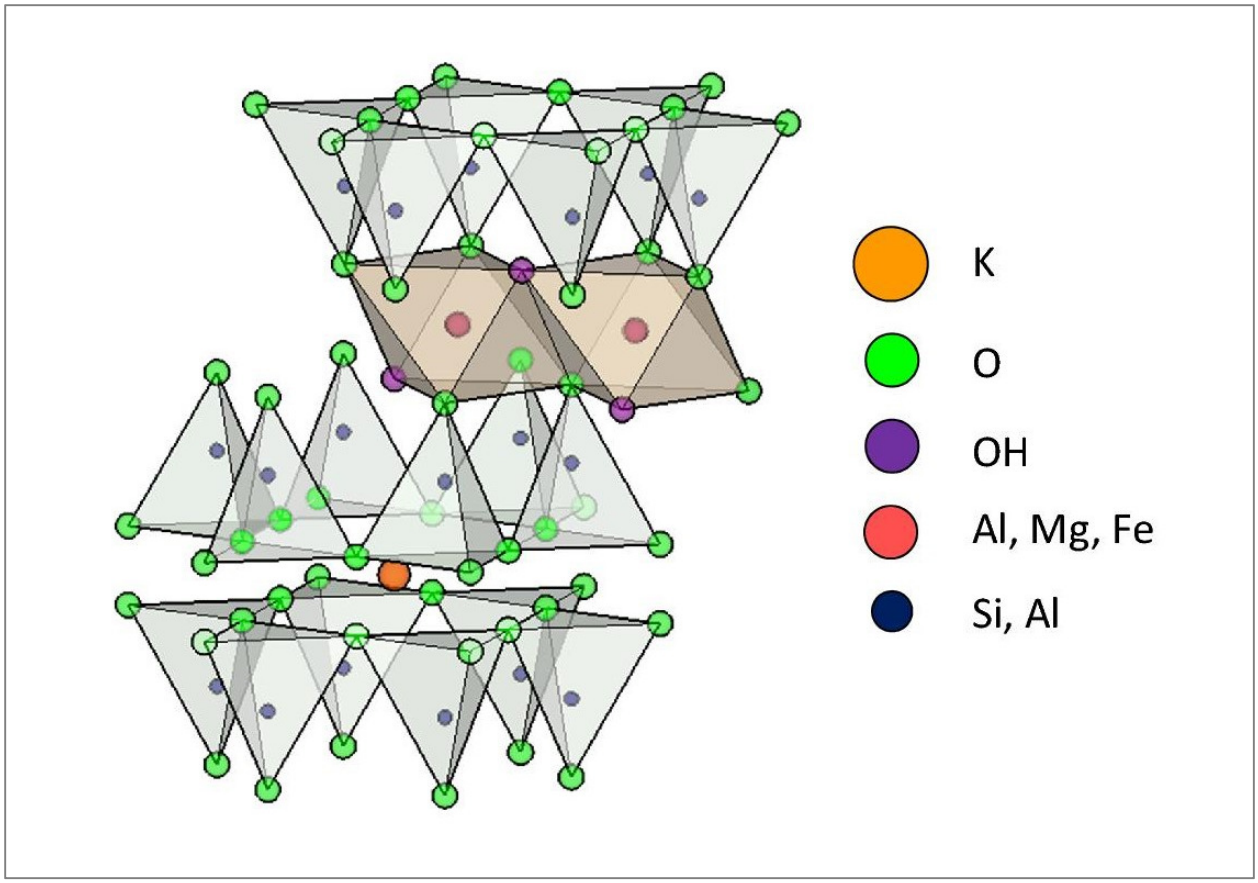

Figure 12 - Ideal structure of Illite (modified by: Serge Renaud, from: (Grim, 1962)).

The GBF shale investigated in this research is primarily composed of the clay mineral, illite, a 2:1 layer silicate mineral with two terahedra layers and an interlayer K^+ cation (Figure 12). Illite is a weathered derivative of mica, which has an imperfect structure that improves the ion exchange capacity of the mineral (Carroll, 1970). In mica, K^+ strongly bonds the layers of the structure, however, in illite some of the K^+ is removed and as a result the structure exposes more fragments, creating more surfaces for ion exchange. Based on the laboratory results and literature, it is hypothesized that during the appropriate environmental conditions interlayer K^+ exchanges with Na^+ ions abundant in the solution (Carroll, 1970; Scott and Smith, 1966; Tournassat et al., 2007)

6 Discussion

The unifying objective of this research was to identify the weathering processes contributing to the degradation of an urban bedrock channel. The environmental parameters measured (stage, water temperature and air temperature) were within the typical ranges for the climate of southern Ontario. Measurements of major cations and anions indicated high concentrations of Na^+ and Cl^- (Section 5.1), which were comparable to the range of chloride concentrations (1390 to 4310 mg/L) measured in Toronto-area creeks (Environment Canada and Health Canada, 2001). Road salting during winter months is a probable explanation for the elevated NaCl concentrations. The water temperature, stage and water chemistry data collected in this study are not representative of an entire year, since the data was collected over a period of four months from January to April.

Prior studies have noted the importance of slaking as a primary weathering agent in shale bedrock channels. Contrary to previous observations by Tinkler and Parish (1998) and Mugridge and Young (1983) who considered slaking as the primary weathering mechanism in shale bedrock channels, this study suggests that slaking may not be the exclusive weathering agent relative to the other mechanisms investigated (Section 5.2). This discrepancy could be attributed to the direct measurements taken in the laboratory on shale samples, without oven drying prior to weathering trials as in Erguler and Ulusay (2009). As well as the lack of field based shale measurements in this study, compared to Mugridge and Young (1983).

Shale samples were exposed to a limited number of weathering cycles, which may not have expressed the full impact of slaking on the samples. When compared to natural conditions, slaking may occur all year long whereas impact from NaCl concentrations and freeze-thaw are limited to winter months, when NaCl concentrations are elevated from road salting practices (Environment Canada and Health Canada, 2001; Perera et al., 2010). Therefore, annual slaking may have a larger timespan to degrade a given geologic unit.

Current findings support the contention that environmental conditions dictate the weathering processes present at any given time or location within a bedrock channel (Carroll, 1970). Freeze-thaw weathering mechanisms have also been documented as a damaging physical weathering mechanism in the breakdown of all rock types, not just shales (Erguler and Ulusay, 2009; Fraser, 1959). This emphasizes that slaking may not predominate weathering mechanisms at all times of the year. The standard conceptual model in which slaking is the

primary agent increasing erodibility of shale bedrock channels (Erguler and Shakoor 2009; Mugridge and Young 1983; Tinkler and Parish 1998) may need to factor in regional and/or climatic conditions and anthropogenic inputs, particularly salt, as additional agents of erosion in some geologic settings.

This study demonstrated that high concentrations of NaCl (5,000 mg/L) in association with winter air temperatures (- 20 ℃) commensurate with the seasonal applications of road salt, in combination with slaking cycles, resulted in the greatest loss of coherent shale sample mass (Section 5.2). Findings here corroborate observations made by Carroll (1970), Scott and Smith (1966) and Tournassat et al. (2007), who suggest that the interlayer K^+ exchanges with Na^+ under the appropriate environmental conditions may exacerbate the rates of particle dislodgement. In addition, these findings further provide causality to previous observations that bedrock channel geometries in some geologic settings are adjusting at historically high rates ((Allen et al., 2002; Allen and Narramore, 1985; Booth, 1990; Tinkler and Parish, 1998)). Nevertheless, this result has not previously been described in shale bedrock channels. The results observed here are contrary to Tinkler and Parish (1998) who examined another bedrock stream channel in the same geologic setting where they speculated that chemical weathering nominally contributed towards channel degradation on the bed material transport load – although in their case chemical analyses were not investigated but postulated. The reason for this discrepancy is not clear; however it may be attributed to the focus of this study on anthropogenic influences on water quality as it relates to geochemical weathering.

The current results should be interpreted with caution as the laboratory experiments were conducted in batch reactions, where the NaCl concentration were approximately constant. Whereas in the field condition, a concentration of 5,000 mg/L NaCl will occur over a shorter time period than six days (as applied in this experiment over 12 wetting/drying cycles). In addition, two levels (high and low bounds) for each parameter were investigated and a relationship between and beyond the high and low bound for each of the three parameter factorial design should not be extrapolated.

Based upon the findings of this study, it can be suggested that changes in water quality due to anthropogenic influences have the potential to increase rates of weathering in shale bedrock channels. A compelling implication is that salt applied to roads for de-icing in the winter, is increasing the erodibility of illite dominant shale bedrock channels. Three management implications of these findings are:

1. storm water management ponds installed adjacent to channels channel may prolong the residence time of road salt solutions in contact with the substrate, thereby increasing the erodibility of select shales. In addition, low impact development techniques may increase the impact of NaCl on the channel by reducing the volume of water and subsequently increasing the salt concentration,
2. managers should adjust de-icing practices to minimize the mass loss through weathering along a shale bedrock channel from the synergistic impact of negative air temperature and high NaCl concentrations. This implication corresponds with Section 64 of the *Canadian Environmental Protection Act, 1999* which has designated inorganic chloride salts as a "toxic" substance (CEPA, 1999), and
3. managers should prescribe techniques for remediation based upon a larger suite of mechanism occurring at the basin-scale of a specific bedrock channel, rather than the symptoms identified at the reach-scale (Rosgen, 1997; Wohl et al., 2015).

Based upon the findings of this study, further research is proposed which includes:

1. investigating changes in water quality and channel weathering in a field based study, with the additional influence of flowing conditions, and
2. expanding the study of chemical weathering to other shale formations as well as aqueous phase chemistry, such as changes in chemistry due to de-icing applications other than NaCl.

This study also hypothesized that the interlayer K^+ cations in the illite mineralogical structure exchanged with the abundant Na^+ cations in solution; this was investigated using a geochemical model. Contrary to expectations, the modelling results were inconclusive and did not identify a significant ion exchange between illite and the NaCl solutions (Section 5.3). In particular the geochemical modelling results were questionable because of the unexplained increase on Na^+ and Cl^- in the LAB: UPPER and LAB: LOWER solutions. The model results also indicated that the greatest loss of illite mass occurred when the mineral was exposed to the LAB: LOWER condition, which directly conflicts with the results of the laboratory experiment as described above. The model did not consider the effect of ambient temperature on the reaction. The results were also in the absence of any physical weathering mechanism therefore, the results support the observation that shale weathering in the absence of physical weathering is a slow process.

7 Conclusion

The unifying objective of this study was to investigate the weathering agents contributing to enhanced degradation of a shale bedrock channel in a temperate environment. This study indicates that freeze-thaw and cation exchange in combination with slaking had the greatest impact on shale weathering relative to slaking exclusively.

The findings of this research suggest that changes to water quality from road salting (the expected source of seasonal increases in NaCl) are contributing to accelerated rates of erosion in shale bedrock channels. Despite its exploratory nature, this study offers insights into the possible land use management modifications required to attenuate rates of channel degradation and highlights the importance of understanding channel mechanism prior to prescribing techniques for restoration.

It was beyond the scope of this study to quantify erosion rates due to increased erodibility from physical and chemical weathering as a result of anthropogenic influences. In addition, these results may not be applicable to weathering mechanism outside the temperate climate of southern Ontario.

Bibliography

Allen, P., Arnold, J. ., and Skipwith, W. (2002). Erodibility of Urban Bedrock and Alluvial Channels, North Texas. *Journal Of The American Water Resources Association*, *38*(5), 1477–1492. https://doi.org/10.1111/j.1752-1688.2002.tb04360.x

Allen, P., and Narramore, R. (1985). Bedrock controls on stream channel enlargement with urbanization, North Central Texas. *American Water Resource Association: Water Resource Bulletin*, *21*(6), 1037–1048.

American Geological Institute. (1976). *Dictionary of Geologic Terms*. New York, NY: Dolphin Books, Doubleday and Company, Inc.

Amos, C. B., and Burbank, D. W. (2007). Channel width response to differential uplift. *Journal of Geophysical Research: Earth Surface*, *112*(2), 1–11. https://doi.org/10.1029/2006JF000672

Aquafor Beech Limited. (1999). *Humber Creek Subwatershed Restoration Plan - Final Report*.

ASTM. (2016). Standard Test Method for Slake Durability of Shales and Similar Weak Rocks (D4644-16). *ASTM Standard Guide*. https://doi.org/10.1520/D4644-08.2

Booth, D. B. (1990). Stream-channel incision following drainage-basin urbanization. *American Water Resource Association: Water Resource Bulletin*, *26*(3), 407–417.

Cao, L. F., Peaker, S. . M., Ahmad, S., and Sirati, A. (2014). Engineering characteristic of Georgian Bay Formation in Toronto. *Geo Regina*.

Carroll, D. (1970). *Rock Weathering*. New York, NY.

CEPA. Canadian Environmental Protection Act , 1999 (1999). Canada. Retrieved from https://laws-lois.justice.gc.ca/PDF/C-15.31.pdf

City of Toronto. (1999). *Humber Creek Subwatershed Restoration Plan*. Toronto, Ontario.

Craddock, W. H., Burbank, D. W., Bookhagen, B., and Gabet, E. J. (2007). Bedrock channel geometry along an orographic rainfall gradient in the upper Marsyandi River valley in central Nepal. *Journal of Geophysical Research: Earth Surface*, *112*(3), 1–17. https://doi.org/10.1029/2006JF000589

Czerewko, M. A., and Cripps, J. C. (2001). Assessing the durability of mudrocks using the modified jar slake index test. *Quarterly Journal of Engineering Geology and Hydrogeology*, *34*, 153–163.

Czurda, K., Winder, C. G., and Quigley, R. M. (1973). Sedimentology, mineral facies, and petrofabric of the Meaford-Dundas Formation (Upper Ordovician) in Southern Ontario. *Canad. J. Earth Sci.*, *10/12*, 1790–1804.

Duvall, A., Kirby, E., and Burbank, D. (2004). Tectonic and lithologic controls on bedrock channel profiles and processes in coastal California. *Journal of Geophysical Research*, *109*, 1–18. https://doi.org/10.1029/2003JF000086

Environment Canada. (2017a). Toronto Intl A Ontario - Daily Weather Data Report. Retrieved

December 28, 2017, from http://climate.weather.gc.ca/climate_data/daily_data_e.html?hlyRange=2013-06-11%7C2017-01-10&dlyRange=2013-06-13%7C2017-01-10&mlyRange=%7C&StationID=51459&Prov=ON&urlExtension=_e.html&searchType=stnProx&optLimit=specDate&StartYear=1840&EndYear=2017&selRow

Environment Canada. (2017b). Toronto Lester B. Pearson Int'l A Ontario - Daily Weather Data Report. Retrieved December 28, 2017, from http://climate.weather.gc.ca/climate_data/daily_data_e.html?hlyRange=1953-01-01%7C2013-06-13&dlyRange=1937-11-01%7C2013-06-13&mlyRange=1937-01-01%7C2013-06-01&StationID=5097&Prov=ON&urlExtension=_e.html&searchType=stnProx&optLimit=specDate&Month=6&Day=10&

Environment Canada, and Health Canada. (2001). *Priority Substance List Assessment Report - Road Salts*. Retrieved from http://ww1.prweb.com/prfiles/2008/02/07/370423/EnvironmentCanadareport.pdf

Erguler, Z. A., and Shakoor, A. (2009). Relative contribution of various climatic processes in disintegration of clay-bearing rocks. *Engineering Geology*, *108*(1–2), 36–42. https://doi.org/10.1016/j.enggeo.2009.06.002

Erguler, Z. A., and Ulusay, R. (2009). Water-induced variations in mechanical properties of clay-bearing rocks. *International Journal of Rock Mechanics and Mining Sciences*, *46*(2), 355–370. https://doi.org/10.1016/j.ijrmms.2008.07.002

Finnegan, N. J., Sklar, L. S., and Fuller, T. K. (2007). Interplay of sediment supply, river incision, and channel morphology revealed by the transient evolution of an experimental bedrock channel. *Journal of Geophysical Research: Earth Surface*, *112*(3), 1–17. https://doi.org/10.1029/2006JF000569

Franklin, J. A., and Chandra, R. (1972). The slake-durability test. *International Journal of Rock Mechanics and Mining Sciences And*, *9*(3), 325–328. https://doi.org/10.1016/0148-9062(72)90001-0

Fraser, J. K. (1959). Freeze-thaw frequencies and mechanical weathering in Canada. *Arctic*, *12*(1), 40–53.

Gamble, J. (1971). *Durability-Pasticity Classification of Shales and Other Agrillaceous Rocks*. Ph.D., University of Illinois.

Gautam, T. P. (2012). *An Investigation of Disintegraion Behavior of Mudrocks based on Laboratory and Field Tests*. Ph.D., Kent State University. https://doi.org/10.1016/j.aqpro.2013.07.003

Gautam, T. P., and Shakoor, A. (2013). Slaking behavior of clay-bearing rocks during a one-year exposure to natural climatic conditions. *Engineering Geology*, *166*, 17–25. https://doi.org/10.1016/j.enggeo.2013.08.003

Gautam, T. P., and Shakoor, A. (2015). An Experimental Study for Evaluating the Disintegration Behavior of Clay-Bearing Rocks under Field Conditions. *Engineering Geology for Society and Territory - Volume 5: Urban Geology, Sustainable Planning and Landscape Exploitation*, *5*, 1285–1288. https://doi.org/10.1007/978-3-319-09048-1

Grim, R. E. (1962). *Applied Clay Mineralogy*. New York, NY: McGraw-Hill.

Guillet, J. (1967). *The clay products industry of Ontario*. Toronto, Ontario.

Guillet, J. (1977). Clay and shale deposits of Ontario. Toronto, Ontario: Ontario Geological Survey Mineral Deposits Circular 15, Ministry of Natural Resources.

Gurgenli, H. (2006). *Geomechanical and Weathering Properties of Weak Roof Shales in Coal Mines*. M.Sc., West Virginia University.

Hale, P., and Shakoor, A. (2003). A Labratory Investigation of the Effects of Cyclic Heating and Cooling, Wetting and Drying, and Freezing and Thawing on the Compressive Strength of Selected Sandstones. *Environmental & Engineering Geoscience*, *IX*(2), 117–130.

Hancock, G. S., Anderson, R. S., and Whipple, K. X. (1998). Beyond Power: Bedrock River Incision Process and Form. In K. J. Tinkler & E. E. Wohl (Eds.), *Geophysical Monograph 107, Rivers Over Rock: Fluvial Processes in Bedrock Channels* (pp. 35–60). Washington, D.C.: American Geophysical Union.

Hancock, G. S., Small, E. E., and Wobus, C. (2011). Modeling the effects of weathering on bedrock-floored channel geometry. *Journal of Geophysical Research: Earth Surface*, *116*(3), 1–13. https://doi.org/10.1029/2010JF001908

Harbor, D. J. (1998). Dynamic Equilibrium Between an Active Uplift and the Sevier River, Utah. *The Journal of Geology*, *106*(2), 181–194. https://doi.org/10.1086/516015

Henshaw, P. C., and Booth, D. B. (2000). Natural Restabilization of Stream Channels in Urban Watersheds. *Journal Of The American Water Resources Association*, *36*(6), 1219–1236.

Hirvonen, J. (2017). *Thresholds and Sediment Transport Dynamics in an Interbedded Shale and Limestone Controlled Urban Watercourse*. M.A.Sc., University of Waterloo.

Humphrey, N. F., and Konrad, S. K. (2000). River incision or diversion in response to bedrock uplift. *Geology*, *28*(1), 43–46. https://doi.org/10.1130/0091-7613(2000)028<0043:RIODIR>2.3.CO;2

International Association for Rock Mechanics. (n.d.). Part 2: Suggested Methods for Determining Swelling and Slake-Durability Index Properties. *International Society for Rock Mechanics*, 151–156.

Jansen, J. D. (2006). Flood magnitude-frequency and lithologic control on bedrock river incision in post-orogenic terrain. *Geomorphology*, *82*, 39–57. https://doi.org/10.1016/j.geomorph.2005.08.018

Johnson, J. P., and Whipple, K. X. (2007). High spatial resolution data acquisition for the geosciences: kite aerial photography. *Earth Surface Processes and Landforms*, *32*, 1048–1062. https://doi.org/10.1002/esp

Kang, R. S., and Marston, R. A. (2006). Geomorphic effects of rural-to-urban land use conversion on three streams in the Central Redbed Plains of Oklahoma. *Geomorphology*, *79*(3–4), 488–506. https://doi.org/10.1016/j.geomorph.2006.06.034

Kolay, E. (2016). Modeling the effect of freezing and thawing for sedimentary rocks. *Environmental Earth Sciences*, *75*(3), 1–12. https://doi.org/10.1007/s12665-015-5005-3

Kolay, E., and Kayabali, K. (2006). Investigation of the effect of aggregate shape and surface roughness on the slake durability index using the fractal dimension approach. *Engineering Geology*, *86*(4), 271–284. https://doi.org/10.1016/j.enggeo.2006.05.007

Koncagul, E. C. (1998). *Comparison of Uniaxial Compressive Strength Test and Slake Durability Index values of Shale Samples from the Breathitt Formation, Kentucky*. Ph.D., University of Missouri. https://doi.org/10.16953/deusbed.74839

Lague, D., Hovius, N., and Davy, P. (2005). Discharge, discharge variability, and the bedrock channel profile. *Journal of Geophysical Research: Earth Surface*, *110*(4), 1–17. https://doi.org/10.1029/2004JF000259

Lavé, J., and Avouac, J. P. (2001). Fluvial incision and tectonic uplift across the Himalayas of central Nepal. *Journal of Geophysical Research: Solid Earth*, *106*(B11), 26561–26591. https://doi.org/10.1029/2001JB000359

Lienhart, D. A. (1988). The Geographic Distribution of Intensity and Frequency of Freeze-Thaw Cycles. *Bulletin of the Association of Engineering Geologists*. https://doi.org/10.2475/ajs.294.6.665

Lienhart, D. A. (1993). The Mechanism of Freeze-Thaw Deterioration of Rock in the Great Lakes Region. In C. McElroy & D. Lienhart (Eds.), *Rock for Erosion Control, ASTM STP1177* (pp. 77–87). Philadelphia: American Society for Testing and Materials.

Massong, T. M., and Montgomery, D. R. (2000). Influence of Sediment Supply, Lithology, and Wood Debris on the Distribution of Bedrock and Alluvial Channels. *Bulletin of the Geological Society of America*, *112*(4), 591–599. Retrieved from https://pubs.geoscienceworld.org/gsabulletin/issue/112/4

Matsuoka, N. (1990). The rate of rock weathering by frost action: Field measurements and predective model. *Earth Surface Processes and Landforms*, *15*, 73–90. https://doi.org/10.1002/esp.3290150108

McGreevy, J. P. (1981). Some Perspectives on frost shattering. *Progress in Physical Geography*, *5*(1), 57–75.

Mitchell, J. K. (1993). *Fundamentals of Soil Behavior*. New York, NY: John Wiley and Sons Ltd.

Montgomery, D. C. (2012). *Design and Analysis of Experiments* (8th ed.). Wiley.

Montgomery, D. R. (2004). Observations on the role of lithology in strath terrace formation and bedrock channel width. *American Journal of Science*, *304*(5), 454–476. https://doi.org/10.2475/ajs.304.5.454

Montgomery, D. R., and Buffington, J. M. (1997). Channel-reach morphology in mountain drainage basins. *Bulletin of the Geological Society of America*, *109*(5), 596–611. https://doi.org/10.1130/0016-7606(1997)109<0596:CRMIMD>2.3.CO

Montgomery, D. R., and Gran, K. B. (2001). Downstream variations in the width of bedrock channels. *Water Resources Research*, *37*(6), 1841–1846.

Moriwaki, Y. (1975). *Causes of Slaking in Agrillaceous Materials*. Ph.D, University of California at Berkeley.

Mugridge, S., and Young, H. R. (1983). Disintegration of Shale by Cyclic Wetting and Drying and Frost Action. *Canadian Journal of Earth Sciences*, *20*, 568–576. https://doi.org/10.1139/e83-108

Murphy, B. P., Johnson, J. P. L., Gasparini, N. M., and Sklar, L. . (2016). Chemical weathering as a mechanism for the climatic control of bedrock river incision. *Nature*, *532*, 223–227.

Oakland, M. W., and Lovell, C. W. (1982). *Classification and Other Standard Tests for Shale Embankments*. Indiana.

Onset. (2018). HOBO 13-Foot Fresh Water Level Data Logger. Retrieved January 3, 2018, from http://www.onsetcomp.com/products/data-loggers/u20-001-04

Ontario Geological Survey. (1991). Bedrock geology of ontario, southern sheet; Ontario Geological Survey, Map 2544, scale 1:1 000 000.

Parish, D. W. (2001). *Slake Durability and Engineering Properties f Durham Triassic Basin Rock*. North Carolina State University. https://doi.org/10.16953/deusbed.74839

Parkhurst, D. L., and Appelo, C. A. J. (2013). PHREEQC for Windows. Version 2.18.00. USGS. Retrieved from https://wwwbrr.cr.usgs.gov/projects/GWC_coupled/phreeqc/

Pearce, S. A., Pazzaglia, F. J., and Eppes, M. C. (2004). Ephemeral stream response to growing folds. *Bulletin of the Geological Society of America*, *116*(9–10), 1223–1239. https://doi.org/10.1130/B25386.1

Perera, N., Gharabaghi, B., Noehammer, P., and Bruce, K. (2010). Road Salt Application in Highland Creek Watershed, Toronto, Ontario - Chloride Mass Balance. *Water Quality Research Journal*, *45*(4), 451–461.

Potter, P., Maynard, B., and Pryor, W. (1980). *Sedimentology of Shale - Study Guide and Reference Source*. New York, NY: Springer-Verlag. Retrieved from https://books.google.ca/books?hl=en&lr=&id=9ZwyBwAAQBAJ&oi=fnd&pg=PA3&dq=Sedimentology+of+Shale&ots=mWqvzzsusA&sig=F_zJGAWv-p3yNunD79l5x-6T_E8#v=onepage&q=Sedimentology of Shale&f=false

Reiche, P. (1950). *A survey of weathering processes and products* (Revised Ed). Albuquerque: University of New Mexico Press.

Robinson, K., Hanson, G., Cook, K., and Kadavy, K. (2001). Erosion of Fractured Material. *Transactions of the ASAE*, *44*, 819–823.

Rosgen, D. L. (1997). A geomorphological approach to restoration of incised rivers. In *Proceedings of the Conference on Management of Landscapes Disturbed by Channel Incision*. Retrieved from http://www.wildlandhydrology.com/assets/A_Geomorphological_Approach_to_Restoration_of_Incised_Rivers.pdf

Russell, D. J. (1982). Controls on shale durability : the response of two Ordovician shales in the slake durability test. *Can. Geotech. J.*, *19*, 1–13.

Rutka, M. A., and Vos, M. A. (1993). *The Clay Products Industry and Shale Resources in Southern Ontario*.

SAS Institute Inc. (2017). SAS. Version 3.71 (Basic Edition). Retrieved from https://uwaterloo.ca/applied-health-sciences-computing/sasr-university-edition

Scott, A. D., and Smith, S. J. (1966). Susceptibility of Interlayer Potassium in Micas to Exchange with Sodium. *Proceedings of the Fourteenth National Conference on Clays and Clay Minerals*, (1234), 69–81. https://doi.org/10.1346/CCMN.1966.0140106

Shepherd, R. G. (1972). Incised River Meanders : Evolution in Simulated Bedrock. *Science*, *178*(4059), 409–411.

Shobe, C. M., Hancock, G. S., Eppes, M. C., and Small, E. E. (2017). Field evidence for the influence of weathering on rock erodibility and channel form in bedrock rivers. *Earth Surface Processes and Landforms*, *42*(13), 1997–2012. https://doi.org/10.1002/esp.4163

Sklar, L. S., and Dietrich, W. E. (2001). Sediment and rock strength control on river incision into bedrock. *Geology*, *29*(12), 1087–1090. https://doi.org/10.1130/0091-7613(2001)029<1087:SARSCO>2.0.CO

Sklar, L. S., and Dietrich, W. E. (2004). A mechanistic model for river incision into bedrock by saltating bed load. *Water Resources Research*, *40*(6), 1–22. https://doi.org/10.1029/2003WR002496

Snyder, N. P., Whipple, K., Tucker, G. E., and Merritts, D. J. (2003a). Importance of a stochastic distribution of floods and erosion thresholds in the bedrock river incision problem. *Journal of Geophysical Research*, *108*(B2), 2388. https://doi.org/10.1029/2003JB002649

Snyder, N. P., Whipple, K. X., Tucker, G. E., and Merritts, D. J. (2003b). Channel response to tectonic forcing: Field analysis of stream morphology and hydrology in the Mendocino triple junction region, northern California. *Geomorphology*, *53*, 97–127. https://doi.org/10.1016/S0169-555X(02)00349-5

Stark, C. P. (2006). A self-regulating model of bedrock river channel geometry. *Geophysical Research Letters*, *33*(4), 1–5. https://doi.org/10.1029/2005GL023193

Stock, J. D., Montgomery, D. R., Collins, B. D., Dietrich, W. E., and Sklar, L. (2005). Field measurements of incision rates following bedrock exposure: Implications for process controls on the long profiles of valleys cut by rivers and debris flows. *Bulletin of the Geological Society of America*, *117*(11–12), 174–194. https://doi.org/10.1130/B25560.1

Tinkler, K. J., and Parish, J. (1998). Recent Adjustments to the Long Profile of Cooksville Creek, an Urbanized Bedrock Channel in Mississauga, Ontairo. *Geophysical Monograph, Rivers Over Rock: Fluvial Processes in Bedrock Channels*, *107*, 167–187.

Tinkler, K. J., and Wohl, E. E. (1998). Field Studies of Bedrock Channels. In K. J. Tinkler & E. E. Wohl (Eds.), *Geophysical Monograph 107, Rivers Over Rock: Fluvial Processes in Bedrock Channels* (pp. 261–277). Washington, D.C.: American Geophysical Union.

Tournassat, C., Gailhanou, H., Crouzet, C., Gautier, A., Lassin, A., Blanc, P., … Gautier, A. (2007). Two cation exchange models for direct and inverse modelling of solution major cation composition in equilibrium with illite surfaces. *Geochimica et Cosmochimica Acta*, *71*(5), 1098–1114. https://doi.org/10.1016/j.gca.2006.11.018

Turowski, J. M., Hovius, N., Meng-Long, H., Lague, D., and Men-Chiang, C. (2008). Distribution

of erosion across bedrock channels. *Earth Surface Processes and Landforms*, *33*, 353–363. https://doi.org/10.1002/esp

Turowski, J. M., Hovius, N., Wilson, A., and Horng, M. J. (2008). Hydraulic geometry, river sediment and the definition of bedrock channels. *Geomorphology*, *99*, 26–38. https://doi.org/10.1016/j.geomorph.2007.10.001

Turowski, J. M., Lague, D., Crave, A., and Hovius, N. (2006). Experimental channel response to tectonic uplift. *Journal of Geophysical Research: Earth Surface*, *111*(3), 1–12. https://doi.org/10.1029/2005JF000306

Turowski, J. M., Lague, D., and Hovius, N. (2007). Cover effect in bedrock abrasion: A new derivation and its implications for the modeling of bedrock channel morphology. *Journal of Geophysical Research: Earth Surface*, *112*(4), 1–16. https://doi.org/10.1029/2006JF000697

Turowski, J. M., Lague, D., and Hovius, N. (2009). Response of bedrock channel width to tectonic forcing: Insights from a numerical model, theoretical considerations, and comparison with field data. *Journal of Geophysical Research: Solid Earth*, *114*(3), 1–16. https://doi.org/10.1029/2008JF001133

Turowski, J. M., and Rickenmann, D. (2009). Tools and cover effects in bedload transport observations in the Pitzbach , Austria. *Earth Surface Processes and Landforms*, *34*, 26–37. https://doi.org/10.1002/esp

Unrug, K. (1997). Weatherability Test of Rocks for Underground Mines. In *16th International Conference on Ground Control in Mining* (pp. 259–266). Morgantown, WV.

Unrug, K., and Padgett, P. (2003). RQD from the Barrel to the Box: Weatherability may be a Better Indicator for Roof Support Design. In *22nd International Conference on Ground Control in Mining* (pp. 162–167). Morgantown, WV.

Van Emden, H. (2008). *Statistics for Terrified Biologists*. Blackwell Publishing Ltd.

Walkinshaw, J. L., and Santi, P. M. (1996). Shales and Other Degradable Materials. In T. R. B. N. R. Council (Ed.), *Landslides: Investigation and Mitigation* (pp. 555–576). Washington, D.C.: National Academy Press.

Westgate, J. A., von Bitter, P. H., Eyles, N., McAndrews, J. H., Timmer, V., and Howard, K. W. F. (1999). The Physical Setting: A Story of Changing Envirnoments through Time. In *Special Places: The Past, Present, and Future of the Ecosystesm of the Toronto Region* (pp. 11–31). University of British Columbia Press.

Whipple, K. X. (2004). Bedrock Rivers and the Geomorphology of Active Orogens. *Annual Review of Earth and Planetary Sciences*, *32*(1), 151–185. https://doi.org/10.1146/annurev.earth.32.101802.120356

Whipple, K. X., Hancock, G. S., and Anderson, R. S. (2000). River incision into bedrock: Mechanics and relative efficacy of plucking, abrasion, and cavitation. *Bulletin of the Geological Society of America*, *112*(3), 490–503. https://doi.org/10.1130/0016-7606(2000)112<490:RIIBMA>2.0.CO

Whittaker, A. C., Cowie, P. A., Attal, M., Tucker, G. E., and Roberts, G. P. (2007a). Bedrock

channel adjustment to tectonic forcing: Implications for predicting river incision rates. *Geology*, *35*(2), 103–106. https://doi.org/10.1130/G23106A.1

Whittaker, A. C., Cowie, P. A., Attal, M., Tucker, G. E., and Roberts, G. P. (2007b). Contrasting transient and steady-state rivers crossing active normal faults: New field observations from the central apennines, Italy. *Basin Research*, *19*(4), 529–556. https://doi.org/10.1111/j.1365-2117.2007.00337.x

Wilson, J. C., Benbow, S., Metcalfe, R., and Leung, H. (2017). Reactive transport modelling of shale-bentonite interactions in a hypersaline environment. *Applied Geochemistry*, *76*, 60–73. https://doi.org/10.1016/j.apgeochem.2016.10.021

Wohl, E. E. (1993). Bedrock Channel Incision along Piccaninny Creek , Australia. *The Journal of Geology*, *101*(6), 749–761.

Wohl, E. E. (1999). Incised Bedrock Channels. In S. E. Darby & A. Simon (Eds.), *Incised River Channels* (pp. 187–218). New York, New York: John Wiley and Sons.

Wohl, E. E., and David, G. C. L. (2008). Consistency of scaling relations among bedrock and alluvial channels. *Journal of Geophysical Research: Earth Surface*, *113*(4), 1–16. https://doi.org/10.1029/2008JF000989

Wohl, E. E., and Ikeda, H. (1998). Patterns of Bedrock Channel Erosion on the Boso Peninsula , Japan. *The Journal of Geology*, *106*(3), 331–345.

Wohl, E. E., Lane, S. N., and Wilcox, A. C. (2015). The science and practice of river restoration. *Water Resources Research*, *51*, 5974–5997. https://doi.org/10.1002/2014WR016874

Wohl, E. E., and Merritt, D. M. (2001). Bedrock channel morphology. *Bulletin of the Geological Society of America*, *113*(9), 1205–1212. https://doi.org/10.1130/0016-7606(2001)113<1205:BCM>2.0.CO;2

Wood, L. E., and Deo, P. (1975). A Suggested System for Classifying Shale Materials for Embankments. *Bulletin of the Association of Engineering Geologists1*, *XII*, 39–55.

Yaalon, D. H. (1962). Mineral Composition of the Average Shale. *Clay Minerals*, *5*(27), 31–36. https://doi.org/10.1180/claymin.1962.5.27.05

Appendix A: Raw Data

Location ID	Sample Date	Sample Time	pH	Water Temperature (°C)	Electrical Conductivity (mS/cm)	Fe (mg/L)	Cl (mg/L - an)	Nitrate (mg/L - an)	Sulfate (mg/L - an)	Na (mg/L -cat)	Mg (mg/L -cat)	K (mg/L -cat)	Ca (mg/L -cat)
XS1	2017-01-06	11:30:00					1692.8	8.7	118.4	746.4	28.6	8.9	167.8
XS1	2017-01-11	00:30:00					1569.1	3.2	52.1	838.4	11.2	4.1	76.1
XS1	2017-01-11	01:00:00					2021.3	2.1	49.6	1160.2	8.0	4.6	46.8
XS1	2017-01-22	16:45:00					1590.7	4.0	107.9	716.2	33.9	16.8	159.6
XS1	2017-01-23	10:20:00					1699.1	4.5	118.5	683.3	37.4	17.5	167.8
XS1	2017-02-07	16:00:00					4459.3	3.5	109.7	2160.8	41.6		199.3
XS1	2017-02-07	17:45:00					9843.4	2.2	105.4	4650.3	8.0		124.6
XS1	2017-02-18	16:00:00					1090.3	1.5	36.6	631.9	7.5		51.9
XS1	2017-02-21	11:50:00	7.5	3.8	5.4		1772.7	3.0	93.4	906.5	18.8		130.4
XS1	2017-03-16	13:15:00	6.5	0.1	10.0		3539.3	5.2	115.9	1476.9	43.2		214.9
XS1	2017-03-24	03:00:00	6.0	2.5	7.6	0.0	2542.6	3.2	114.2	1163.9	30.4		191.6
XS1	2017-03-24	04:30:00	6.5	2.5	7.1	0.3	2459.0	3.1	111.6	1076.3	32.9		187.5
XS1	2017-03-24	05:30:00		2.4	7.1	0.3	2426.3	3.1	110.3	979.8	42.0		195.1
XS1	2017-03-24	06:15:00	6.5	2.5	6.9	0.3	2365.8	3.2	109.0	965.1	39.3		174.8
XS1	2017-03-24	07:00:00	6.0	2.4	9.3	0.6	3627.7	3.1	100.6	1584.9	27.9		152.2
XS1	2017-03-24	07:15:00		3.1	7.7	0.5	2711.9	2.9	92.7	1323.1	21.9		136.3
XS1	2017-03-24	07:45:00	6.0	3.5	9.3	1.1	3373.5	3.0	93.5	1344.3	29.6		119.6
XS1	2017-03-24	08:15:00	6.0	3.2	6.2	0.9	2163.5	1.7	58.9	986.3	-4.7		54.0
XS1	2017-03-24	08:45:00	6.5	3.2	3.6	0.7	1178.2	1.8	37.6	535.4	-3.6		12.7
XS1	2017-03-24	09:15:00	6.0	3.1	2.6	0.3	906.7	1.4	30.2	509.6	2.7		41.5
XS1	2017-03-24	09:45:00	6.5	3.1	2.6	0.6	819.2	1.4	29.2	434.9	-7.7		31.8
XS1	2017-03-24	10:15:00	6.0	3.2	2.6	0.3	818.2	1.5	29.4	397.4	-1.5		42.3
XS1	2017-03-24	10:45:00	6.0	3.6	2.6	0.4	799.7	1.6	30.0	390.2	2.6		42.8
XS1	2017-04-20	10:45:00	7.0	9.4	4.4	0.1	1316.5	3.2	105.9	677.1	16.5		154.0
XS1	2017-04-20	11:15:00	7.0	8.4	4.3	0.4	1329.7	5.7	105.8	691.7	18.6		159.5
XS1	2017-04-20	11:45:00	7.5	7.9	3.0	0.6	885.0	4.1	74.8	471.0	12.1		92.7
XS1	2017-04-20	11:50:00	7.0	8.4	2.2	0.4	616.3	3.3	55.0	340.9	7.2		66.8
XS1	2017-04-20	12:00:00	7.0	8.7	3.6	0.9	1084.0	3.3	84.4	544.9	15.6		115.8
XS1	2017-04-20	12:10:00	7.0	8.8	4.0	0.8	1217.6	4.6	89.9	592.5	26.8		120.9
XS1	2017-04-20	12:25:00	6.5	7.5	1.6	1.2	515.4	2.7	42.0	352.9	16.0		46.5
XS1	2017-04-20	14:10:00	7.0	8.5	0.6	0.4	124.3	1.4	15.4	82.5	6.6		11.6

Sample No.	Wet and Dry Mass					Density					
	Initial wt.	Final wt.	A (long)	B (int.)	C (short)	Initial WL	Final WL	ΔWL	Volume of sample	Wet Density	Dry Density
	g	g	mm	mm	mm	mm	mm	mm	cm^3	g/cm^3	g/cm^3
1m	679.5	634.1	193	115	20						
2m	30.4	28.9	78	34	5						
3m	12.6	11.9	47	37	4						
4m	18.7	17.9	55	42	3						
5m	14.1	13.4	38	21	15						
6m	36.3	34.6	101	34	3						
7m	18.3	17.7	45	35	5						
8m	13.4	13	52	23	4						
9m	13.6	12.9	37	27	10						
10m	12.7	12.4	55	25	5						
11m	34.1	32.9	79	35	8						
12m	64.9	62.1	105	58	7						
13m	19.9	19	68	30	5						
14m	47.7	45.6	73	40	10						
15m	14.8	14.3	60	20	8						
16m	16.2	15.4	50	32	8						
17m	57.7	55.3	75	48	10						
18m	83.4	80.5	95	40	15						
19m	60.9	58.5	80	44	10						
20m	93.5	88.5	123	40	5						
21m	85.2	81.5	75	60	18						
22m	11.8	11.5	53	27	5						
23m	16	15.3	93	20	7						
24m	14.7	14	55	27	6						
25m	31.2	29.6	75	36	5						
26m	153.2	145.3	114	80	18						
27m	84.9	81.6	100	60	10						
28m	69.1	65.5	105	40	9						
29m	27.2	25.8	65	45	4						
30m	58.8	56.4	95	43	10						
31m	94.9	90.7	90	70	10						
32m	65.4	63.7	81	32	13						
33m	49.3	46.7	113	63	2						
34m	206.5	196.5	155	65	17						
35m	202	191.8	145	75	15						
36m	53.8	52.1	81	30	10						
37m	33.6	32.2	60	37	5						
38m	25.1	23.8	68	44	3						
39m	25.3	24	65	40	5						
40m	86.6	81.8	98	55	7						
41m	116.7	111.6	150	62	5						
42m	134.5	128.4	95	67	20						
43m	122.6	116.4	165	45	8						
44m	207.5	197.5	170	65	10						
45m	264.6	251.2	240	55	13						
46m	477.2	468.1	165	55	34	58	64	6	161.28151	2.958802	2.902379
47m	502.8	482.4	185	80	20	59	65	6	161.28151	3.11753	2.991043
48m	78.5	77.2	107	27	25						
49m	140.6	133.5	115	65	5						
50m	117.2	111	125	100	3						
51m	172	162.7	125	118	6						
52m	116.6	110.9	117	78	5						
53m	148.2	141.8	126	64	4						
54m	133	126.1	155	57	4						

Sample No.	Wet and Dry Mass					Density					
	Initial wt.	Final wt.	A (long)	B (int.)	C (short)	Initial WL	Final WL	ΔWL	Volume of sample	Wet Density	Dry Density
	g	g	mm	mm	mm	mm	mm	mm	cm^3	g/cm^3	g/cm^3
55m	141.6	134.9	113	67	18						
56m	164.8	157.5	110	82	17						
57m	175.9	168.2	130	88	8						
58m	316.8	301.7	155	85	12	58	62	4	107.52101	2.946401	2.805963
59m	197.2	189.1	110	72	12						
60m	157	149.2	140	75	8						
61m	178.9	170.1	137	50	10						
62m	123.6	117.5	120	80	7						
63m	179.9	170.9	135	90	7						
64m	182.5	173.3	139	97	5						
65m	110.6	105.9	100	60	10						
66m	228.1	218.1	140	70	8						
67m	577.2	548.6	190	101	16	57	63.5	6.5	174.72164	3.30354	3.139851
68m	528.9	504.3	145	93	17						
69m	215.5	205.1	135	78	7						
70m	431	425.1	165	100	16	57	62.5	5.5	147.84139	2.915287	2.875379
71m	115.2	110.2	90	73	9						
72m	528.4	502.1	279	90	8	57	63	6	161.28151	3.276259	3.11319
73m	99.9	94.5	135	50	12						
74m	603.4	573	137	90	30	56	64	8	215.04202	2.805963	2.664596
75m	477.5	459.8	151	97	8						
76m	415.2	396.1	147	110	18						
77m	122.1	119.6	130	53	7						
78m	287.2	272.8	172	60	17	70	74	4	107.52101	2.671106	2.537179
79m	292.1	275.9	170	75	16	69	73	4	107.52101	2.716678	2.56601
80m	293.4	280.1	200	85	16	68	72	4	107.52101	2.728769	2.605072
81m	550.3	525	176	109	23	67	75	8	215.04202	2.559035	2.441383
82m	345.6	327.1	175	110	10	67	71	4	107.52101	3.214256	3.042196
83m	339.2	324.4	160	93	15	65.5	70	4.5	120.96113	2.804206	2.681853
84m	359.3	343.7	145	118	15	65	70	5	134.40126	2.673338	2.557268
85m	455.6	431.6	158	145	15	64	70	6	161.28151	2.824874	2.676066
86m	595.9	565.9	180	105	14	64	71	7	188.16176	3.166956	3.007519
87m	471.8	447.5	Broke in half								
88m	600.2	582.5	145	100	20	63	71	8	215.04202	2.791082	2.708773
89m	532.3	512	170	128	17	62.5	69.5	7	188.16176	2.828949	2.721063
90m	158.7	151	130	83	10	61.5	63.5	2	53.760504	2.951981	2.808753
91m	361.7	344	185	125	8	61	66	5	134.40126	2.691195	2.5595
92m	417.5	401.1	170	80	11	61	66	5	134.40126	3.10637	2.984347
93m	333.4	321	140	90	12	60	64	4	107.52101	3.100789	2.985463
94m	277.8	264.3	163	70	18	59	63	4	107.52101	2.583681	2.458124

Note: Drying the samples, then immersing them in water (for the density calculation), causese the samples to fall apart very easily.

Experimental Conditions							Sample Number	Before Weathering					After Weathering				Analysis Parameters	
Trial No.	No. cycles	Time Dry	Time Wet	Air Temp	Water Temp	Water Conc.		Wet Mass	Dry Mass*	A (long)	B (int.)	C (short)	Dry Mass of All Rem. + Tin(s)	Mass of Tin(s)	Dry Mass of All Rem.	Dry Mass of Largest Elements Rem.	Weatherability Index (WI)	Inverse Durability Index (ISDI)
		Hrs	Hrs	Deg. C	Deg. C	mg/L NaCl		g	g	mm	mm	mm	g	g	g	g	% weight lost from sample	% weight lost from sample
23	12	8	4	20	4	5000	99	247.8	236.6	137	122	12	235.4	0	235.4	234.7	0.8	0.5
							100	240.3	229.4	130	83	13	229.3	0	229.3	229.2	0.1	0.1
							101	199.9	190.9	127	75	7	190.9	0	190.9	190.9	0.0	0.0
							102	156.9	149.8	130	105	7	147.9	0	147.9	143.6	4.2	1.3
							103	157.8	150.7	120	67	10	152.2	0	152.2	152.2	-1.0	-1.0
24	12	8	4	20	4	0	104	152.2	145.3	122	87	5	144.5	0	144.5	144.3	0.7	0.6
							105	154.6	147.6	78	75	18	148.2	0	148.2	148.2	-0.4	-0.4
							106	209.9	200.4	130	64	8	200	0	200	200	0.2	0.2
							107	249.1	237.9	138	95	8	238.7	0	238.7	238.6	-0.3	-0.4
							108	229	218.7	138	80	15	220.4	0	220.4	217.8	0.4	-0.8
25	12	8	4	20	20	0	109	162.3	155.0	97	58	14	157.4	0	157.4	157.4	-1.6	-1.6
							110	177.9	169.9	113	56	5	168.1	0	168.1	168	1.1	1.0
							111	172.1	164.3	138	97	5	163.1	0	163.1	159.5	2.9	0.8
							112	224.7	214.6	150	80	10	213.2	0	213.2	213.2	0.6	0.6
							113	238.9	228.1	105	100	15	229.1	0	229.1	228.9	-0.3	-0.4
26	12	8	4	20	20	5000	114	170.5	162.8	150	85	5	162.1	0	162.1	162	0.5	0.4
							115	153.9	147.0	133	70	10	147.6	0	147.6	143.9	2.1	-0.4
							116	209.1	199.7	175	89	9	198.8	0	198.8	197.9	0.9	0.4
							117	226.9	216.7	135	80	10	216.8	0	216.8	208.4	3.8	-0.1
							118	240.8	229.9	136	115	4	230.6	0	230.6	230.6	-0.3	-0.3
27	12	8	4	-20	4	5000	119	167.3	159.8	165	65	9	157.1	11.7	145.4	122.7	23.2	9.0
							120	248.1	236.9	115	100	15	238.9	11.8	227.1	216.2	8.7	4.1
							121	218.9	209.0	130	80	16	213.3	11.9	201.4	191.3	8.5	3.6
							122	196.8	187.9	147	82	15	192.6	12	180.6	163	13.3	3.9
							123	163.9	156.5	122	85	10	163	11.7	151.3	132.1	15.6	3.3
28	12	8	4	-20	4	0	124	242.7	231.7	115	70	18	240.6	4.1	236.5	232.3	-0.2	-2.1
							125	235.1	224.5	136	80	10	235.9	13.1	222.8	220	2.0	0.8
							126	203.6	194.4	145	114	10	204	13.1	190.9	186.5	4.1	1.8
							127	174.2	166.4	121	90	10	177.3	13.1	164.2	154.8	6.9	1.3
							128	145.3	138.8	142	65	6	150.8	13	137.8	135.9	2.1	0.7
29	12	8	4	-20	20	5000	129	145.6	139.0	130	80	10	136.4	11.9	124.5	101.4	27.1	10.5
							130	220.4	210.5	145	80	15	204	11.8	192.2	165.6	21.3	8.7
							131	248.4	237.2	125	80	10	251.2	11.7	239.5	238	-0.3	-1.0
							132	182.7	174.5	138	85	12	175	11.9	163.1	132.6	24.0	6.5
							133	197.4	188.5	124	95	12	182.2	11.7	170.5	152.4	19.2	9.5
30	12	8	4	-20	20	0	134	193.3	184.6	120	100	10	187.2	4.1	183.1	178.7	3.2	0.8
							135	177	169.0	158	87	10	179.8	13	166.8	158.5	6.2	1.3
							136	165.2	157.8	115	105	10	167.1	13	154.1	129.4	18.0	2.3
							137	247	235.8	130	100	11	244.4	13.1	231.3	213.1	9.6	1.9
							138	213.1	203.5	120	116	12	213.3	13.1	200.2	184.2	9.5	1.6

* Dry mass (before weathering without oven drying the sample) was calculated using the linear regression model derived from the relationship between oven dried mass and saturated mass of GBF shale samples

Appendix B: Statistical Program (SAS) Output

Class Level Information		
Class	Levels	Values
Air_Temp__DC_	2	20 -20
Water_Temp__DC_	2	4 20
Water_Conc___mg_LNaCl_	2	0 5000

Number of Observations Read	40
Number of Observations Used	40

Dependent Variable: Inverse_Durability_Index

Source	DF	Sum of Squares	Mean Square	F Value	Pr > F
Model	7	243.4224026	34.7746289	8.77	<.0001
Error	32	126.8984005	3.9655750		
Corrected Total	39	370.3208031			

R-Square	Coeff Var	Root MSE	Inverse_Durability_Index Mean
0.657328	114.8273	1.991375	1.734236

Source	DF	Type I SS	Mean Square	F Value	Pr > F
Air_Temp__DC_	1	115.6823104	115.6823104	29.17	<.0001
Water_Temp__DC_	1	6.4958657	6.4958657	1.64	0.2098
Water_Conc___mg_LNaC	1	59.9800586	59.9800586	15.13	0.0005
Air_Temp_*Water_Temp	1	5.8459303	5.8459303	1.47	0.2336
Air_Temp_*Water_Conc	1	54.1082525	54.1082525	13.64	0.0008
Water_Tem*Water_Conc	1	0.1922117	0.1922117	0.05	0.8271
Air_Te*Water_*Water_	1	1.1177733	1.1177733	0.28	0.5991

Source	DF	Type III SS	Mean Square	F Value	Pr > F
Air_Temp__DC_	1	115.6823104	115.6823104	29.17	<.0001
Water_Temp__DC_	1	6.4958657	6.4958657	1.64	0.2098
Water_Conc___mg_LNaC	1	59.9800586	59.9800586	15.13	0.0005
Air_Temp_*Water_Temp	1	5.8459303	5.8459303	1.47	0.2336
Air_Temp_*Water_Conc	1	54.1082525	54.1082525	13.64	0.0008
Water_Tem*Water_Conc	1	0.1922117	0.1922117	0.05	0.8271
Air_Te*Water_*Water_	1	1.1177733	1.1177733	0.28	0.5991

Least Squares Means
Adjustment for Multiple Comparisons: Tukey

Air_Temp__DC_	Inverse_Durability_Index LSMEAN	H0:LSMean1=LSMean2 Pr > |t|
20	0.03363041	<.0001
-20	3.43484064	

Air_Temp__DC_	Inverse_Durability_Index LSMEAN	99% Confidence Limits	
20	0.033630	-1.185774	1.253035

Air_Temp__DC_	Inverse_Durability_Index LSMEAN	99% Confidence Limits	
-20	3.434841	2.215436	4.654245

Least Squares Means for Effect Air_Temp__DC_				
i	j	Difference Between Means	Simultaneous 99% Confidence Limits for LSMean(i)-LSMean(j)	
1	2	-3.401210	-5.125585	-1.676836

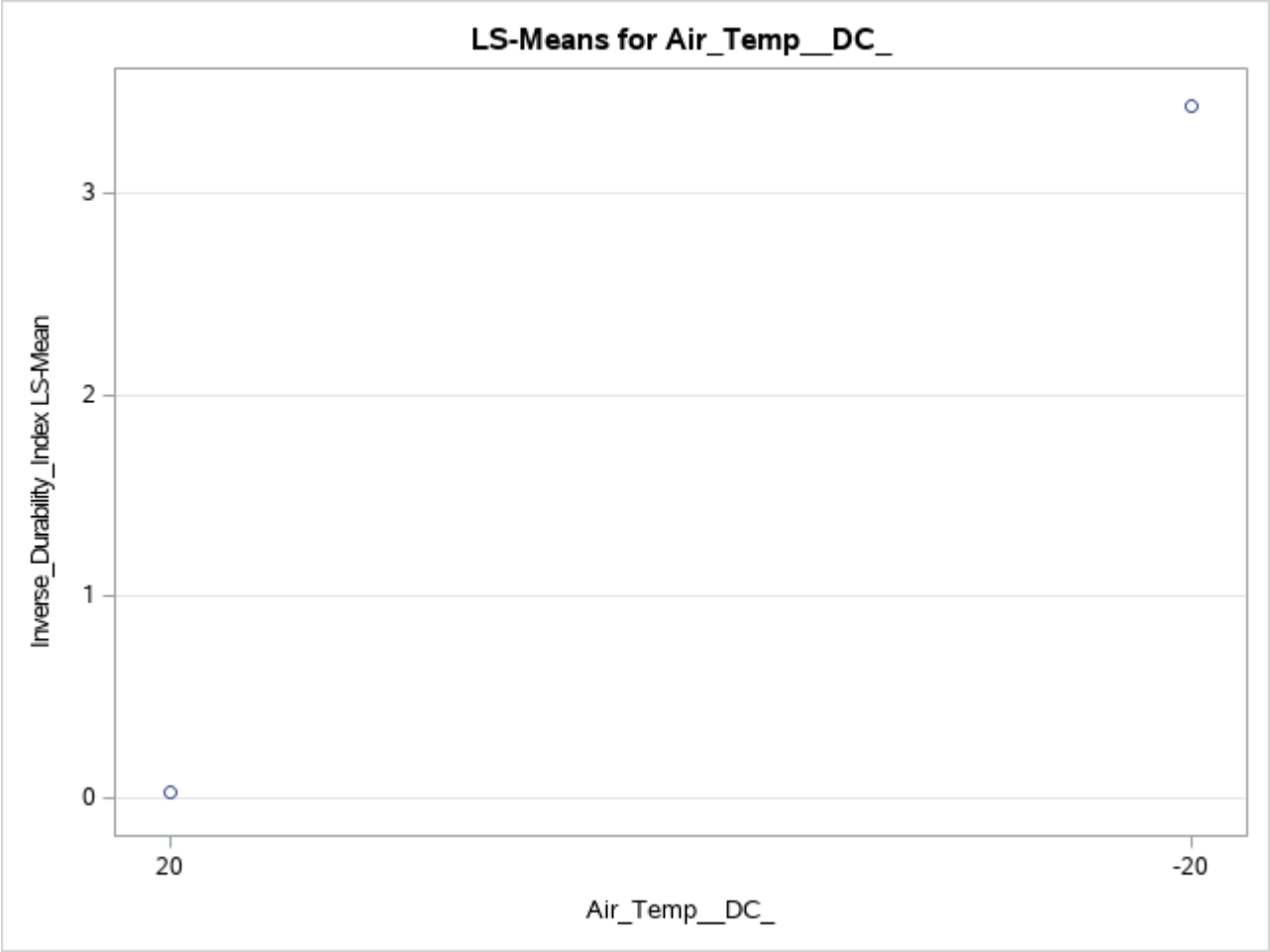

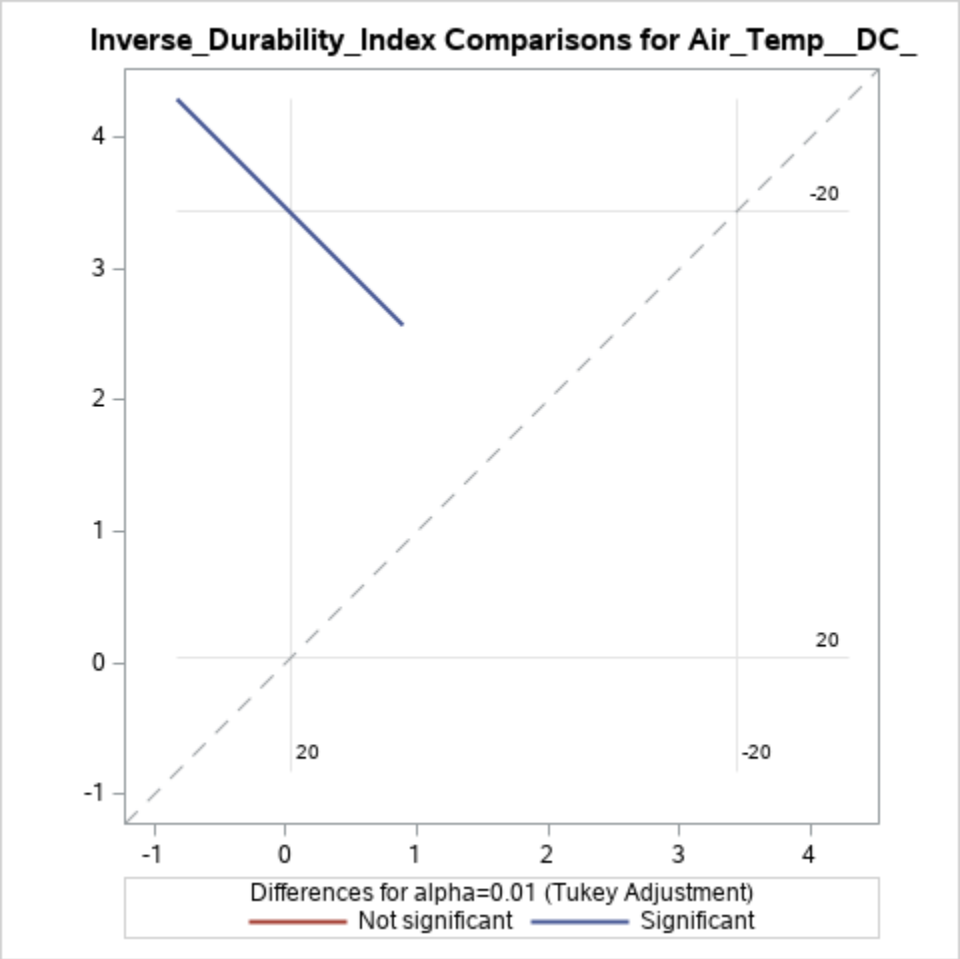

Least Squares Means
Adjustment for Multiple Comparisons: Tukey

Water_Temp__DC_	Inverse_Durability_Index LSMEAN	H0:LSMean1=LSMean2 Pr > |t|
4	1.33125085	0.2098
20	2.13722019	

Water_Temp__DC_	Inverse_Durability_Index LSMEAN	99% Confidence Limits	
4	1.331251	0.111846	2.550656
20	2.137220	0.917815	3.356625

Least Squares Means for Effect Water_Temp__DC_				
i	j	Difference Between Means	Simultaneous 99% Confidence Limits for LSMean(i)-LSMean(j)	
1	2	-0.805969	-2.530344	0.918405

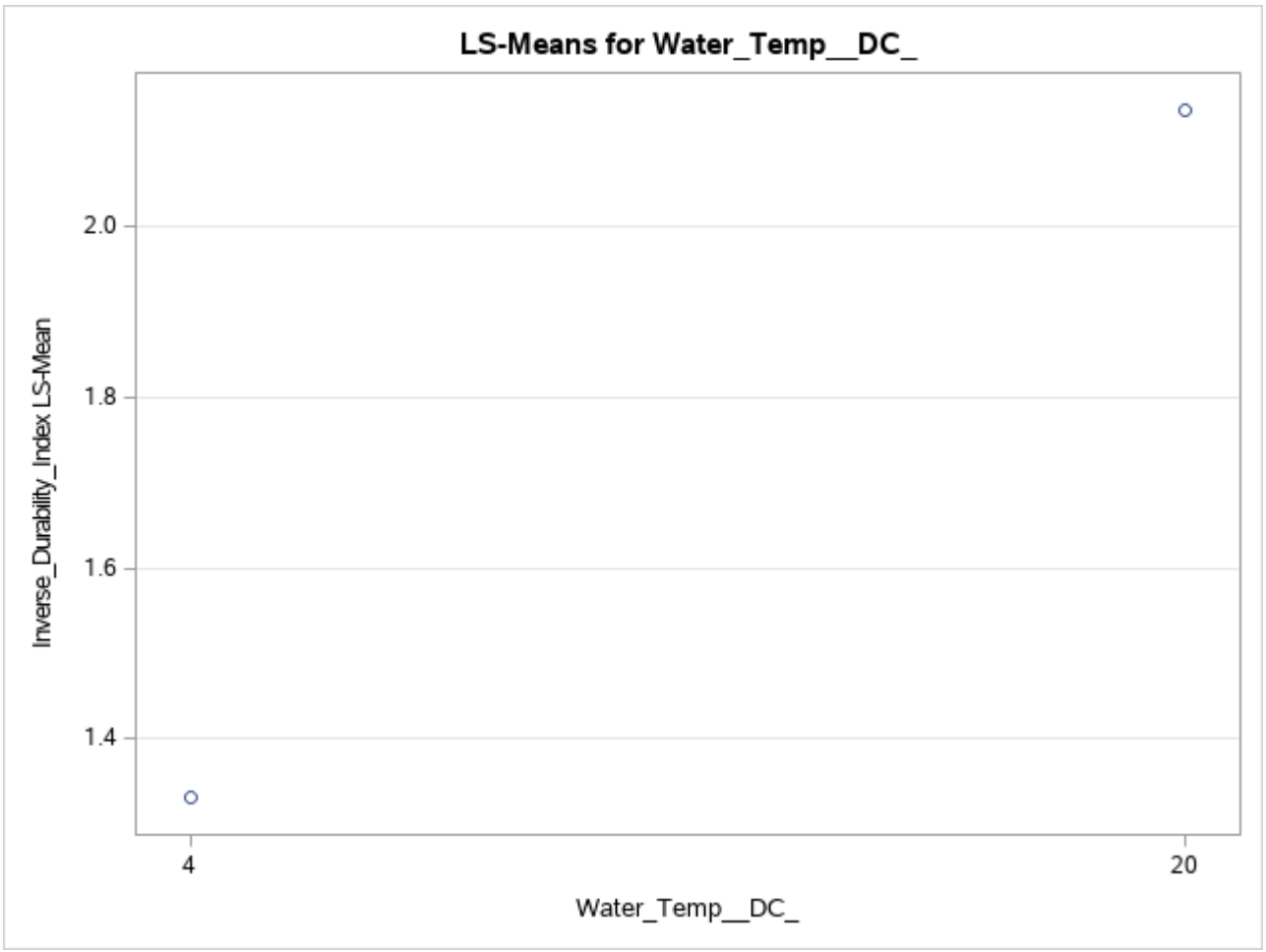
LS-Means for Water_Temp__DC_
Inverse_Durability_Index LS-Mean
2.0
1.8
1.6
1.4
4
20
Water_Temp__DC_

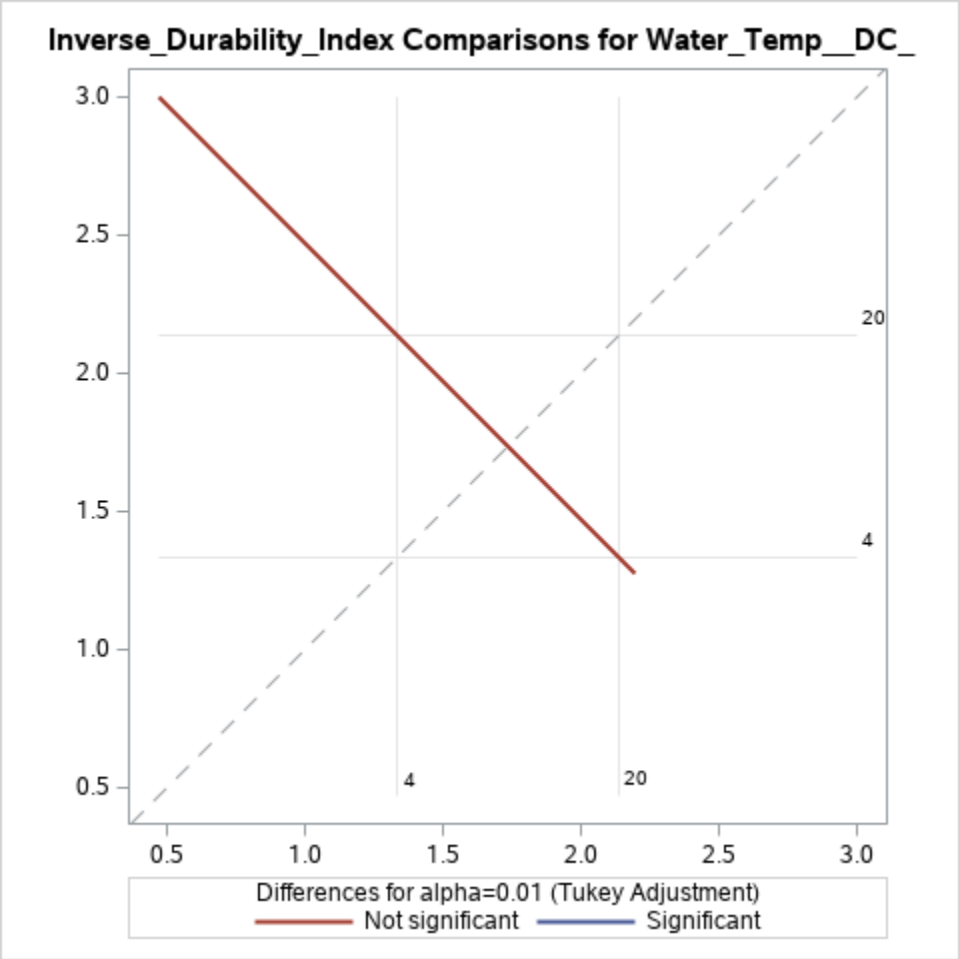

Least Squares Means
Adjustment for Multiple Comparisons: Tukey

Water_Conc___mg_LNaCl_	Inverse_Durability_Index LSMEAN	H0:LSMean1=LSMean2 Pr > |t|
0	0.50969419	0.0005
5000	2.95877685	

Water_Conc___mg_LNaCl_	Inverse_Durability_Index LSMEAN	99% Confidence Limits	
0	0.509694	-0.709711	1.729099
5000	2.958777	1.739372	4.178182

Least Squares Means for Effect Water_Conc___mg_LNaC				
i	j	Difference Between Means	Simultaneous 99% Confidence Limits for LSMean(i)-LSMean(j)	
1	2	-2.449083	-4.173457	-0.724708

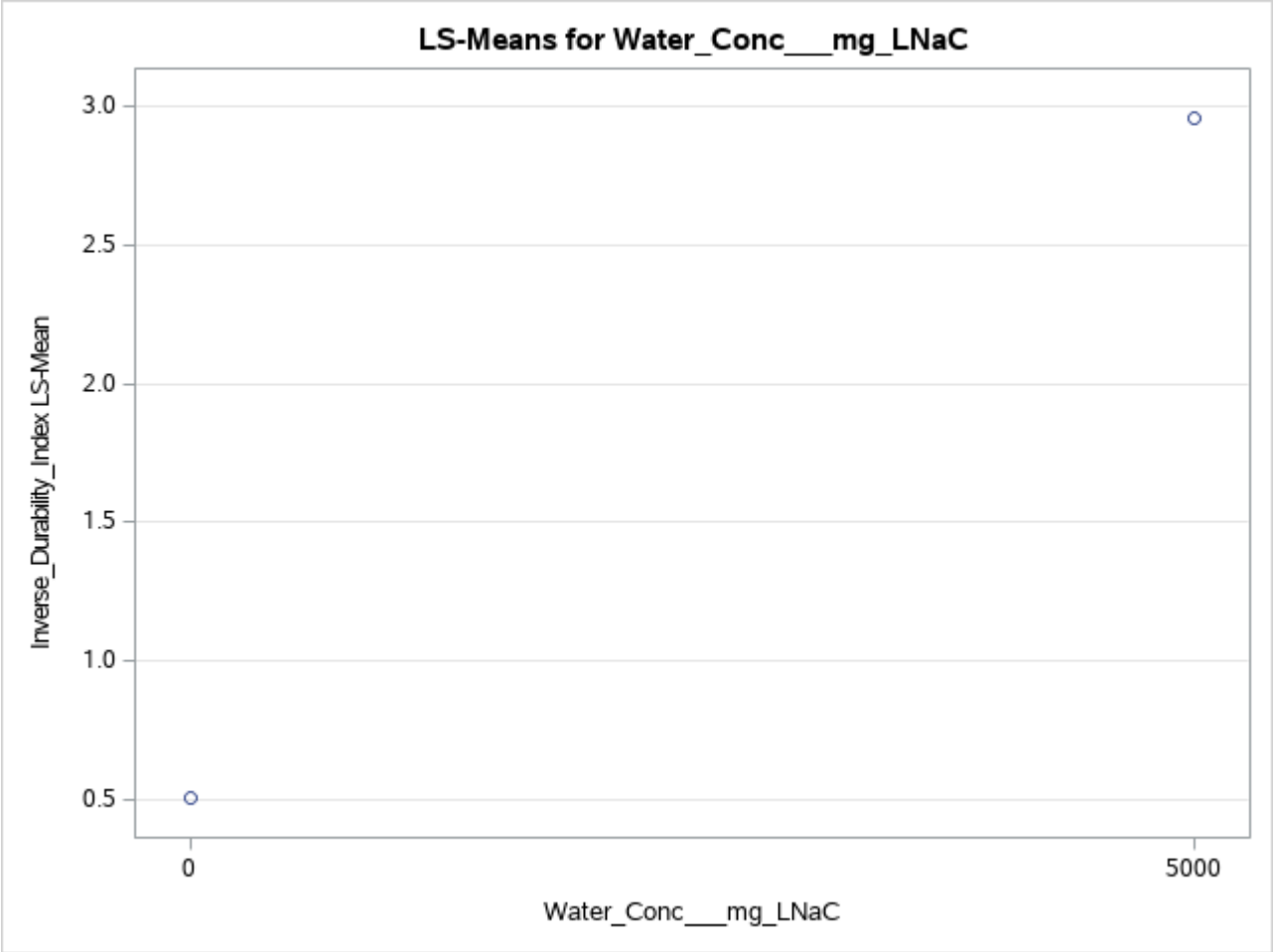
LS-Means for Water_Conc___mg_LNaC
Inverse_Durability_Index LS-Mean
3.0
2.5
2.0
1.5
1.0
0.5
0
5000
Water_Conc___mg_LNaC

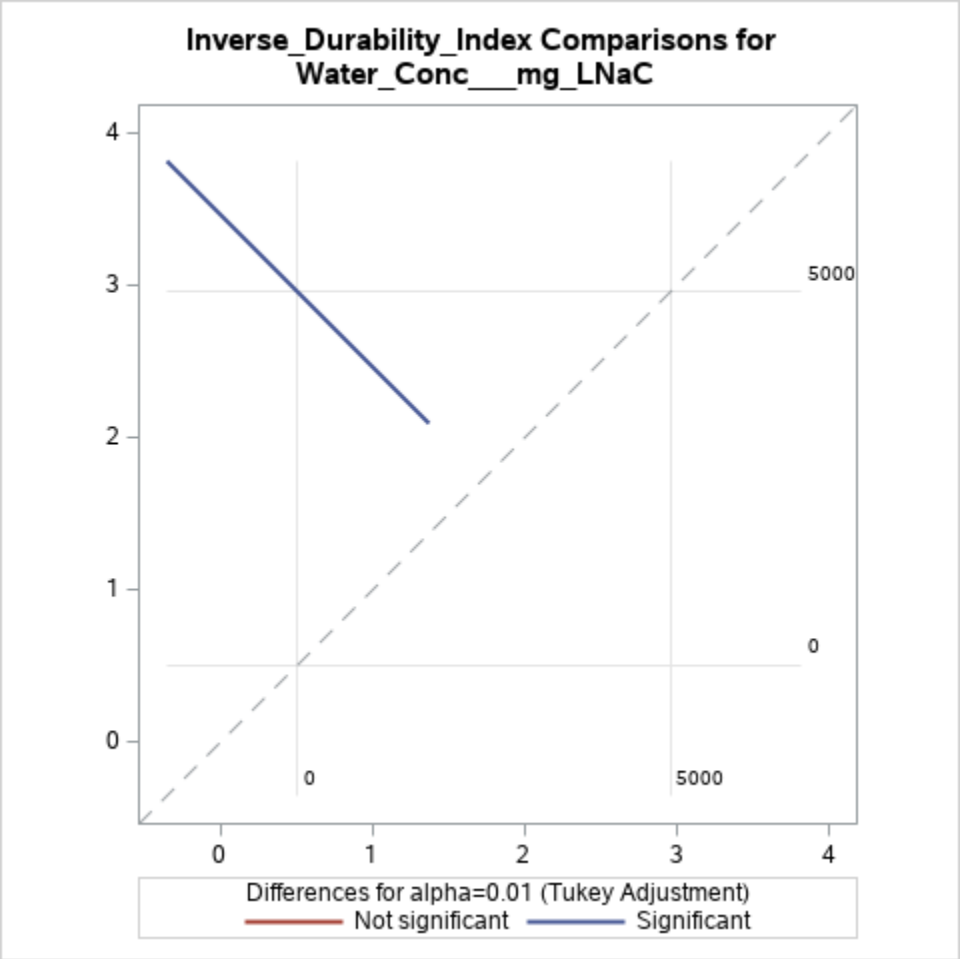

Least Squares Means
Adjustment for Multiple Comparisons: Tukey

Air_Temp__DC_	Water_Temp__DC_	Inverse_Durability_Index LSMEAN	LSMEAN Number
20	4	0.01293916	1
20	20	0.05432165	2
-20	4	2.64956255	3
-20	20	4.22011873	4

Least Squares Means for effect Air_Temp_*Water_Temp
Pr > |t| for H0: LSMean(i)=LSMean(j)

Dependent Variable: Inverse_Durability_Index

i/j	1	2	3	4
1		1.0000	0.0279	0.0002
2	1.0000		0.0312	0.0003
3	0.0279	0.0312		0.3091
4	0.0002	0.0003	0.3091	

Air_Temp__DC_	Water_Temp__DC_	Inverse_Durability_Index LSMEAN	99% Confidence Limits	
20	4	0.012939	-1.711560	1.737438
20	20	0.054322	-1.670177	1.778820
-20	4	2.649563	0.925064	4.374061
-20	20	4.220119	2.495620	5.944618

Least Squares Means for Effect Air_Temp_*Water_Temp				
i	j	Difference Between Means	Simultaneous 99% Confidence Limits for LSMean(i)-LSMean(j)	
1	2	-0.041382	-3.046917	2.964152
1	3	-2.636623	-5.642158	0.368911
1	4	-4.207180	-7.212714	-1.201645
2	3	-2.595241	-5.600776	0.410294
2	4	-4.165797	-7.171332	-1.160262
3	4	-1.570556	-4.576091	1.434978

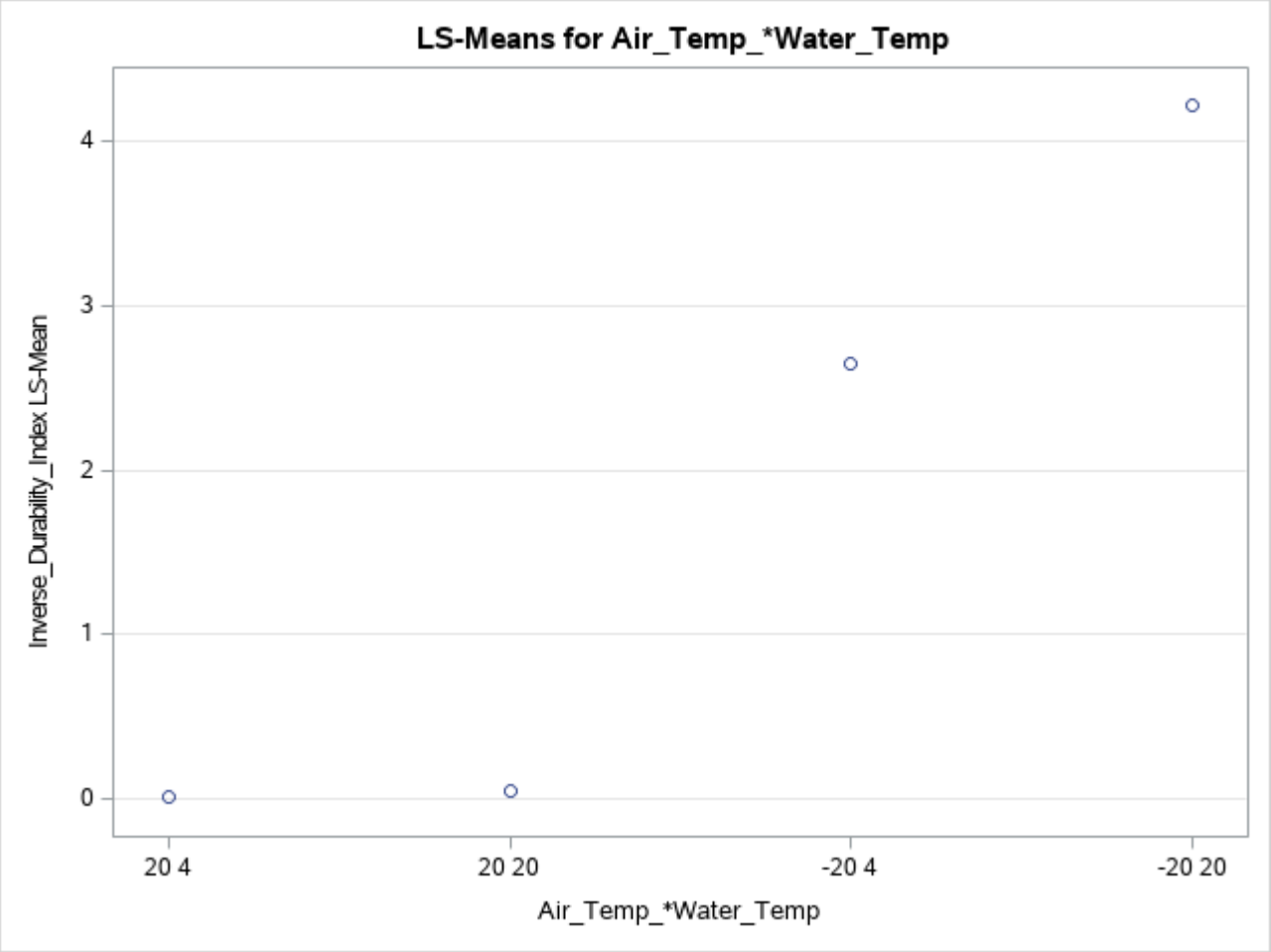

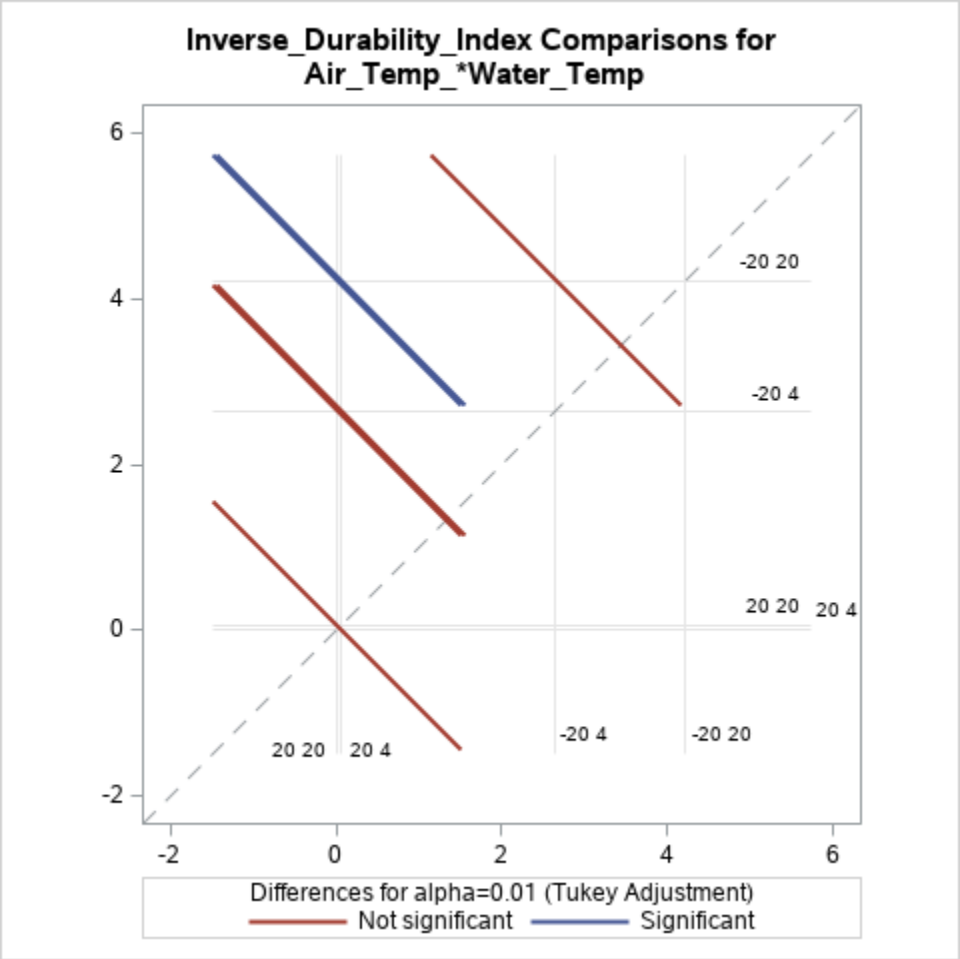

Least Squares Means
Adjustment for Multiple Comparisons: Tukey

Air_Temp__DC_	Water_Conc___mg_LNaCl_	Inverse_Durability_Index LSMEAN	LSMEAN Number
20	0	-0.02785189	1
20	5000	0.09511270	2
-20	0	1.04724028	3
-20	5000	5.82244100	4

Least Squares Means for effect Air_Temp_*Water_Conc
Pr > |t| for H0: LSMean(i)=LSMean(j)

Dependent Variable: Inverse_Durability_Index

i/j	1	2	3	4
1		0.9990	0.6269	<.0001
2	0.9990		0.7104	<.0001
3	0.6269	0.7104		<.0001
4	<.0001	<.0001	<.0001	

Air_Temp__DC_	Water_Conc___mg_LNaCl_	Inverse_Durability_Index LSMEAN	99% Confidence Limits	
20	0	-0.027852	-1.752351	1.696647
20	5000	0.095113	-1.629386	1.819611
-20	0	1.047240	-0.677259	2.771739
-20	5000	5.822441	4.097942	7.546940

Least Squares Means for Effect Air_Temp_*Water_Conc				
i	j	Difference Between Means	Simultaneous 99% Confidence Limits for LSMean(i)-LSMean(j)	
1	2	-0.122965	-3.128499	2.882570
1	3	-1.075092	-4.080627	1.930442
1	4	-5.850293	-8.855828	-2.844758
2	3	-0.952128	-3.957662	2.053407
2	4	-5.727328	-8.732863	-2.721794
3	4	-4.775201	-7.780735	-1.769666

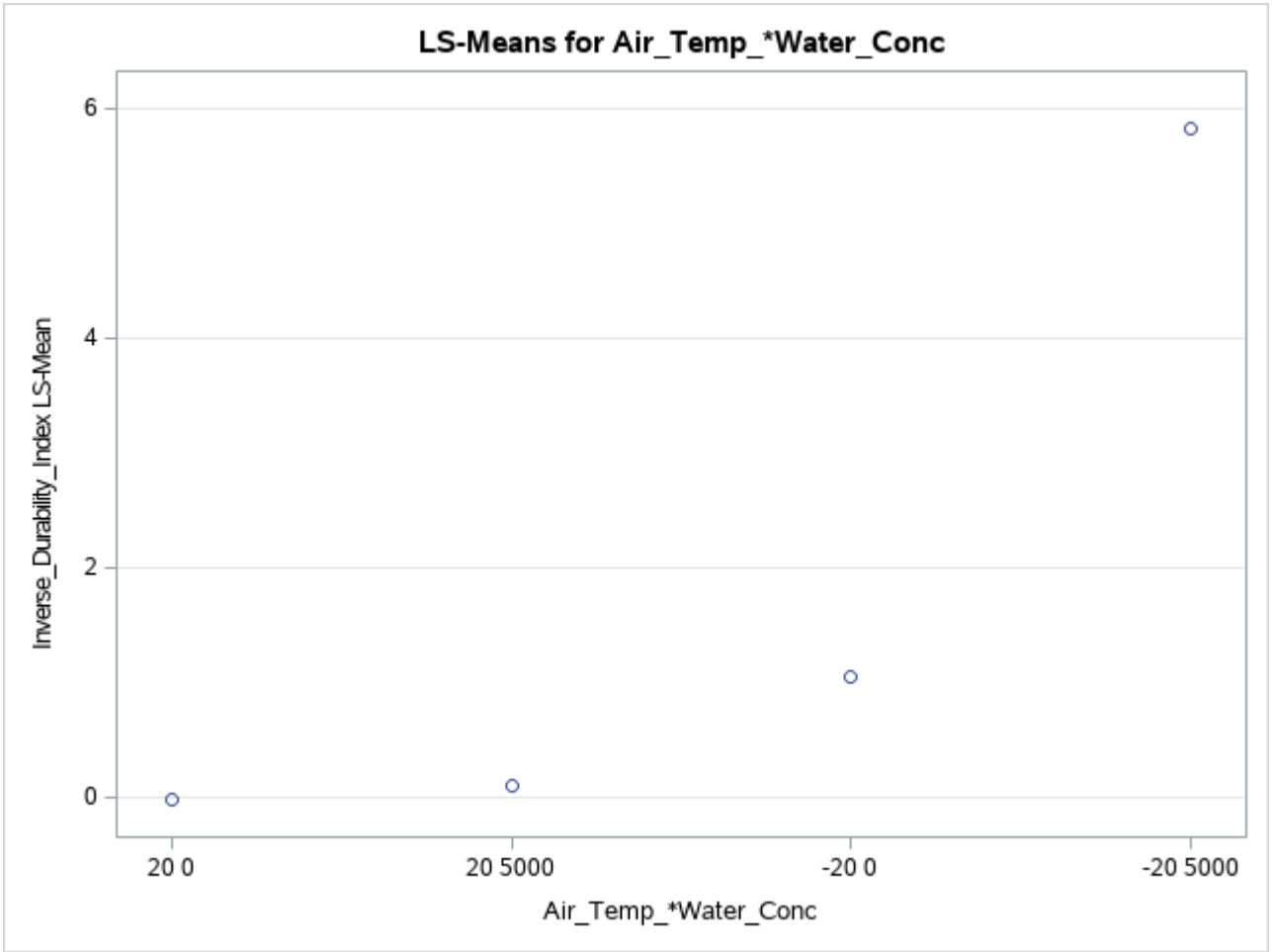

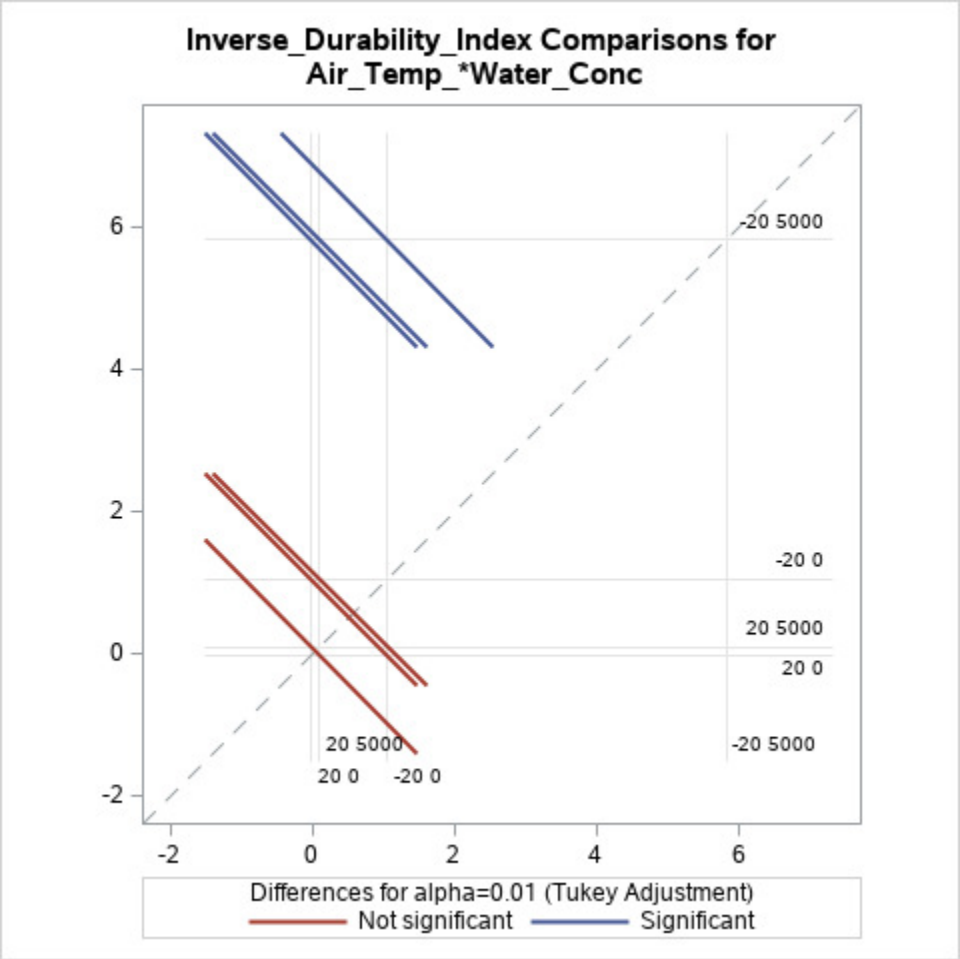

Least Squares Means
Adjustment for Multiple Comparisons: Tukey

Water_Temp__DC_	Water_Conc___mg_LNaCl_	Inverse_Durability_Index LSMEAN	LSMEAN Number
4	0	0.17602975	1
4	5000	2.48647196	2
20	0	0.84335864	3
20	5000	3.43108174	4

Least Squares Means for effect Water_Tem*Water_Conc
Pr > |t| for H0: LSMean(i)=LSMean(j)

Dependent Variable: Inverse_Durability_Index

i/j	1	2	3	4
1		0.0645	0.8763	0.0048
2	0.0645		0.2717	0.7154
3	0.8763	0.2717		0.0318
4	0.0048	0.7154	0.0318	

Water_Temp__DC_	Water_Conc___mg_LNaCl_	Inverse_Durability_Index LSMEAN	99% Confidence Limits	
4	0	0.176030	-1.548469	1.900529
4	5000	2.486472	0.761973	4.210971
20	0	0.843359	-0.881140	2.567857
20	5000	3.431082	1.706583	5.155581

Least Squares Means for Effect Water_Tem*Water_Conc				
i	j	Difference Between Means	Simultaneous 99% Confidence Limits for LSMean(i)-LSMean(j)	
1	2	-2.310442	-5.315977	0.695092
1	3	-0.667329	-3.672864	2.338206
1	4	-3.255052	-6.260587	-0.249517
2	3	1.643113	-1.362421	4.648648
2	4	-0.944610	-3.950144	2.060925
3	4	-2.587723	-5.593258	0.417812

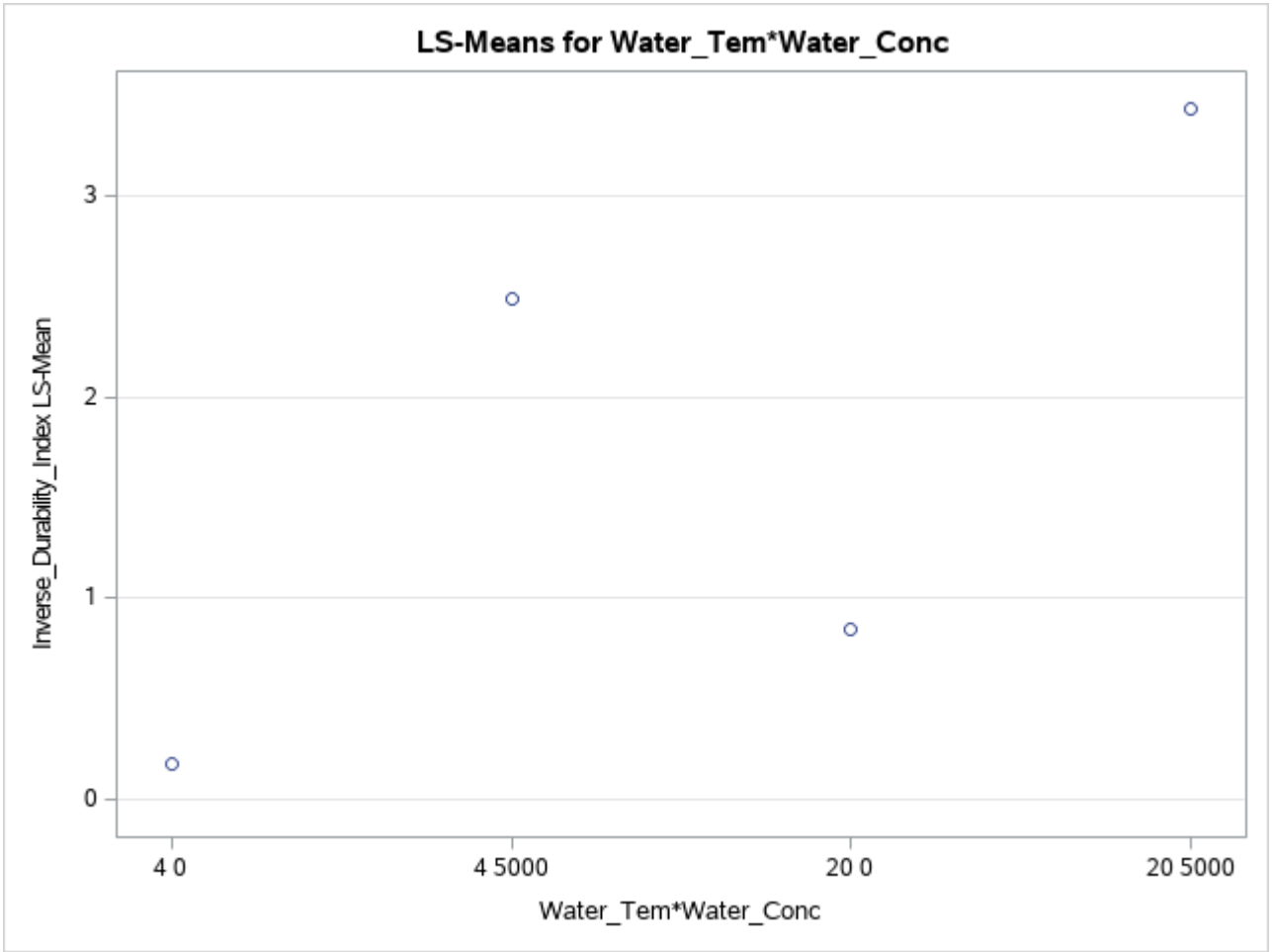

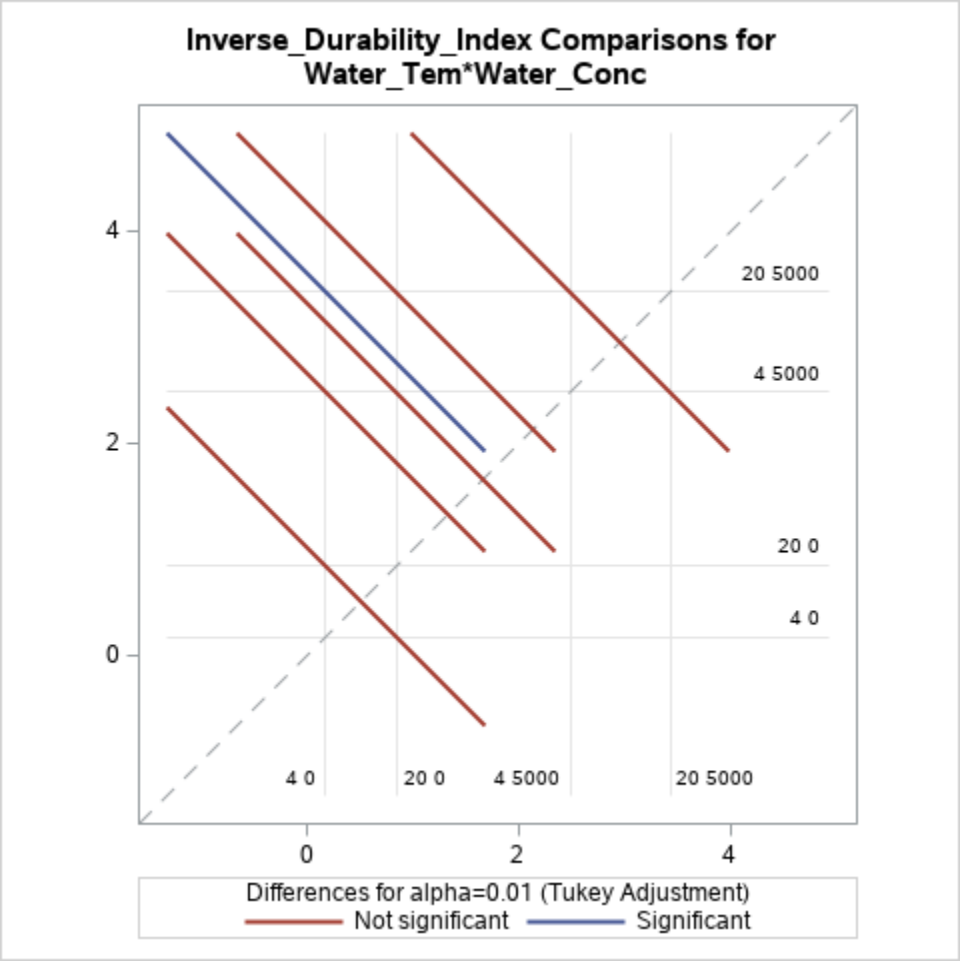

Least Squares Means
Adjustment for Multiple Comparisons: Tukey

Air_Temp__DC_	Water_Temp__DC_	Water_Conc___mg_LNaCl_	Inverse_Durability_Index LSMEAN	LSMEAN Number
20	4	0	-0.14638850	1
20	4	5000	0.17226681	2
20	20	0	0.09068472	3
20	20	5000	0.01795859	4
-20	4	0	0.49844799	5
-20	4	5000	4.80067711	6
-20	20	0	1.59603256	7
-20	20	5000	6.84420489	8

Least Squares Means for effect Air_Te*Water_*Water_
Pr > |t| for H0: LSMean(i)=LSMean(j)

Dependent Variable: Inverse_Durability_Index

i/j	1	2	3	4	5	6	7	8
1		1.0000	1.0000	1.0000	0.9995	0.0090	0.8580	<.0001
2	1.0000		1.0000	1.0000	1.0000	0.0173	0.9450	0.0002
3	1.0000	1.0000		1.0000	1.0000	0.0147	0.9274	0.0002
4	1.0000	1.0000	1.0000		0.9999	0.0127	0.9091	0.0001
5	0.9995	1.0000	1.0000	0.9999		0.0329	0.9866	0.0004
6	0.0090	0.0173	0.0147	0.0127	0.0329		0.2138	0.7337

Least Squares Means for effect Air_Te*Water_*Water_
Pr > |t| for H0: LSMean(i)=LSMean(j)

Dependent Variable: Inverse_Durability_Index

i/j	1	2	3	4	5	6	7	8
7	0.8580	0.9450	0.9274	0.9091	0.9866	0.2138		0.0048
8	<.0001	0.0002	0.0002	0.0001	0.0004	0.7337	0.0048	

Air_Temp__DC_	Water_Temp__DC_	Water_Conc___mg_LNaCl_	Inverse_Durability_Index LSMEAN	99% Confidence Limits	
20	4	0	-0.146388	-2.585198	2.292421
20	4	5000	0.172267	-2.266543	2.611076
20	20	0	0.090685	-2.348125	2.529494
20	20	5000	0.017959	-2.420851	2.456768
-20	4	0	0.498448	-1.940362	2.937258
-20	4	5000	4.800677	2.361868	7.239487
-20	20	0	1.596033	-0.842777	4.034842
-20	20	5000	6.844205	4.405395	9.283014

Least Squares Means for Effect Air_Te*Water_*Water_

i	j	Difference Between Means	Simultaneous 99% Confidence Limits for LSMean(i)-LSMean(j)	
1	2	-0.318655	-5.216113	4.578803
1	3	-0.237073	-5.134531	4.660385
1	4	-0.164347	-5.061805	4.733111
1	5	-0.644836	-5.542294	4.252621
1	6	-4.947066	-9.844523	-0.049608
1	7	-1.742421	-6.639879	3.155037
1	8	-6.990593	-11.888051	-2.093136
2	3	0.081582	-4.815876	4.979040
2	4	0.154308	-4.743150	5.051766
2	5	-0.326181	-5.223639	4.571277
2	6	-4.628410	-9.525868	0.269048
2	7	-1.423766	-6.321224	3.473692
2	8	-6.671938	-11.569396	-1.774480
3	4	0.072726	-4.824732	4.970184
3	5	-0.407763	-5.305221	4.489695
3	6	-4.709992	-9.607450	0.187465
3	7	-1.505348	-6.402806	3.392110
3	8	-6.753520	-11.650978	-1.856062
4	5	-0.480489	-5.377947	4.416968
4	6	-4.782719	-9.680176	0.114739
4	7	-1.578074	-6.475532	3.319384
4	8	-6.826246	-11.723704	-1.928788
5	6	-4.302229	-9.199687	0.595229
5	7	-1.097585	-5.995042	3.799873
5	8	-6.345757	-11.243215	-1.448299
6	7	3.204645	-1.692813	8.102102
6	8	-2.043528	-6.940986	2.853930
7	8	-5.248172	-10.145630	-0.350714

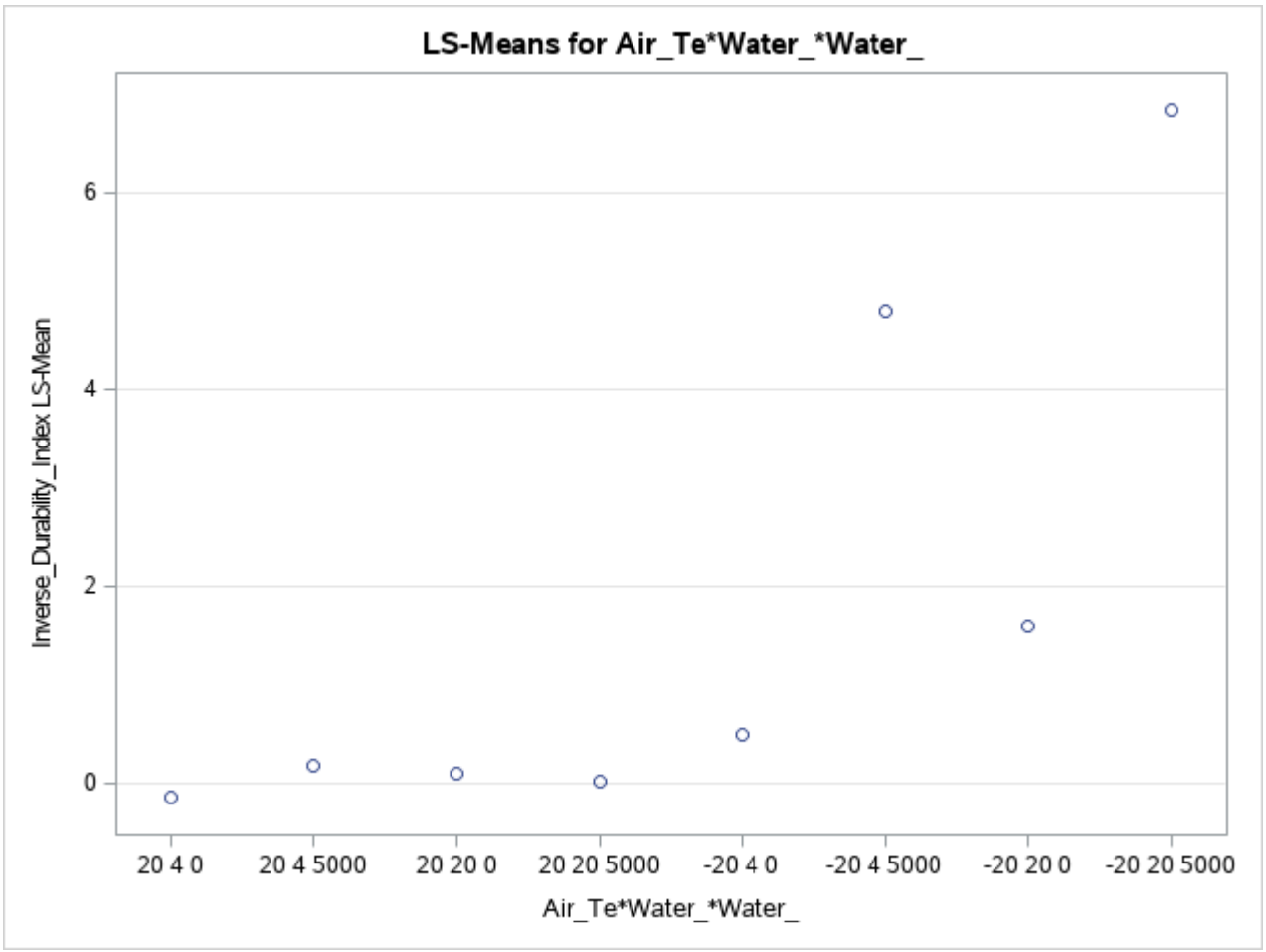
LS-Means for Air_Te*Water_*Water_
Inverse_Durability_Index LS-Mean
6
4
2
0
20 4 0
20 4 5000
20 20 0
20 20 5000
-20 4 0
-20 4 5000
-20 20 0
-20 20 5000
Air_Te*Water_*Water_

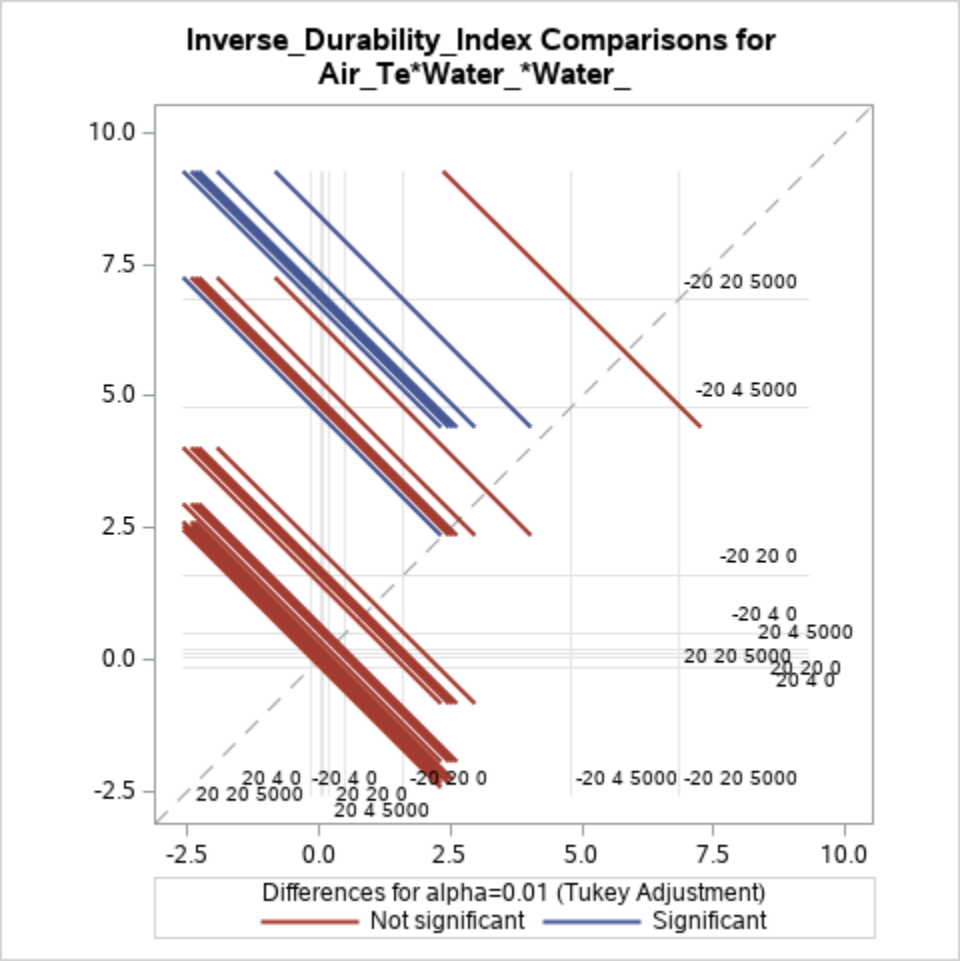
Inverse_Durability_Index Comparisons for Air_Te*Water_*Water_
10.0
7.5
5.0
2.5
0.0
-2.5
-2.5
0.0
2.5
5.0
7.5
10.0
-20 20 5000
-20 4 5000
-20 20 0
-20 4 0
20 4 5000
20 20 5000
20 20 0
20 4 0
20 4 0
-20 4 0
-20 20 0
20 20 5000
20 20 0
20 4 5000
-20 4 5000
-20 20 5000
Differences for alpha=0.01 (Tukey Adjustment)
Not significant
Significant

Class Level Information		
Class	Levels	Values
Air_Temp__DC_	2	20 -20
Water_Temp__DC_	2	4 20
Water_Conc___mg_LNaCl_	2	0 5000

Number of Observations Read	40
Number of Observations Used	40

Dependent Variable: WeatherIndex

Source	DF	Sum of Squares	Mean Square	F Value	Pr > F
Model	7	1718.376040	245.482291	9.79	<.0001
Error	32	802.105590	25.065800		
Corrected Total	39	2520.481630			

R-Square	Coeff Var	Root MSE	WeatherIndex Mean
0.681765	84.74662	5.006576	5.907700

Source	DF	Type I SS	Mean Square	F Value	Pr > F
Air_Temp__DC_	1	1074.533172	1074.533172	42.87	<.0001
Water_Temp__DC_	1	86.049190	86.049190	3.43	0.0732
Water_Conc___mg_LNaC	1	284.948493	284.948493	11.37	0.0020
Air_Temp_*Water_Temp	1	58.827919	58.827919	2.35	0.1354
Air_Temp_*Water_Conc	1	209.221054	209.221054	8.35	0.0069
Water_Tem*Water_Conc	1	2.021115	2.021115	0.08	0.7783
Air_Te*Water_*Water_	1	2.775097	2.775097	0.11	0.7415

Source	DF	Type III SS	Mean Square	F Value	Pr > F
Air_Temp__DC_	1	1074.533172	1074.533172	42.87	<.0001
Water_Temp__DC_	1	86.049190	86.049190	3.43	0.0732
Water_Conc___mg_LNaC	1	284.948493	284.948493	11.37	0.0020
Air_Temp_*Water_Temp	1	58.827919	58.827919	2.35	0.1354
Air_Temp_*Water_Conc	1	209.221054	209.221054	8.35	0.0069
Water_Tem*Water_Conc	1	2.021115	2.021115	0.08	0.7783
Air_Te*Water_*Water_	1	2.775097	2.775097	0.11	0.7415

Least Squares Means
Adjustment for Multiple Comparisons: Tukey

		H0:LSMean1=LSMean2
Air_Temp__DC_	WeatherIndex LSMEAN	Pr > |t|
20	0.7247150	<.0001
-20	11.0906842	

Air_Temp__DC_	WeatherIndex LSMEAN	99% Confidence Limits	
20	0.724715	-2.341027	3.790457

Air_Temp__DC_	WeatherIndex LSMEAN	99% Confidence Limits	
-20	11.090684	8.024942	14.156426

Least Squares Means for Effect Air_Temp__DC_				
i	j	Difference Between Means	Simultaneous 99% Confidence Limits for LSMean(i)-LSMean(j)	
1	2	-10.365969	-14.701271	-6.030667

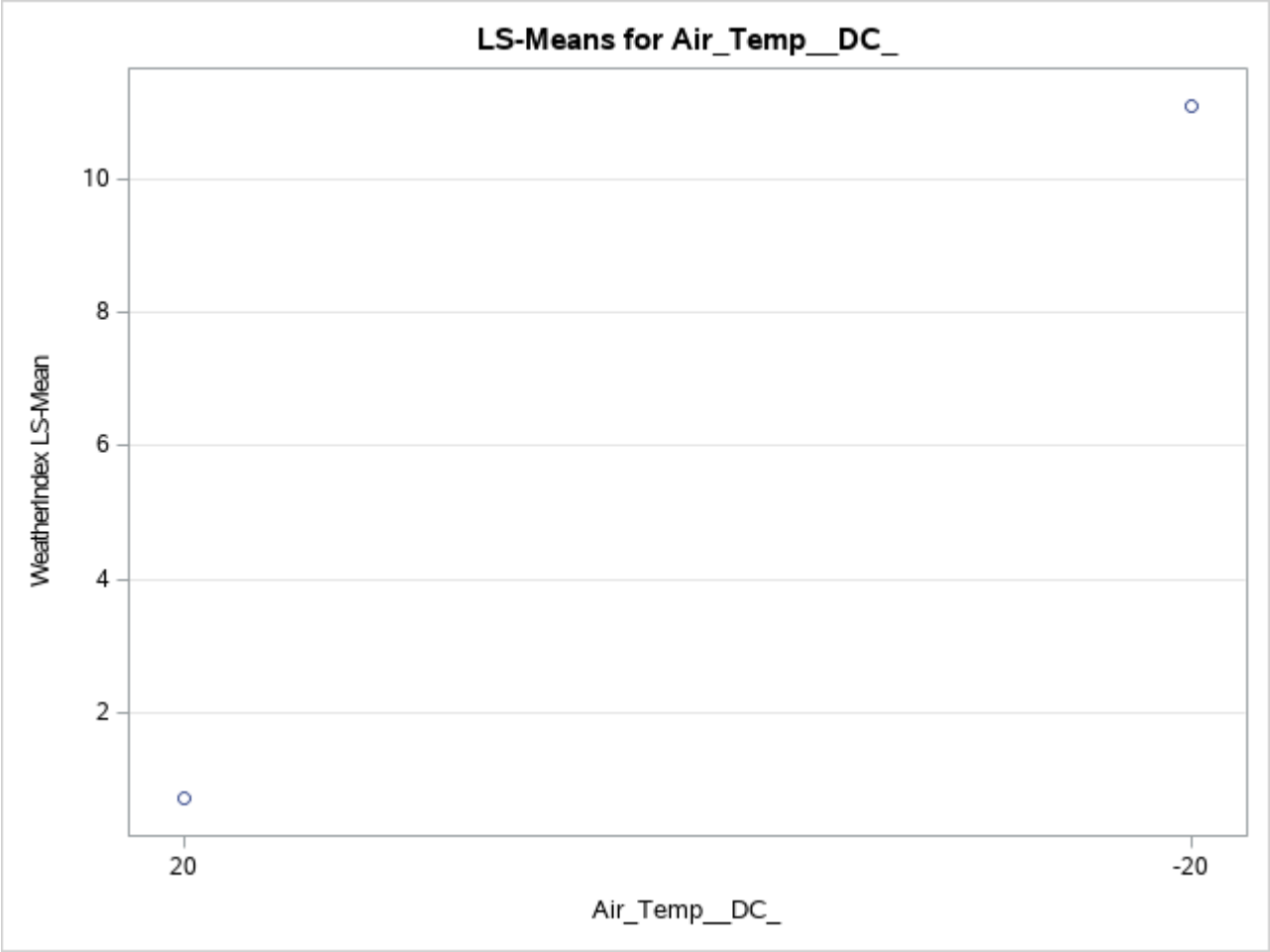

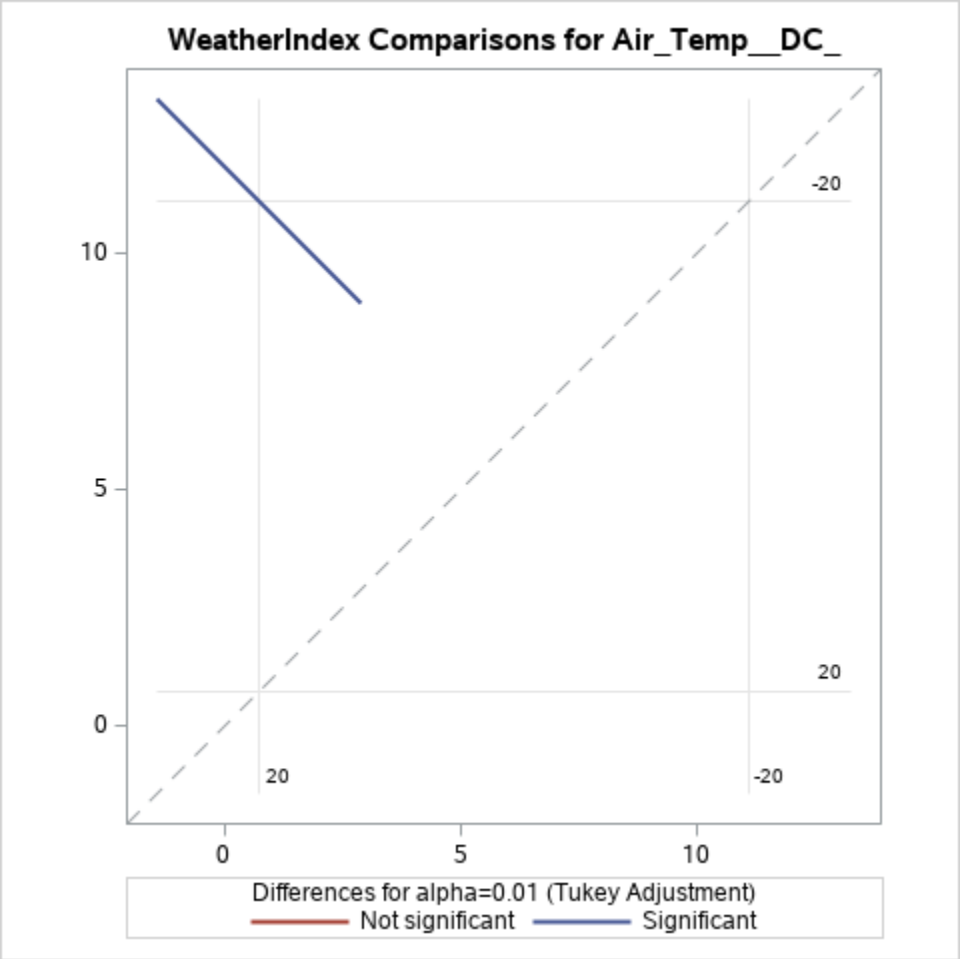

Least Squares Means
Adjustment for Multiple Comparisons: Tukey

Water_Temp__DC_	WeatherIndex LSMEAN	H0:LSMean1=LSMean2 Pr > |t|
4	4.44099251	0.0732
20	7.37440673	

Water_Temp__DC_	WeatherIndex LSMEAN	99% Confidence Limits	
4	4.440993	1.375251	7.506734
20	7.374407	4.308665	10.440149

Least Squares Means for Effect Water_Temp__DC_				
i	j	Difference Between Means	Simultaneous 99% Confidence Limits for LSMean(i)-LSMean(j)	
1	2	-2.933414	-7.268716	1.401888

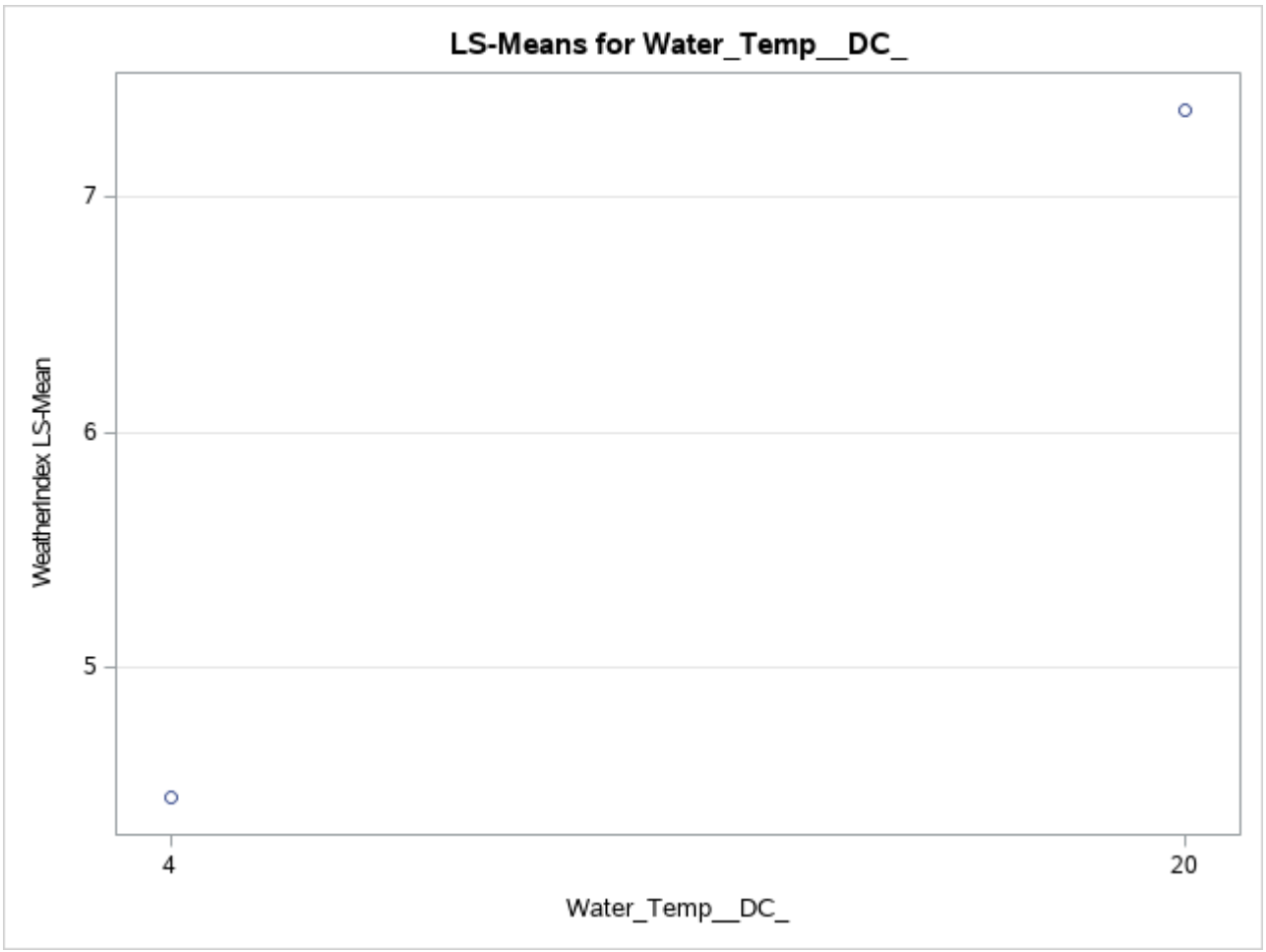
LS-Means for Water_Temp__DC_
Weatherindex LS-Mean
7
6
5
4
20
Water_Temp__DC_

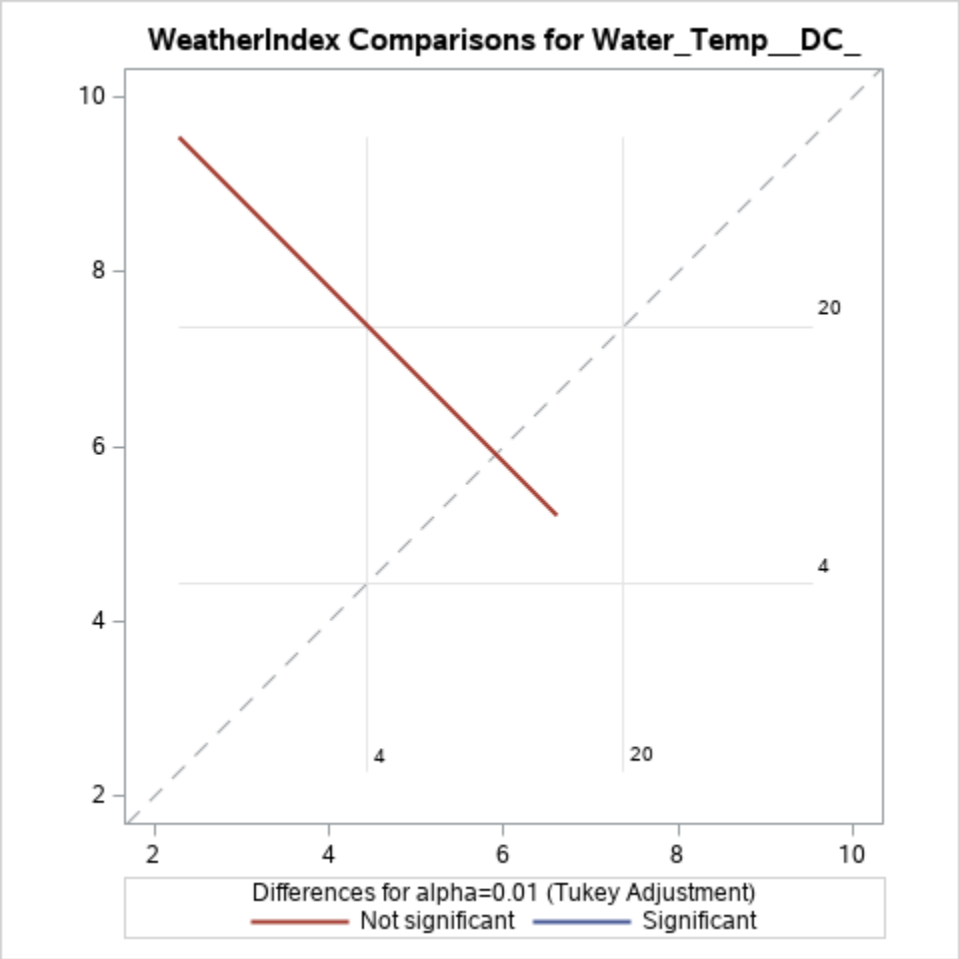

Least Squares Means
Adjustment for Multiple Comparisons: Tukey

Water_Conc___mg_LNaCl_	WeatherIndex LSMEAN	H0:LSMean1=LSMean2 Pr > |t|
0	3.23867127	0.0020
5000	8.57672797	

Water_Conc___mg_LNaCl_	WeatherIndex LSMEAN	99% Confidence Limits	
0	3.238671	0.172929	6.304413
5000	8.576728	5.510986	11.642470

Least Squares Means for Effect Water_Conc___mg_LNaC				
i	j	Difference Between Means	Simultaneous 99% Confidence Limits for LSMean(i)-LSMean(j)	
1	2	-5.338057	-9.673358	-1.002755

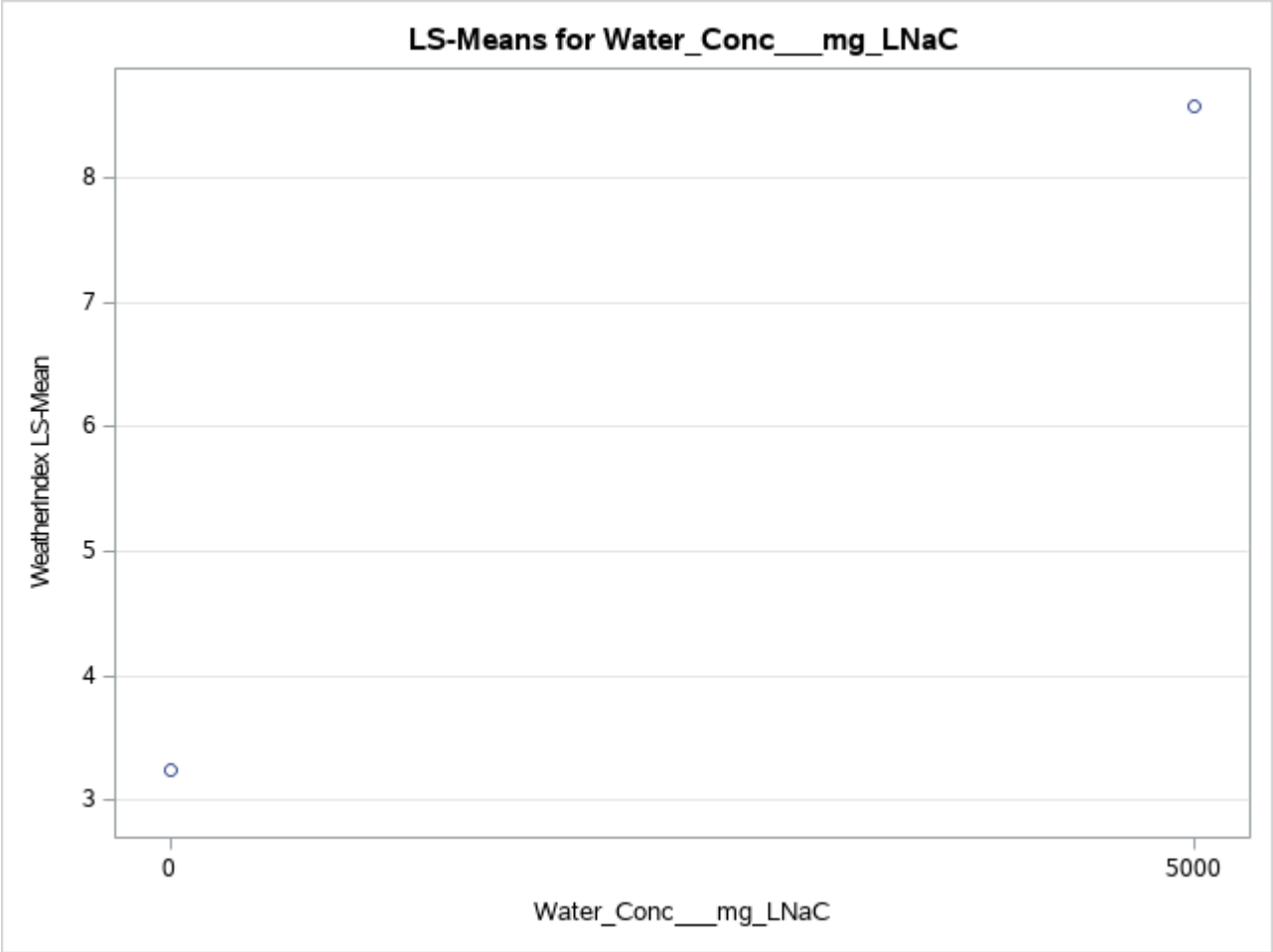
LS-Means for Water_Conc___mg_LNaC
Weatherindex LS-Mean
8
7
6
5
4
3
0
5000
Water_Conc___mg_LNaC

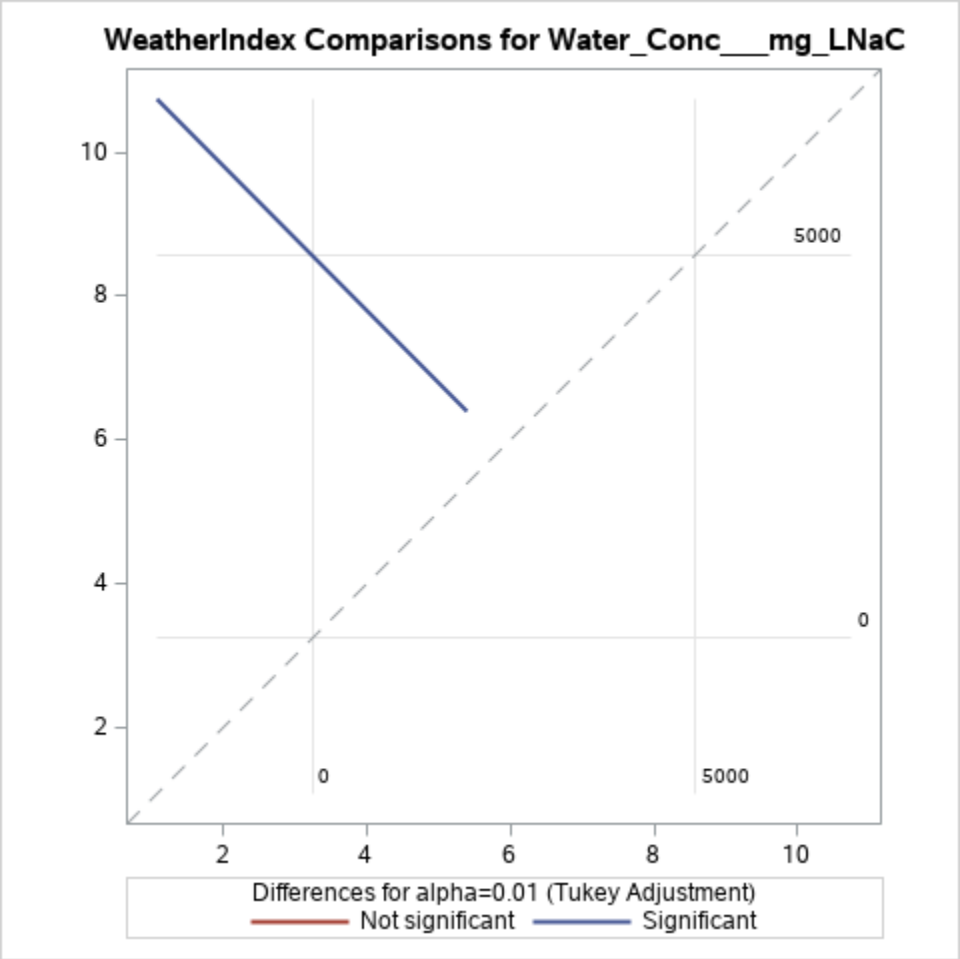

Least Squares Means
Adjustment for Multiple Comparisons: Tukey

Air_Temp__DC_	Water_Temp__DC_	WeatherIndex LSMEAN	LSMEAN Number
20	4	0.4707313	1
20	20	0.9786988	2
-20	4	8.4112537	3
-20	20	13.7701147	4

Least Squares Means for effect Air_Temp_*Water_Temp
Pr > |t| for H0: LSMean(i)=LSMean(j)

Dependent Variable: WeatherIndex

i/j	1	2	3	4
1		0.9958	0.0064	<.0001
2	0.9958		0.0115	<.0001
3	0.0064	0.0115		0.0988
4	<.0001	<.0001	0.0988	

Air_Temp__DC_	Water_Temp__DC_	WeatherIndex LSMEAN	99% Confidence Limits	
20	4	0.470731	-3.864883	4.806345
20	20	0.978699	-3.356915	5.314313
-20	4	8.411254	4.075640	12.746868
-20	20	13.770115	9.434501	18.105729

Least Squares Means for Effect Air_Temp_*Water_Temp				
i	j	Difference Between Means	Simultaneous 99% Confidence Limits for LSMean(i)-LSMean(j)	
1	2	-0.507967	-8.064272	7.048337
1	3	-7.940522	-15.496827	-0.384218
1	4	-13.299383	-20.855688	-5.743079
2	3	-7.432555	-14.988859	0.123749
2	4	-12.791416	-20.347720	-5.235112
3	4	-5.358861	-12.915165	2.197443

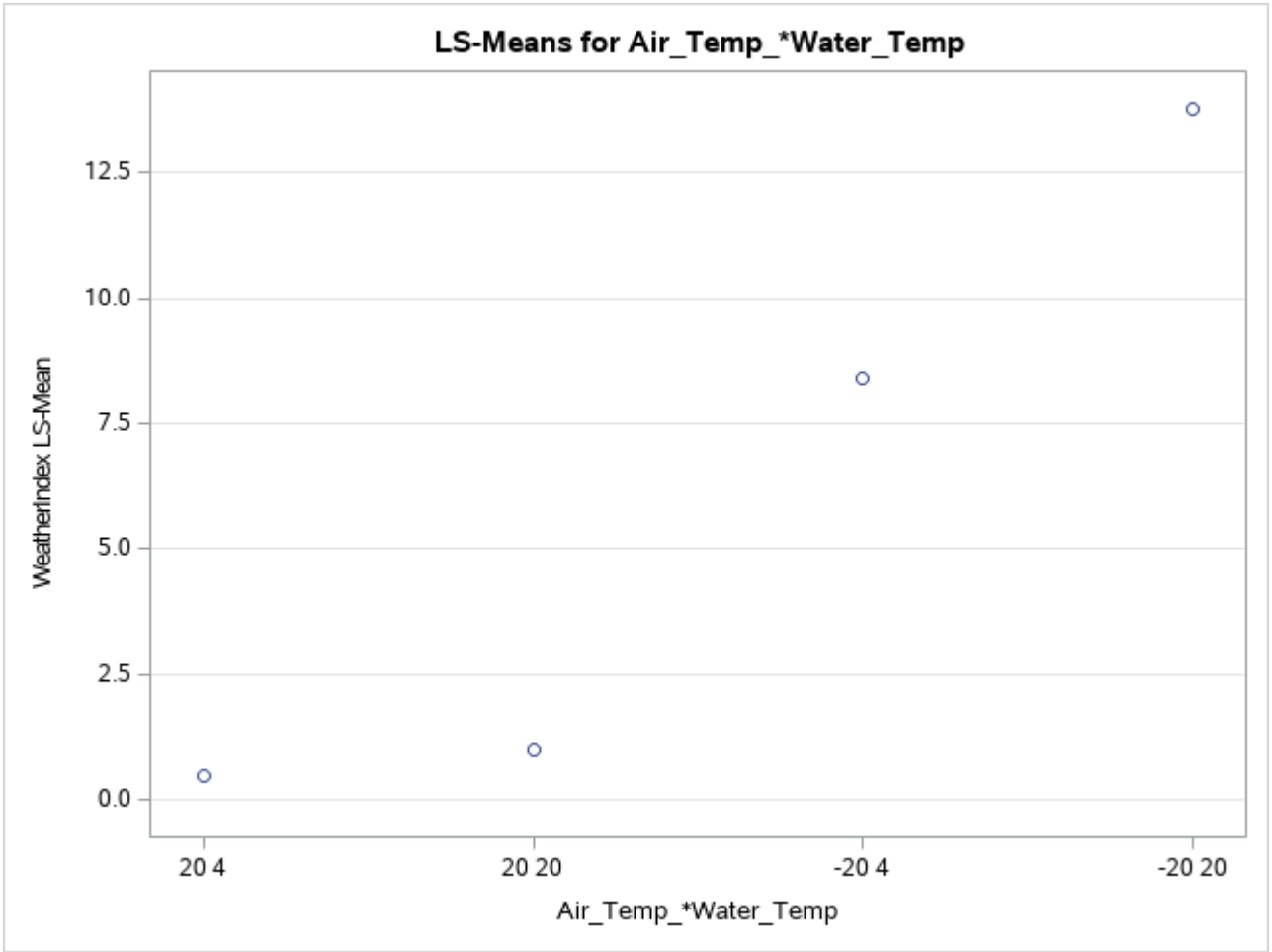

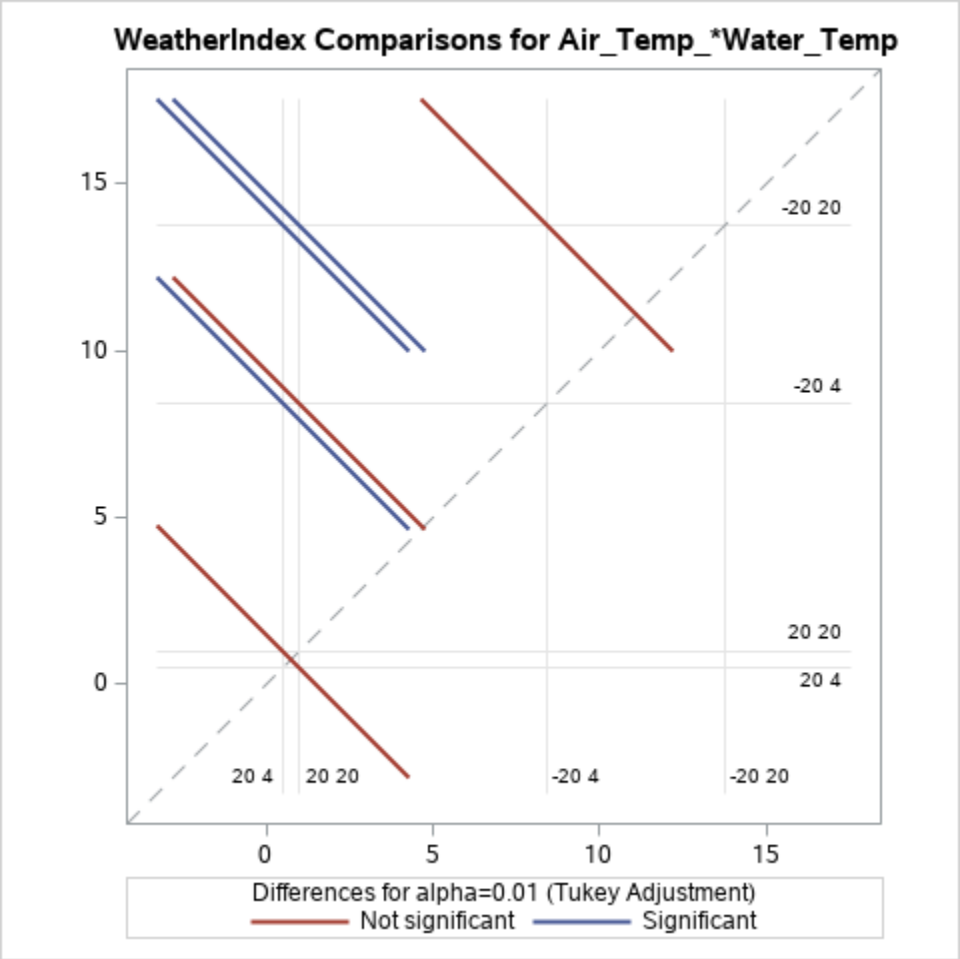

Least Squares Means
Adjustment for Multiple Comparisons: Tukey

Air_Temp__DC_	Water_Conc___mg_LNaCl_	WeatherIndex LSMEAN	LSMEAN Number
20	0	0.3427211	1
20	5000	1.1067090	2
-20	0	6.1346215	3
-20	5000	16.0467470	4

Least Squares Means for effect Air_Temp_*Water_Conc
Pr > |t| for H0: LSMean(i)=LSMean(j)

Dependent Variable: WeatherIndex

i/j	1	2	3	4
1		0.9861	0.0656	<.0001
2	0.9861		0.1327	<.0001
3	0.0656	0.1327		0.0006
4	<.0001	<.0001	0.0006	

Air_Temp__DC_	Water_Conc___mg_LNaCl_	WeatherIndex LSMEAN	99% Confidence Limits	
20	0	0.342721	-3.992893	4.678335
20	5000	1.106709	-3.228905	5.442323
-20	0	6.134621	1.799008	10.470235
-20	5000	16.046747	11.711133	20.382361

Least Squares Means for Effect Air_Temp_*Water_Conc				
i	j	Difference Between Means	Simultaneous 99% Confidence Limits for LSMean(i)-LSMean(j)	
1	2	-0.763988	-8.320292	6.792316
1	3	-5.791900	-13.348205	1.764404
1	4	-15.704026	-23.260330	-8.147722
2	3	-5.027912	-12.584217	2.528392
2	4	-14.940038	-22.496342	-7.383734
3	4	-9.912125	-17.468430	-2.355821

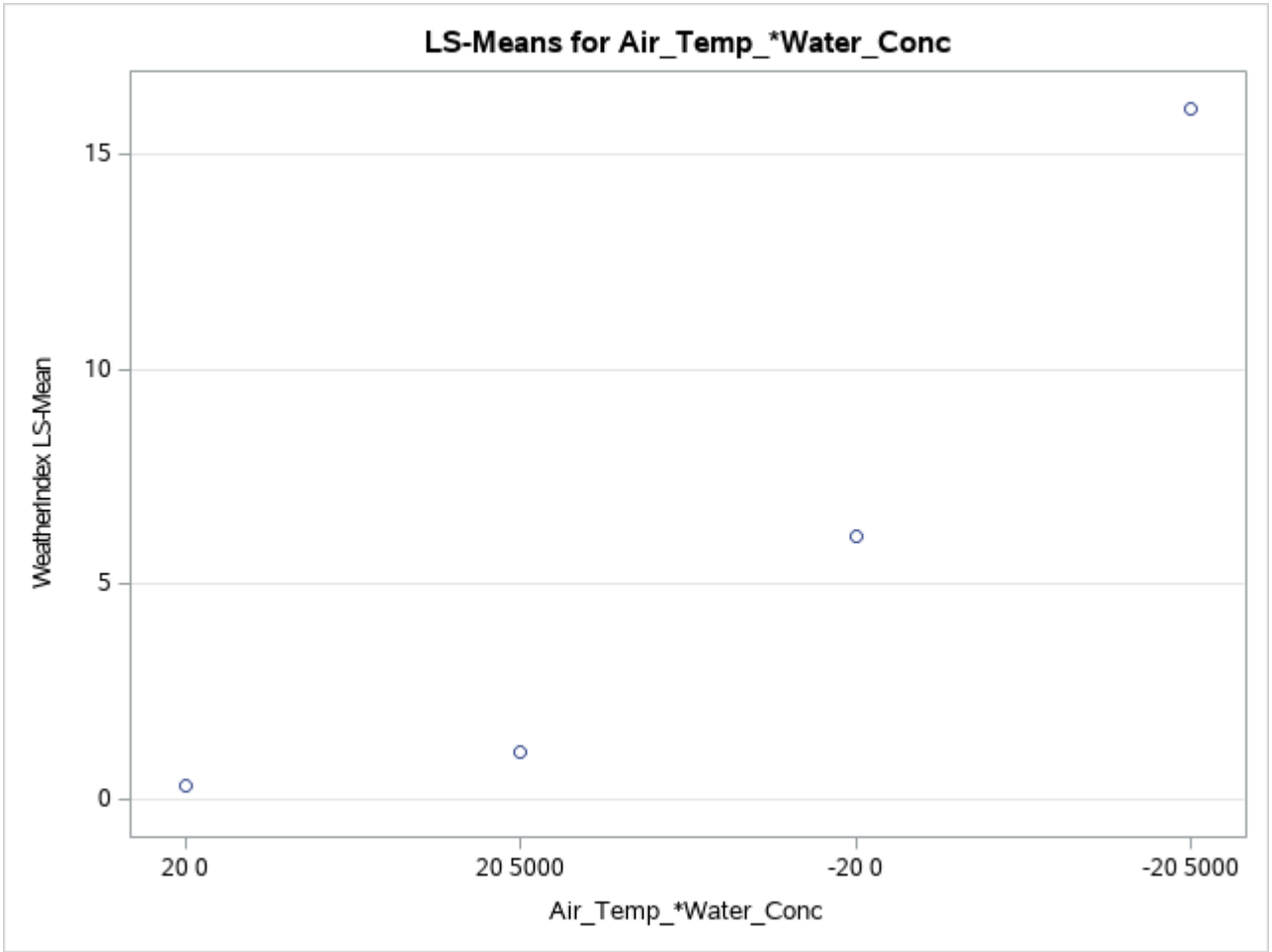

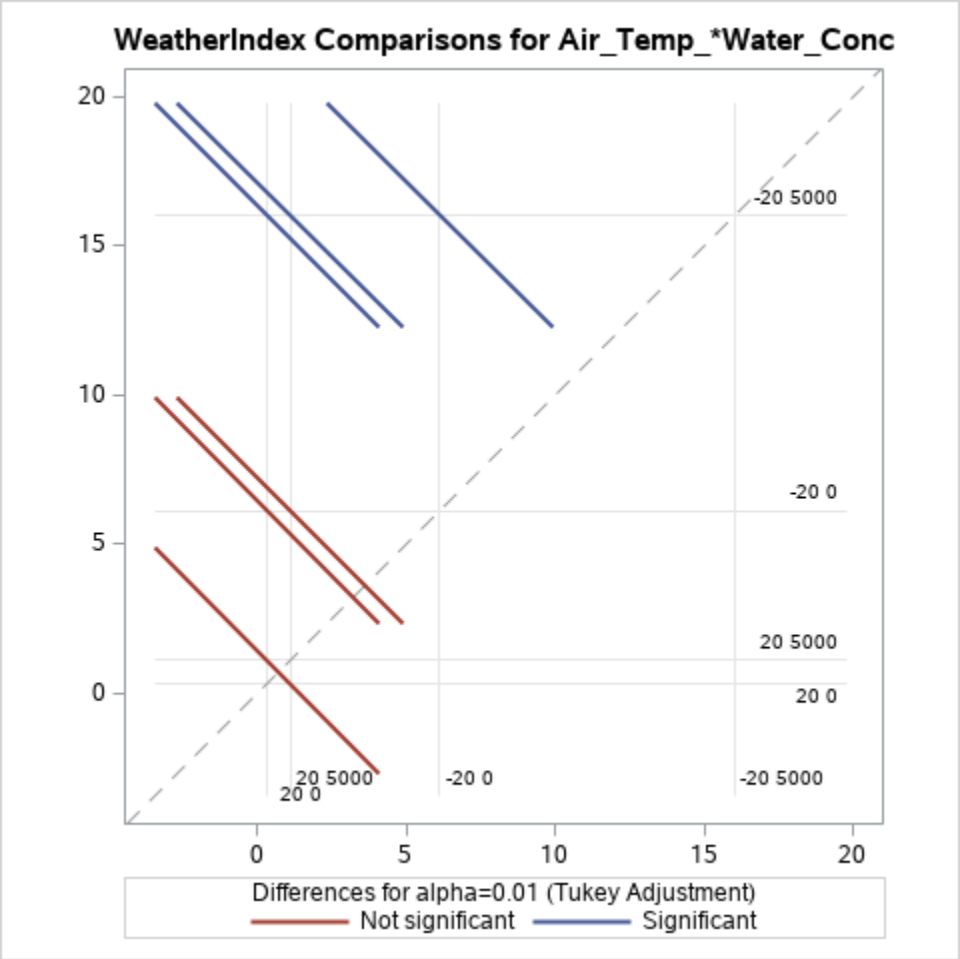

Least Squares Means
Adjustment for Multiple Comparisons: Tukey

Water_Temp__DC_	Water_Conc___mg_LNaCl_	WeatherIndex LSMEAN	LSMEAN Number
4	0	1.54718010	1
4	5000	7.33480491	2
20	0	4.93016244	3
20	5000	9.81865102	4

Least Squares Means for effect Water_Tem*Water_Conc
Pr > |t| for H0: LSMean(i)=LSMean(j)

Dependent Variable: WeatherIndex

i/j	1	2	3	4
1		0.0659	0.4430	0.0043
2	0.0659		0.7076	0.6865
3	0.4430	0.7076		0.1496
4	0.0043	0.6865	0.1496	

Water_Temp__DC_	Water_Conc___mg_LNaCl_	WeatherIndex LSMEAN	99% Confidence Limits	
4	0	1.547180	-2.788434	5.882794
4	5000	7.334805	2.999191	11.670419
20	0	4.930162	0.594549	9.265776
20	5000	9.818651	5.483037	14.154265

Least Squares Means for Effect Water_Tem*Water_Conc				
i	j	Difference Between Means	Simultaneous 99% Confidence Limits for LSMean(i)-LSMean(j)	
1	2	-5.787625	-13.343929	1.768679
1	3	-3.382982	-10.939287	4.173322
1	4	-8.271471	-15.827775	-0.715167
2	3	2.404642	-5.151662	9.960947
2	4	-2.483846	-10.040150	5.072458
3	4	-4.888489	-12.444793	2.667816

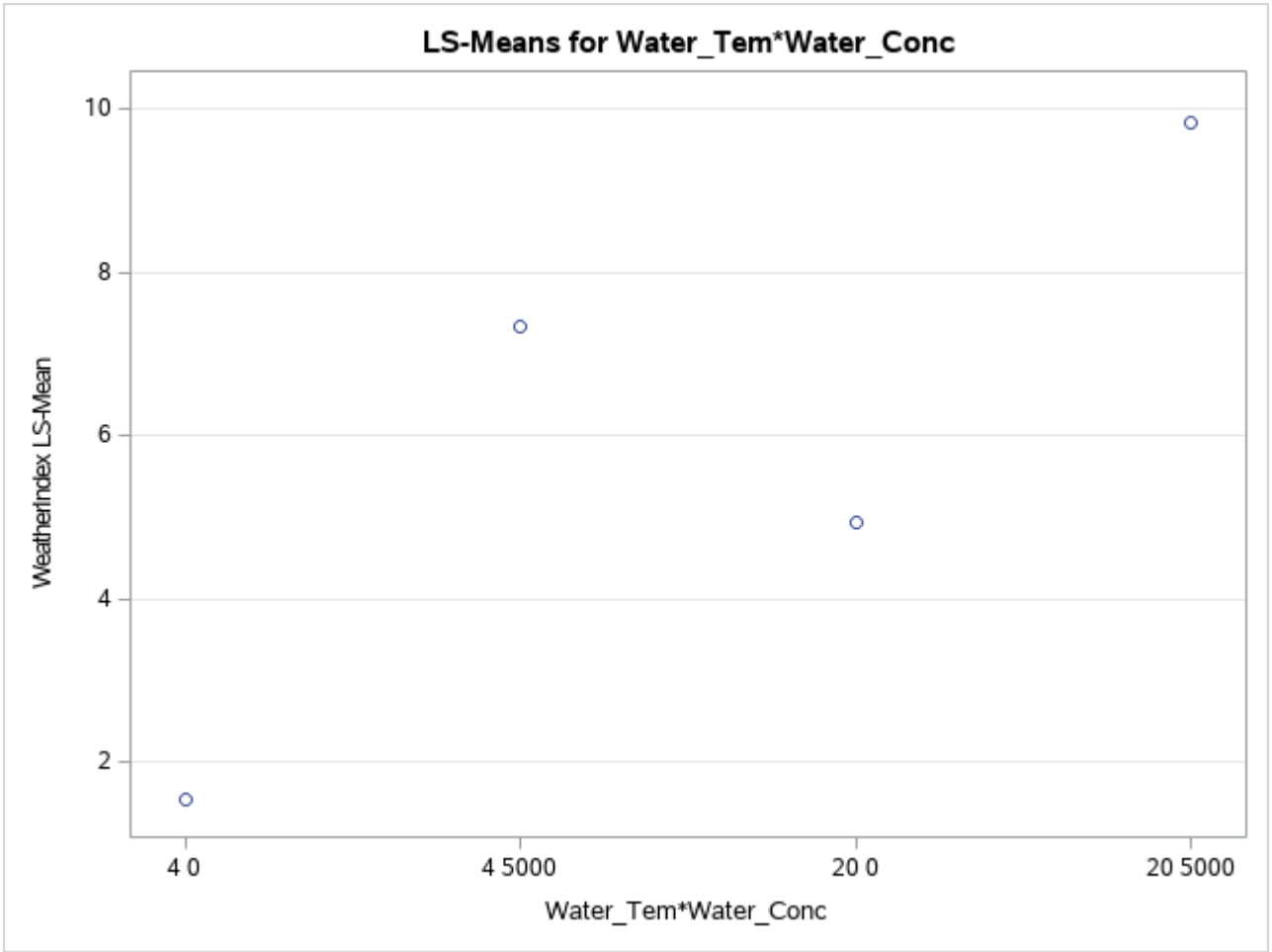

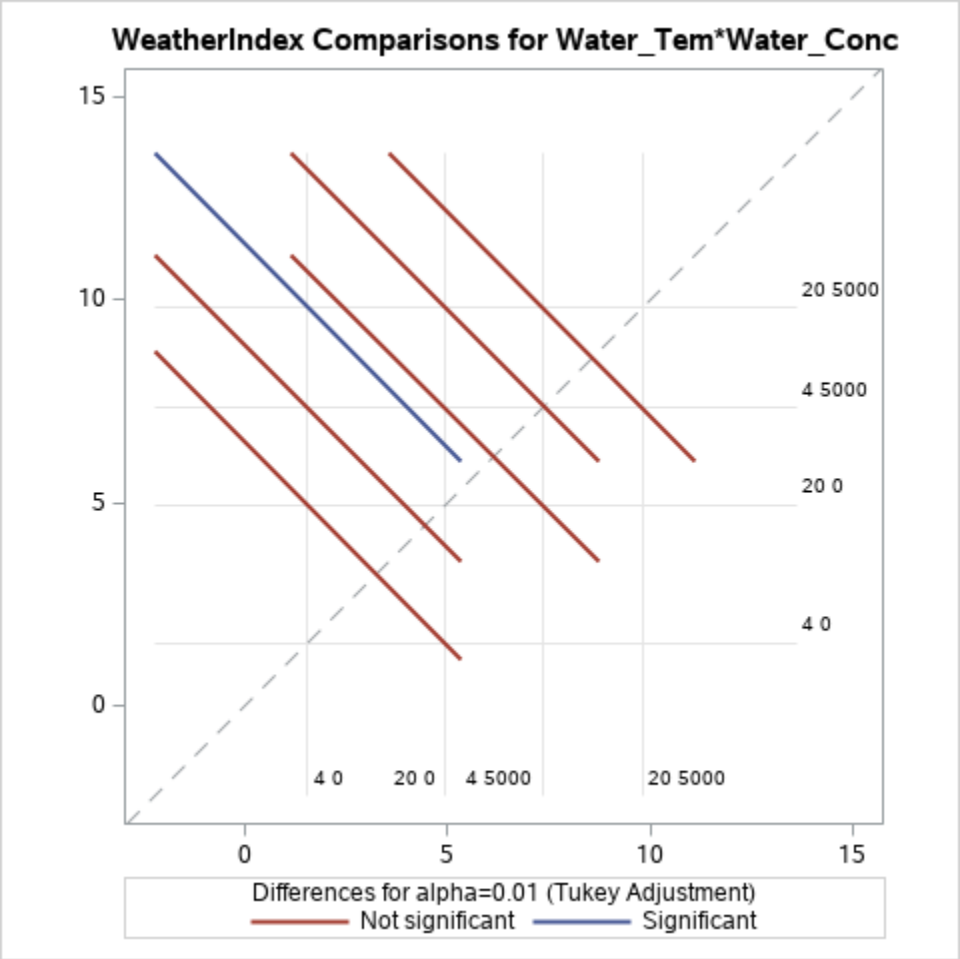

Least Squares Means
Adjustment for Multiple Comparisons: Tukey

Air_Temp__DC_	Water_Temp__DC_	Water_Conc___mg_LNaCl_	WeatherIndex LSMEAN	LSMEAN Number
20	4	0	0.1273492	1
20	4	5000	0.8141133	2
20	20	0	0.5580929	3
20	20	5000	1.3993046	4
-20	4	0	2.9670110	5
-20	4	5000	13.8554965	6
-20	20	0	9.3022320	7
-20	20	5000	18.2379974	8

Least Squares Means for effect Air_Te*Water_*Water_
Pr > |t| for H0: LSMean(i)=LSMean(j)

Dependent Variable: WeatherIndex

i/j	1	2	3	4	5	6	7	8
1		1.0000	1.0000	0.9999	0.9843	0.0030	0.1067	<.0001
2	1.0000		1.0000	1.0000	0.9970	0.0054	0.1655	0.0001
3	1.0000	1.0000		1.0000	0.9940	0.0044	0.1411	<.0001
4	0.9999	1.0000	1.0000		0.9996	0.0089	0.2334	0.0002
5	0.9843	0.9970	0.9940	0.9996		0.0311	0.4970	0.0008
6	0.0030	0.0054	0.0044	0.0089	0.0311		0.8328	0.8577

Least Squares Means for effect Air_Te*Water_*Water_
Pr > |t| for H0: LSMean(i)=LSMean(j)

Dependent Variable: WeatherIndex

i/j	1	2	3	4	5	6	7	8
7	0.1067	0.1655	0.1411	0.2334	0.4970	0.8328		0.1248
8	<.0001	0.0001	<.0001	0.0002	0.0008	0.8577	0.1248	

Air_Temp__DC_	Water_Temp__DC_	Water_Conc___mg_LNaCl_	WeatherIndex LSMEAN	99% Confidence Limits	
20	4	0	0.127349	-6.004135	6.258833
20	4	5000	0.814113	-5.317371	6.945597
20	20	0	0.558093	-5.573391	6.689577
20	20	5000	1.399305	-4.732179	7.530788
-20	4	0	2.967011	-3.164473	9.098495
-20	4	5000	13.855496	7.724013	19.986980
-20	20	0	9.302232	3.170748	15.433716
-20	20	5000	18.237997	12.106514	24.369481

Least Squares Means for Effect Air_Te*Water_*Water_

i	j	Difference Between Means	Simultaneous 99% Confidence Limits for LSMean(i)-LSMean(j)	
1	2	-0.686764	-12.999609	11.626081
1	3	-0.430744	-12.743588	11.882101
1	4	-1.271955	-13.584800	11.040889
1	5	-2.839662	-15.152506	9.473183
1	6	-13.728147	-26.040992	-1.415302
1	7	-9.174883	-21.487727	3.137962
1	8	-18.110648	-30.423493	-5.797803
2	3	0.256020	-12.056824	12.568865
2	4	-0.585191	-12.898036	11.727653
2	5	-2.152898	-14.465742	10.159947
2	6	-13.041383	-25.354228	-0.728538
2	7	-8.488119	-20.800963	3.824726
2	8	-17.423884	-29.736729	-5.111039
3	4	-0.841212	-13.154056	11.471633
3	5	-2.408918	-14.721763	9.903927
3	6	-13.297404	-25.610248	-0.984559
3	7	-8.744139	-21.056984	3.568706
3	8	-17.679905	-29.992749	-5.367060
4	5	-1.567706	-13.880551	10.745138
4	6	-12.456192	-24.769037	-0.143347
4	7	-7.902927	-20.215772	4.409917
4	8	-16.838693	-29.151538	-4.525848
5	6	-10.888486	-23.201330	1.424359
5	7	-6.335221	-18.648066	5.977624
5	8	-15.270986	-27.583831	-2.958142
6	7	4.553265	-7.759580	16.866109
6	8	-4.382501	-16.695346	7.930344
7	8	-8.935765	-21.248610	3.377079

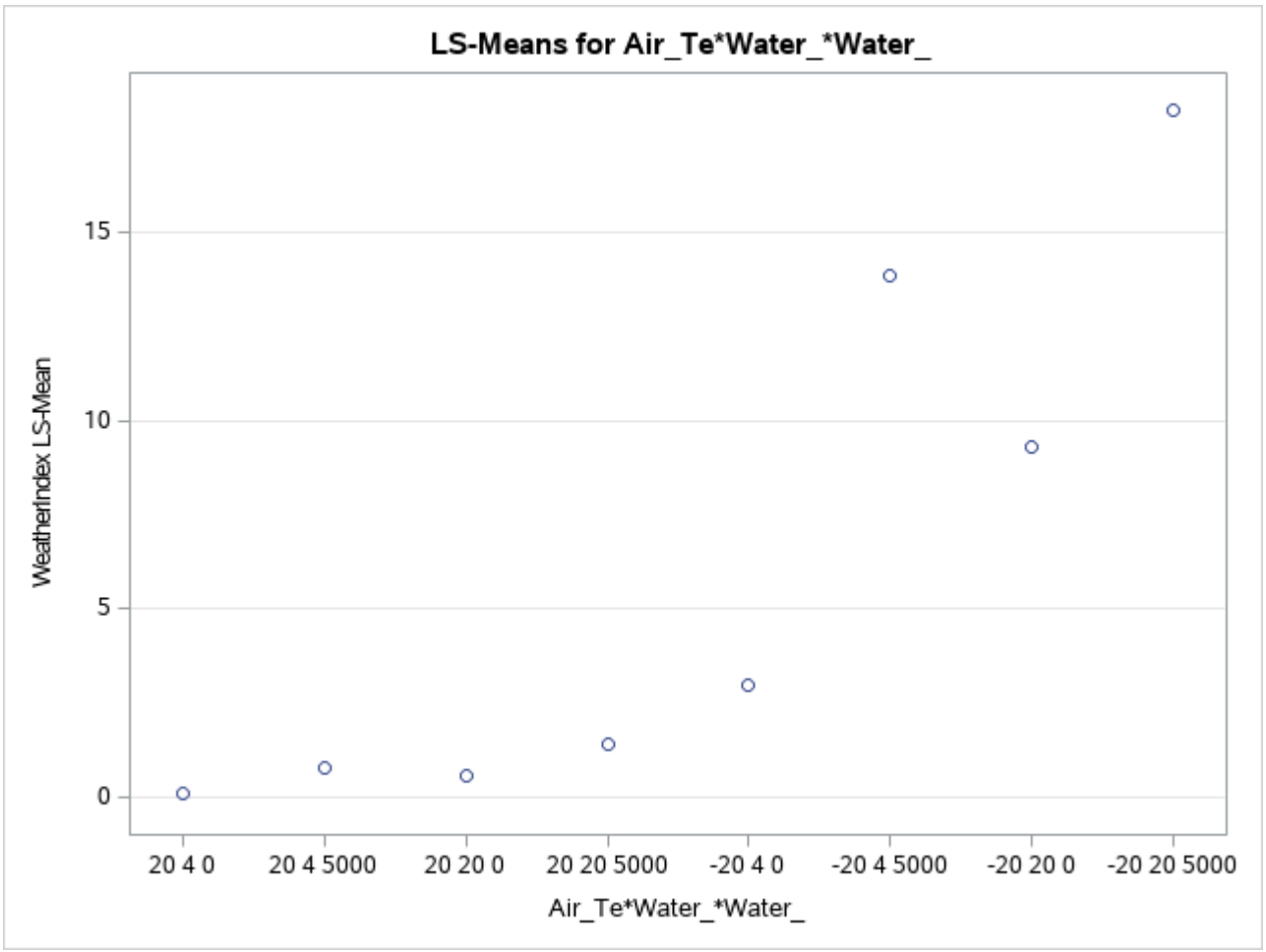
LS-Means for Air_Te*Water_*Water_
Weatherindex LS-Mean
15
10
5
0
20 4 0
20 4 5000
20 20 0
20 20 5000
-20 4 0
-20 4 5000
-20 20 0
-20 20 5000
Air_Te*Water_*Water_

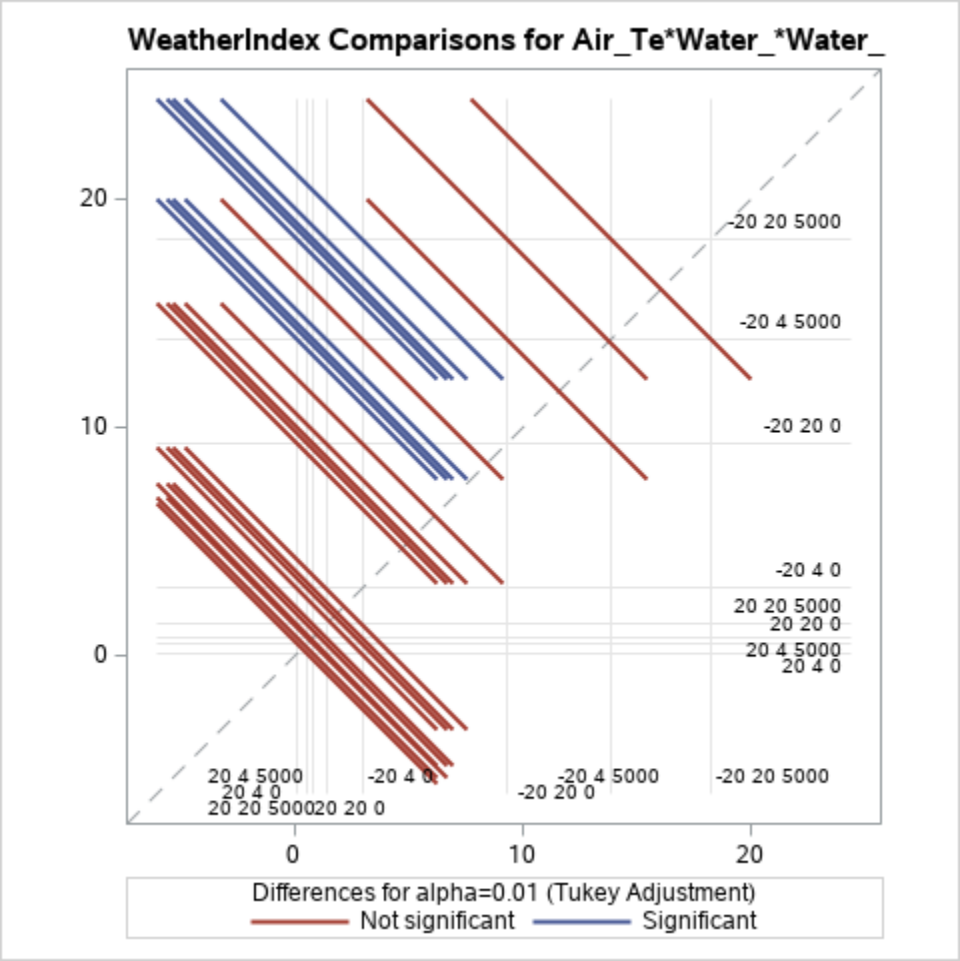
WeatherIndex Comparisons for Air_Te*Water_*Water_
20
10
0
-20 20 5000
-20 4 5000
-20 20 0
-20 4 0
20 20 5000
20 20 0
20 4 5000
20 4 0
20 4 5000
20 4 0
20 20 5000
-20 4 0
20 20 0
-20 4 5000
-20 20 0
-20 20 5000
0
10
20
Differences for alpha=0.01 (Tukey Adjustment)
Not significant
Significant